QATAR UNIVERSITY

COLLEGE OF ENGINEERING

INTEGRATED SUPERCRITICAL CO_2 POWER CYCLE WITH CONCETRATED SOLAR POWER TOWER WITH 50MW POWER CAPACITY

BY

AHMED IDRIS IBRAHIM GAMIL

A Thesis Submitted to the

Department of Mechanical and Industrial Engineering

College of Engineering

in Partial Fulfillment of the Requirements for the Degree of

Master of Science in Mechanical Engineering

June 2021

COMMITTEE PAGE

The members of the Committee approve the Thesis of
Ahmed Idris Ibrahim Gamil defended on 01/06/2021.

Prof. Ahmad K. Sleiti
Thesis/Dissertation Supervisor

Dr. Mohammad Azizur Rahman
Committee Member

Dr. Jamil Renno
Committee Member

Dr. John-John Cabibihan
Committee Member

Approved:

Khalid Kamal Naji, Dean, College of Engineering

ABSTRACT

GAMIL, AHMED IDRIS IBRAHIM, Masters: June : 2021, Master of Mechanical Engineering. Title: INTEGRATED SUPERCRITICAL CO_2 POWER CYCLE WITH CONCENTRATED SOLAR POWER TOWER WITH 50MW POWER CAPACITY, Supervisor: Prof. Ahmad K. Sleiti.

As a part of the world's efforts to mitigate the impact of global warming via carbon neutrality plan by 2050, a novel supercritical carbon dioxide (sCO_2) power cycle is presented that is integrated with concentrated solar power (CSP) tower system and oxy combustor. The system capacity is 50MW and its by-product are pure drinking water and small amount of CO_2 that can be exported for other commercial purposes. The integrated cycle (CONF3) is investigated in comparison to two other cycle configurations in which CONF1 cycle configuration solely depends on oxy combustor and CONF2 cycle configuration solely depends on CSP. Energy and exergy analyses are performed for all 3 cycle configurations and results were presented in a comparative study. Furthermore, the impact of the solar radiation on the cycle's receiver outlet temperature, thermal and exergy efficiencies are investigated. In addition, receiver outlet temperature impact on fuel, exportation of CO_2 and Oxygen consumption is presented for the selected cycle configurations. The study concluded that CONF3 cycle configuration has a promising potential as it has achieved 42.4% of thermal efficiency and 82.77% of exergy efficiency while consuming 1.645 kg/s and 6.579 kg/s of fuel and oxygen, respectively. In addition, 3.621 kg/s of potable water was produced by the integrated CONF3 cycle as a byproduct to the electricity generation, which contributes to resolving the world's scarcity of potable water specially in remote areas. This novel concept of the integrated sCO2 and CSP system is considered as a major step towards

transformation to a full free carbon emission energy production.

The present study also suggested future research directions that include investigating more promising integrated sCO2 and CSP systems; performing levelized cost of electricity and optimization analysis; and investigating more efficient air separation units, turbines, compressors, and heat exchangers.

DEDICATION

I dedicate this novel study to my family and my thesis supervisor for their marvelous support, infinite patience, and continuous encouragement. I really hope that this work will contribute to the realization of carbon neutrality and providing power and clean drinking water for remote and developing parts of the world which is really in need mutual efforts to combat deforestation and climate change effects and accordingly save lives of millions.

ACKNOWLEDGMENTS

I would like to express my special gratitude for my supervisor and mentor Prof. Ahmad K. Sleiti for his unlimited support throughout the preparation of this study. Furthermore, I would like to acknowledge the efforts and support provided to me by Prof. Sleiti's research team members for guidance with the preparation of the EES model. Finally, I would like to thank those who provided me with services of reviewing and editing and those who helped me in bringing this study to an existence.

TABLE OF CONTENTS

LIST OF TABLES

LIST OF FIGURES

CHAPTER 1: INTRODUCTION

1.1 Motivation

Due to the overwhelmingly growth of population around the globe, energy demands increases exponentially pushed further and forward by the modern life-style in which the vast majority of people depends on energy on a daily basis. [1].

Figure 1 shows a graphical representation of the world energy demand from 1980 to 2019 and a forecasted energy demand up to 2030. As shown in Figure 1, the energy demand around the globe is increasing rapidly, which mandates reliable technical solutions to meet this increase.

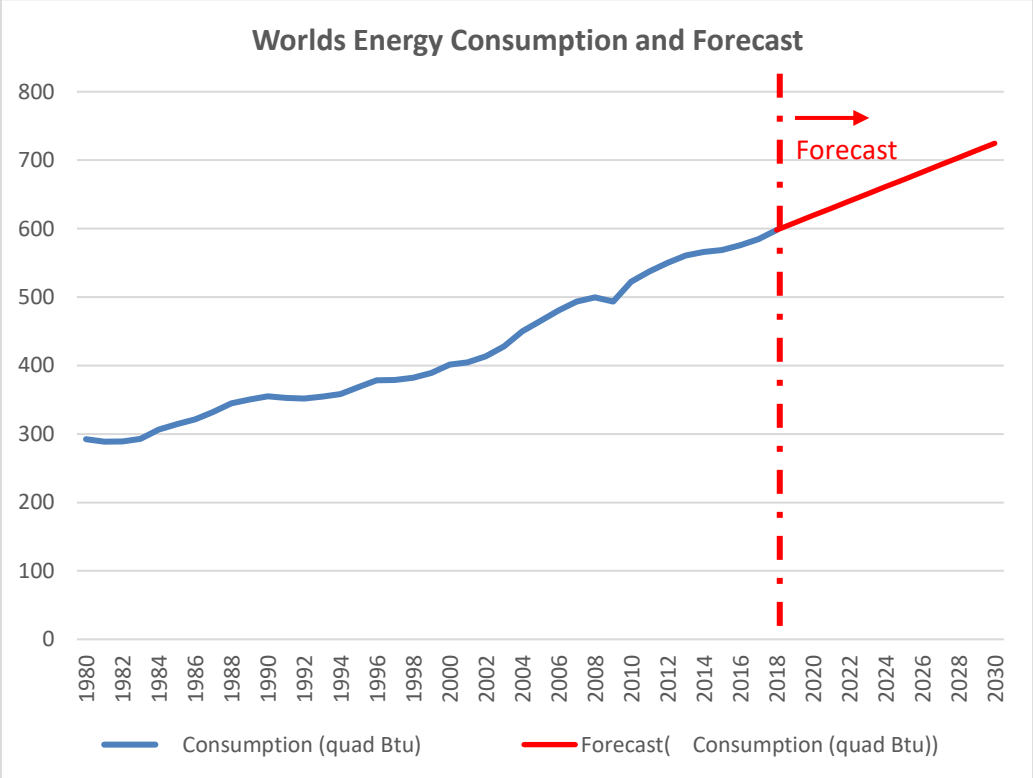

Figure 1. Relative growth in world's population and energy's demand [2]

This rapid increase in energy's demand requires the energy conversion technology stakeholders including governments to adapt and to transform to new

promising technologies. Currently, most of energy conversion technologies depend on fossil fuels , which have three main challenges:

1- Availability of sufficient resources:

   This is mainly caused by the fact that hydrocarbon resources are depleting rapidly.

2- Green House Effect:

   This is caused by the emission of carbon dioxide which is being released by the burning of fossil fuels.

3- Instability of fossil fuel reserves regions:

   Most of known fossil fuels reserve are allocated in parts of the world which are politically instable. Any disturbance to the energy extractions facilities or the shipping routes will directly impact the supply of energy worldwide.

Fossil fuels are mainly used around the globe by the transportation sector and energy (Electricity) production industry. Around 64% of the electricity produced worldwide is dependent on fossil fuels (Coal, Natural Gas and Oil) [2]. In the gulf region, this percentage is even more [3–11]. Figure 2 presents the produced energy worldwide categorized by source of production for the year of 2018.

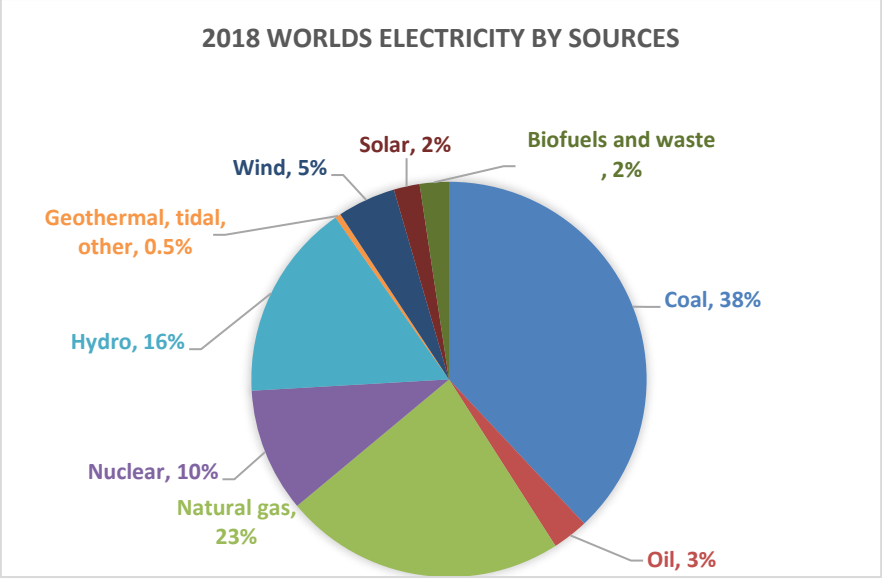

Figure 2. 2018 World's Electricity Production by Source [2]

Carbon Dioxide emissions are really a worldwide concern due to its contribution to the greenhouse effect and subsequently global warming. Although there are ongoing researches with hope to solve the intermittency of power supply and to reduce the electricity generation cost of renewable's technologies in order to permanently replace fossil fuels, those researches are expected to take decades to be materialize and to make them commercially feasible (if successful). In the meantime, the world will continue using fossil fuels and shall suffer from the consequence of using fossil fuels to generate electricity [2] which will negatively impact our lives today and for upcoming generations. Accordingly, the impact of the global warming is a big concern for the world's governments and its citizens. As a foreseeable result of such impact is taking place due to the increase of the global average surface temperature which results in ice melting, rising of sea-water level (it is event anticipated that some countries will be flooded by water [12]), migration of natural habitats, scarcity of some vegetables and crops and which might lead to demo-graphic change and may lead to wars and conflicts over natural resources [13]. That's why international organizations

(like the United Nations) urge countries to invest in reducing carbon emissions at national level and encourage research institutes to innovate or discover a technological breakthrough to either contribute to the reduction of carbon emission or limits its impact on humanity. The United Nation hosts Paris Agreement Framework (COP21) and its Nationally Determined Contributions (NDC) summit for countries and government to demonstrate their plans toward Carbon Neutrality by 2050 and their progress toward that goal.

The current trend considering Sustainable Technologies for Energy Production Systems (STEPS) of worlds carbon emission is not really promising as the world needs to engage into more stricter scenarios like Sustainable Development Scenario (SDS) which will contribute to the carbon neutrality by 2070 and Net Zero program which result in carbon neutrality by 2050 [14]. Figure 3 illustrates the worlds current position and the potential scenarios and its impact.

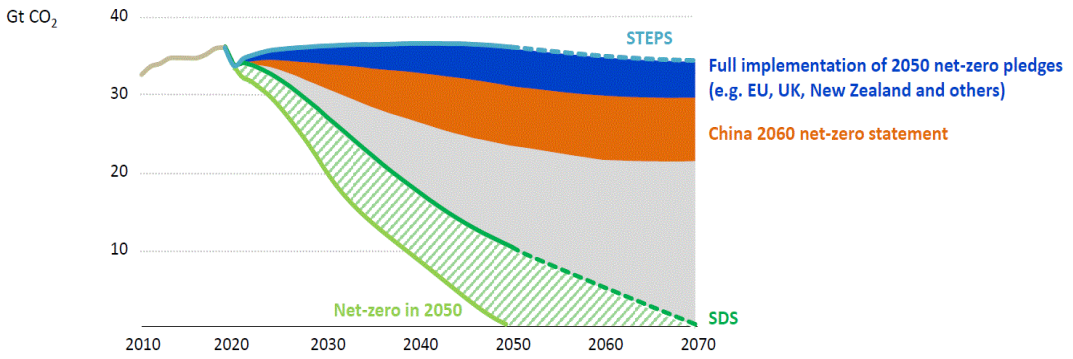

Figure 3. Carbon neutrality scenarios and the world's current position [14]

Following the efforts exerted by UN and other partners to adopt precautional polices and procedure, some parts of the world initiated the transformation in using traditional power generation technologies that depend on fossil fuels. There is an

obvious move to a more sustainable power generation technologies like renewable energy technologies. Since this thesis integrates with the solar power technology, a review on the solar technology's growth are presented below as follow. Solar power (PhotoVoltaics) technology use has been drastically increased and, in fact, further increase is expected as reported by the Energy Information Agency [14]. Figure 4 represents the contribution of the Solar PhotoVoltaics technology in energy industry in the last decade, its current momentum considering (STEPS) and its forecasted growth considering (SDS).

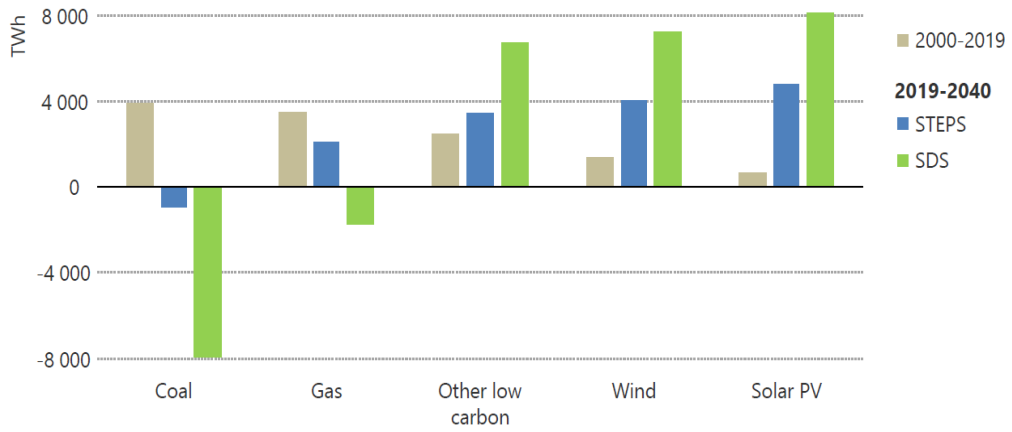

Figure 4. Solar (PV) contribution, current status and its forecasted growth [14]

On the other hand, solar thermal technology has achieved remarkable progress in the period from 2010 to 2017. The technology has been proven to be reliable technology as an energy conversion technology as presented in the in Figures 5 and 6 below. Figure 5 illustrates the growth of solar thermal between the period from 2010 to 2017 and Figure 6 demonstrate the expected growth of this technology in comparison to the achieved development in the previous period.

Part of the motivations behind this project is to contribute in securing energy for developing remote communities and avail them the opportunity to get electricity and potable water and to asset in finding a suitable application for uses of the pressurized CO_2 (rather than emitting it to the atmosphere) by exporting it as by-product which will result in a cleaner environment by drastically reducing the dependency of fossil fuels as the system is integrated with CSP.

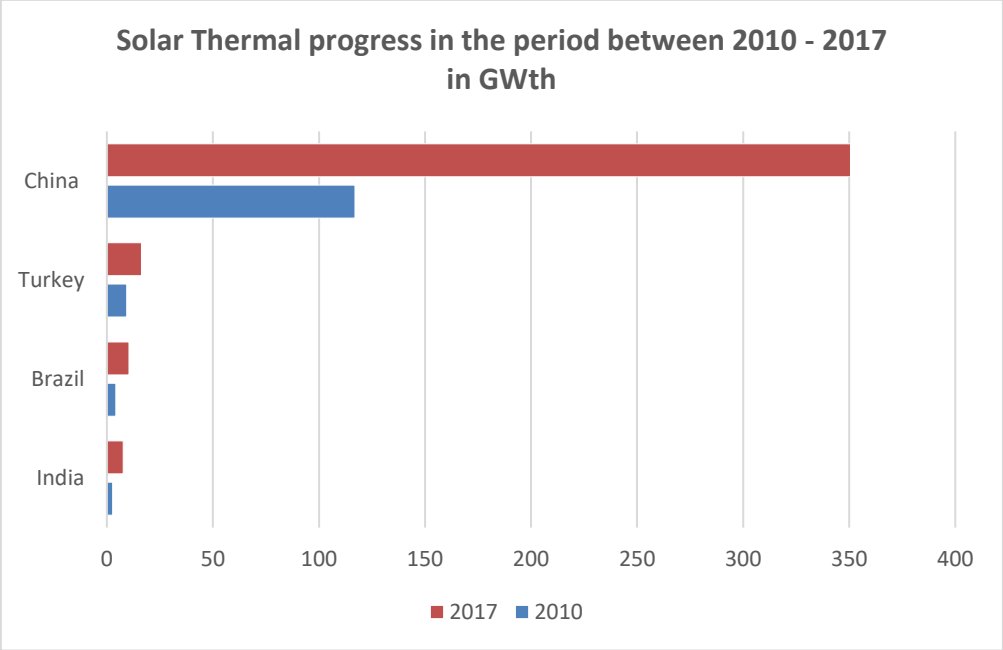

Figure 5. World solar thermal growth between the period from 2010 to 2017 [15]

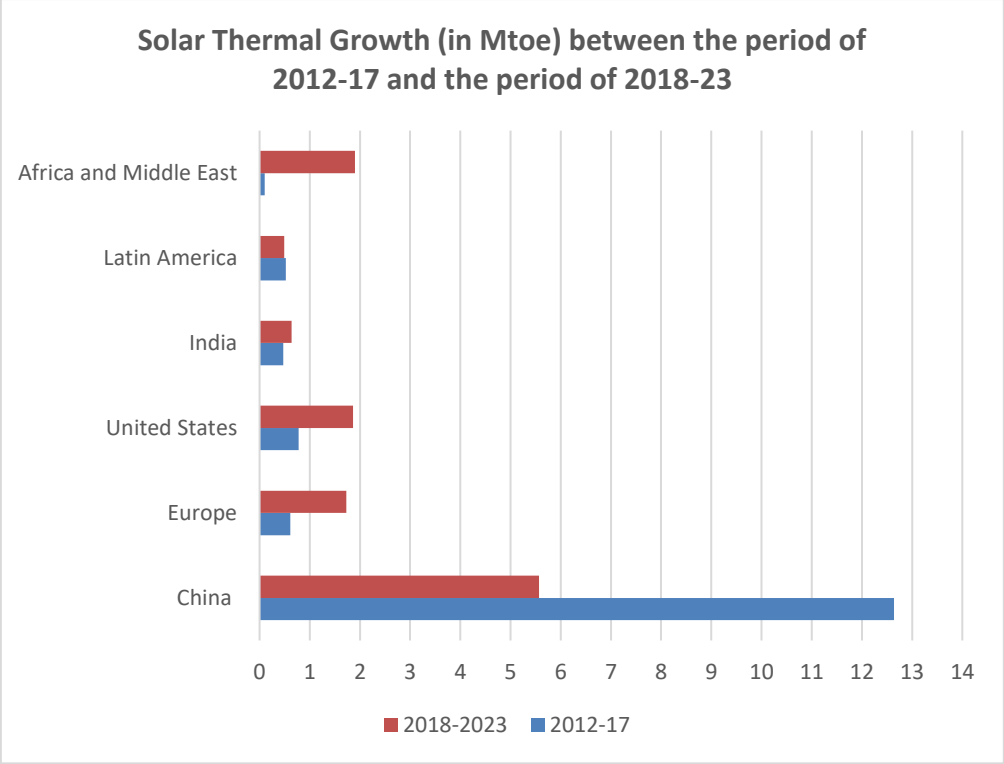

Figure 6. Solar thermal development between 2012 and 2017 in comparision to the forecasted growth between the period between 2018 and 2023 [16]

1.2 Background

As the world is busy exploring alternative energy sources (such as Solid Oxide Fuel Cells, Renewables, Nuclear, etc) and securing efficient operation of the existing energy conversion technologies, the Supercritical Carbon Dioxide Power Cycle (also known as Allam Cycle [17]) has gained the interest of researches around the world due to its promising potential to contribute to efficient and cleaner energy conversion environment [18]. The scientific research journey in this field started by Sulzer (trans-critical cycle) in around 1940 [19]. Few years later Angelino and Feher had concentrated more into sCO_2 power cycles taking independent approaches as explained in [20]. Since then, the subject didn't attract much interest until Dostal revived this area of research in 2004 by investigating hybrid sCO_2 power cycles for various energy

conversion applications like renewable and nuclear power generation industries [21]. The first sCO_2 power cycle combined with the oxy combustor (Allam Cycle) was developed by 8 Rivers Capital in La Port, Texas which was considered as an enormous progress toward commercialization of the such power plants (50 MW_{th}) [17]. The main advantage of such power cycles is the ability to capture the produced Carbon Dioxide resulting from the oxy combustion process in addition to its high efficiency. The cycle combustor uses the natural gas as a fuel to the combustion process. Major project's stakeholders were Heatric (Recuperators Manufacturers) and Toshiba (Combustor and Turbine Manufacturers).

There are various layouts studied in the literature with the purpose of improving the sCO_2 cycle performance by altering the cycle processes flow (by adding/removing of changing of cycle component/layout) [22] or via the integration of sCO_2 power cycle with other application like Nuclear applications [23], CSP-PT [24] and Parabolic Trough Collector [25]. Standard sCO_2 cycle consists of a compressor, turbine, heater (combustor), cooler and recuperators (in some cases). However, in the trans-critical sCO_2 cycle, the compressor and cooler were replaced with pump and condenser respectively because the lower pressure of the cycle is imposed by the condenser. Researchers concluded that the best way to overcome this problem is by introducing a pre-compression process integrated within the cycle. From cycle efficiency prospective, two recuperators (HTR and LTR) were used to recover some of the waste heat, minimize the cooling load on the cooler (before the compressor) and reduce the effect of cycle's irreversibility [26]. Researches, however, show that it is theoretically possible to enhance the conventional Brayton cycle efficiency with the addition of one of the component like a preheater/reheater, multi-stage compression/expansion and intercooling which will be explained in details in the Literature Review Chapters.

1.3 Thesis Objectives and Contribution

One of the objectives of this project is come up with a technological solution to the increasing power demand that results in environmentally friendly, affordable, and reliable technology. This proposed novel power cycle is studied and analyzed thermodynamically via EES and energy/exergy analysis of the system. In addition, this proposed novel power cycle generates clean potable water and pressurized Carbon Dioxide (for other industry applications) as a by-product with the aim to contribute to the solving of the needs for potable water in places of water scarcity, in addition to the industry's demand on Carbon Dioxide for commercial applications.

The novelty of this project is to generate electricity via a hybrid system between Oxy combustion and CSP via utilizing sCO_2 to run the turbine, producing electricity with by-products of pure water (drinking water) and pressurized Carbon Dioxide for commercial use. The difference between 8 River Capital plant [17] and this proposed cycle is the integration of the oxy combustor and CSP to the cycle where the oxy combustor contribute to the production of sCO_2 and water as a by-product of this cycle. On the other hand, the CSP works as a pre-heater to the combustion process during the day time, this layout will have a positive outcome of the consumption of the fuel (natural gas/Methane) used for the combustion process as it will be discussed in detailed later in this document. The concept of this thesis is that both systems will be integrated where the Concentrated Solar Power Tower will act as a pre-heater to the sCO_2 before it enters the oxy combustion chamber to reduce the dependency of the thermal energy produced by the oxy combustor (and subsequently fuel and oxygen consumption). The CSP-PT is capable to work independently if it is able to generates enough heat (depending on the geographical location and its solar flux), however, the systems efficiency will be drastically decreased as presented below in CONF2 model.

1.4 Thesis Layout

This thesis is presented by firstly reviewing the literature review about the topic in general with special emphasis to similar system in Chapter 2. In this chapter, all CO_2 thermodynamic power cycles and its various cycle's configuration in addition to its integration with various energy sources are presented the Literature Review chapter. More specifically, all publications relating to sCO_2 power cycles integrated with CSP and oxy combustor have been investigated in detail and its different from the proposed novel sCO_2 power cycle (CONF3). In chapter 3, the proposed sCO_2 power cycle integrated with CSP and oxy-combustor cycle configuration (CONF3) is being presented in comparison to other similar cycles (CONF1 and CONF2). Each one of the three cycle's configurations are being presented and discussed and illustrating the differences between across all three investigated sCO_2 power cycle layout. In chapter 4, the energy and exergy models are being presented for the all the three different sCO_2 power cycles highlighting the assumptions and equations used to generate the model. Chapter 5 represents the verification and validation performed in comparison to CONF1 and CONF2 cycles which are available in the literature to reassure the accuracy of the model. In addition, the energy and exergy models' results were discussed for all the three models and compared to each other, the best sCO_2 cycle configuration was recommend supported by the evidences and the results were compared to the other two sCO_2 cycle configurations. Chapter 6 draws the conclusion to this thesis and restate the obtained results and the evidence behind the claim that the novel sCO_2 cycle (CONF3) is achieving better than the other compared to $\mathbf{sCO_2}$ cycles, recommendations are also presented in this chapter for further cycle's enhancement and potential future work.

CHAPTER 2: LITERATURE REIVEW

An overview of the literature related to this subject is presented in this chapter including published papers, articles, thesis documents and other research materials in relation to the proposed $\mathbf{sCO_2}$ power cycles integrated with CSP and/or oxy combustor as described in the below sub-sections.

2.1 sCO_2 Cycle Configurations, Energy Source and Analysis Type

Recently, Sleiti and Al-Ammari [27] studied and reviewed the research on $\mathbf{sCO_2}$ power cycles available in the literature and classified the studies cycles according to their energy sources, cycle configurations and the analysis types carried on the subject. The results of this review and classification is shown in Figure 7 [27].

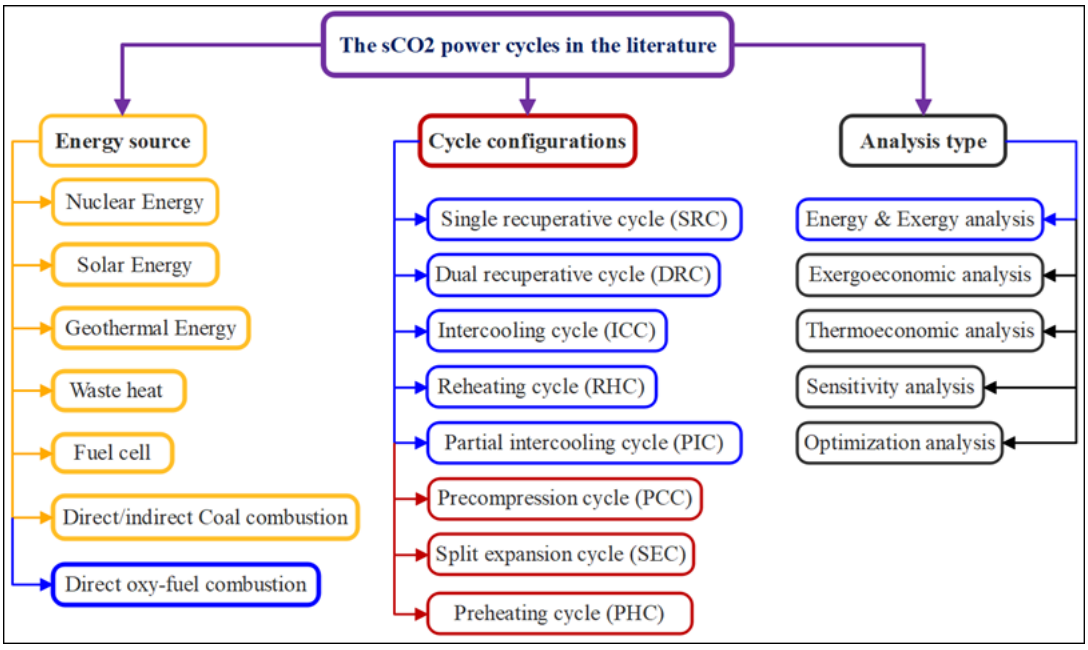

Figure 7. Heat sources, cycle configurations, and analyses of the $\mathbf{sCO_2}$ power cycles in the literature [27]

Feher and Angelino had introduced to the scientific world the use of $\mathbf{sCO_2}$ power cycle. It a was a breakthrough which paved the way to other researches where

the proposed thermodynamic cycle achieved a thermal efficiency of 90% of Carnot efficiency under ideal conditions [23].

In January 1968, Feher's research has trigged a lot of researches in the field of capturing and utilizing Carbon Dioxide for the thermodynamic supercritical power cycle. Dostal in 2004 has carried out his PhD research paper in studying the effective potential using of Carbon Dioxide. In his published research by MIT library [21] the use of $\mathbf{sCO_2}$ was recommended for the application of nuclear application for power generation purposes which will lead to a cheaper production of electricity and contribute to solving the world's problem of carbon dioxide emissions.

On the other hand, Angelino's researches [20] focused around the lower efficiency of Brayton cycle compared to Rankine cycle at similar Turbine Inlet Temperature. To overcome this challenge of irreversibility, a series of various power cycle layout has been investigated, and it was concluded that recompression cycle layout is the most efficient cycle layout whereas low carbon dioxide stream shall be split into parallel compressors. However, it was noted that the above cycle main disadvantage was the turbine exhaust temperature was restricted to the condenser pressure. Accordingly, a modification was introduced with the addition of one additional compressor to ensure the ensure the pressure flexibility and ultimately overcome the identified problem above. This modified cycle is known as Partial Condensation with Pre-Compression cycle. Another proposal by Angelino to reduce the turbine inlet pressure (for the purpose to simplify the turbine design) is by re-routing the recycled high-temperature Carbon Dioxide before it enters the combustor (or boiler, receiver, etc) into a moderate temperature turbine, this will ensure lower pressure and simpler turbine design is required. This design is known as Partial Condensation with Pre-Expansion Cycle.

In a review paper by Francesco [20] and another research by Sleiti and Al-Ammari [27], various s$\mathbf{CO_2}$ power cycle were analyzed based on their Energy source, Cycle Configuration and Analysis Type. Around 200 papers were summarized with all layouts presented in all those review papers, those were categorized as Single Recuperative Cycle (SRC), Dual Recuperative Cycle (DRC), Intercooling Cycle (ICC), Reheating Cycle (RHC), Partial Intercooling Cycle (PIC), Precompression (PCC) and Split Expansion Cycle (SEC). Each of the above cycle category will be briefly discussed in the following sub-chapters.

2.1.1 Single/Dual Recuperative Cycle (SRC) & (DRC)

This cycle is a simple recuperated Brayton cycle adapted at the Carbon Dioxide supercritical region. This cycle layout generally aims avoid general Brayton cycle constrains high compression work and the large area required for the heat transfer process. The thermodynamic properties of the Carbon Dioxide at supercritical region has a positive impact in the overall cycle efficiency as the work required for the compression process is lesser and the compressor outlet temperature is also lower and lower pressure which lead to a less complex recuperator process and higher efficiency. One of the main application for such power cycle layout is low-temperature waste heat recovery applications [20]. The major difference between both cycles (SRC & DRC) is the number of recuperative available. Generally, the Dual Recuperative Cycles (DRC) are more efficient compared to the Single Recuperative Cycles (SRC) because they allow for more hot turbine outlet heat recovery with the help of Low Temperature Recuperator (LTR) and High Temperature Recuperator (HTR) without pinch-point effect occurring at the recuperative. On the contrary, the Single Recuperative Cycle (SRC) usually affected by the pinch-point effect due to the large size of the recuperative which also adds a challenge in terms of transportation, handling and the installation of

the recuperative onsite. Figure 8 illustrates the basic description of Single and Dual Recuperative Cycle.

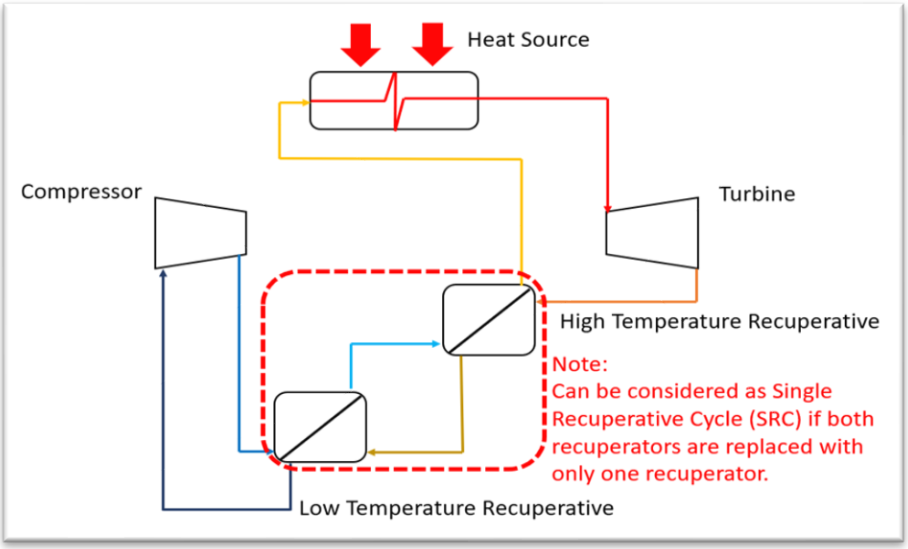

Figure 8. Single/Dual Recuperative Cycle Configuration

In general, standard Brayton cycle efficiency is considerably low (ranges between 15% - 20%), However, many researches were made to enhance the efficiencies of the Brayton Cycle by carrying out the compression and cooling processes at multi-stages and the introduction of multi-recuperators drastically contribute the enhancement of the cycle efficiency [28] [19]. In addition, in the research carried out by Sleiti & Al-Ammari [19] a comparative scenarios were studied using a supercritical carbon dioxide without a preheater, with a preheater parallel to the Low Temperature Recuperators and a preheater parallel to both the Low Temperature and the High Temperature Recuperators. It was concluded that the addition of the preheater parallel to both recuperators will enhance the efficiency of the cycle which reaches up to 53%. The research paper proposed to utilize a nearby high temperature waste heat source as a preheater which leads to even higher efficiency of the Brayton Cycle. Figure 9

represents the proposed cycle by Sleiti which increased the efficiency of Brayton cycle up to 53%.

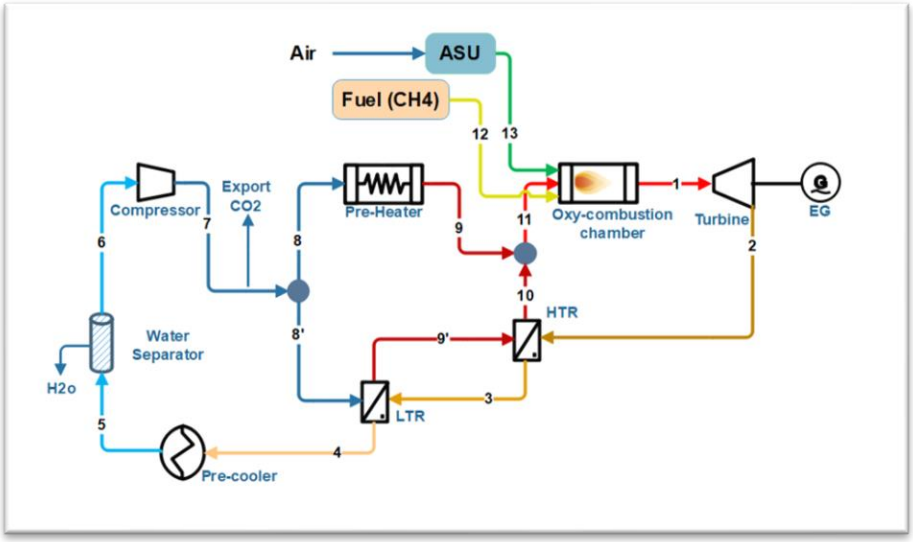

Figure 9. Oxy combustion cycle proposed by Sleiti and Al-Ammari [19]

It is worth mentioning that there are other techniques proposed in the scientific literature to improve the efficiency of Brayton Cycle like the research carried out by Invernizzi [29] to investigate the potential use of various gas mixtures ranges from hydrocarbons, Perfluoro compounds, Halogen Compound and mixtures with Carbon Dioxide (as a primary component), it was noted that a mixture of Carbon Dioxide will drastically influence the performance of the cycle depending on the thermal stability of the secondary component thermal stability. Accordingly, the Carbon Dioxide mixture with a secondary component is mainly dependent on the thermal stability of the secondary component.

2.1.2 Intercooling Cycle (ICC)

This power cycle layout is basically a simple recuperated cycle with multi-compression phases separated by intercoolers in between them. Hot day, Brayton s$\mathbf{CO_2}$

GT, Intercooling II and Allam Cycles are classified as sub-category of this type of power cycle. Although Allam cycle uses Oxy-fired fuel, Natural Gas, Syngas or any other source of use waste heat, it still shares all the main component of this cycle and that is the reason why Allam cycle is classifies as a regeneration with Intercooled compression. Figure 10 below illustrates the basic component of the Intercooling Cycle with the introduction of a pre-cooler and intercooler

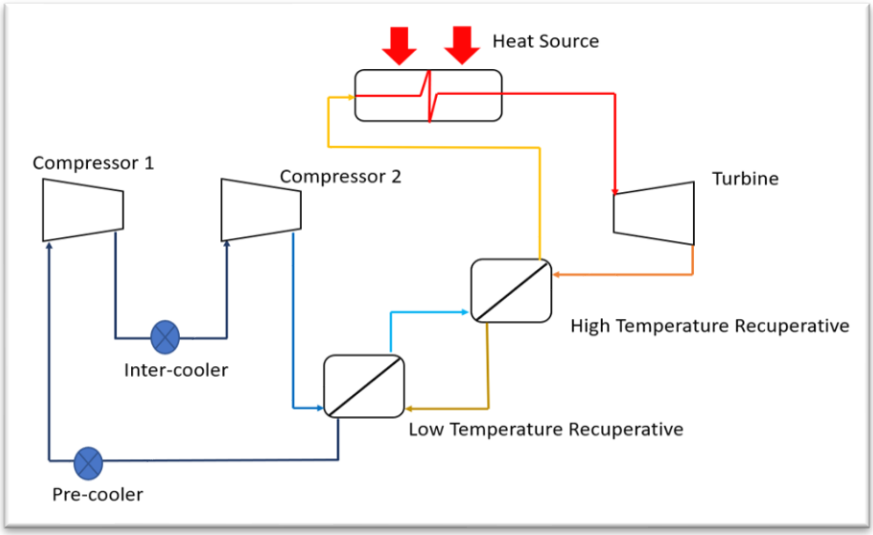

Figure 10. Intercooling cycle configuration

The main purpose of the addition of the pre-cooler and inter-cooler is it reduces the compression power by the cooling the $\mathbf{sCO_2}$ prior compression which will lead into lesser compression work required.

Ma [30] has carried out a thermodynamic study of the intercooling cycle, it was concluded that the integration of the Intercooled Compression does have a positive impact to the overall cycle efficiency (2.65% cycle efficiency improvement) and optimized compressor operation. The impact would be more apparent in higher cycle's temperature, low temperature, and low pressure. Another analysis was carried out by

Osorio [31] to review the integration of the CSP with the $\mathbf{sCO_2}$ power cycle (ICC layout) and its effect on such power cycles (1.2 MW). It was noted that about 0.7% improvement was noted in the overall process efficiency and a 12.6%, 14.3%, 16.2% and 15.6% average efficiency enhancement using the paper proposed layout (ICC).

It is worth noting that [32] had carried out an assessment for the cycle off-design behavior in nuclear application in which the research concluded that it is recommended to have some sort of independent control of the compressor (pressure ratio) is necessary to avoid operation instability by significant drop in both IHX power and cycle efficiency when the heat sink temperature increases.

2.1.3 Reheating Cycle (RHC)

This cycle layout emphasizes on the two-stage heating process as a preparation for the expansion process. The heating source can be the same [20] or independent heating source [22] in comparison to the main heating source. In the cases of the same heating source can be used/reused from the same heating source [33] or via using recuperators to benefit from the turbine hot outlet [19]. This cycle layout can be integrated with single or dual expansion (in sequence or in parallel) process depending on various factors of the design (power requirements, TIT achieved, system dependency and other decisive design factors). Figure 11 illustrates the standard reheating cycle.

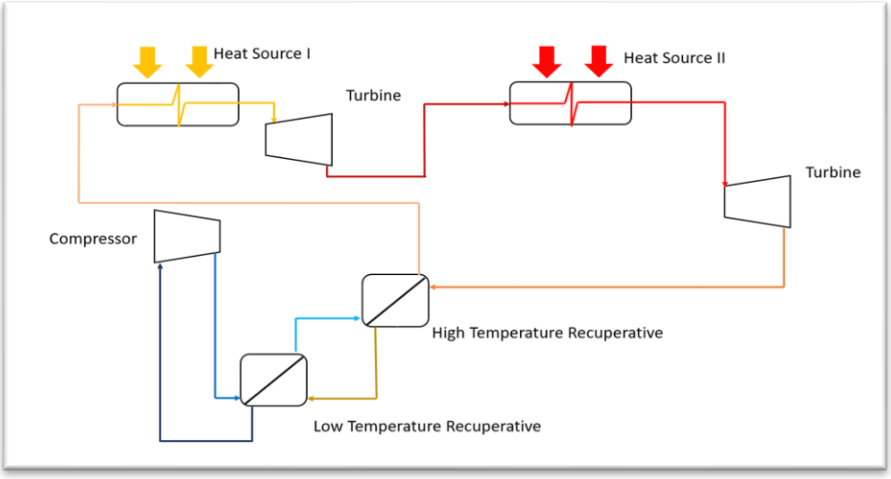

Figure 11. Reheating cycle configuration

It is worth noting that the Reheating Cycle may come into different Configurations and setup depending on the cycle and available equipment like turbines, recuperators, and the available heat source. Francesco [20] has elaborated more into the different Reheating Cycle configurations combined with recuperative and intercooling cycles as shown in the Figure 12.

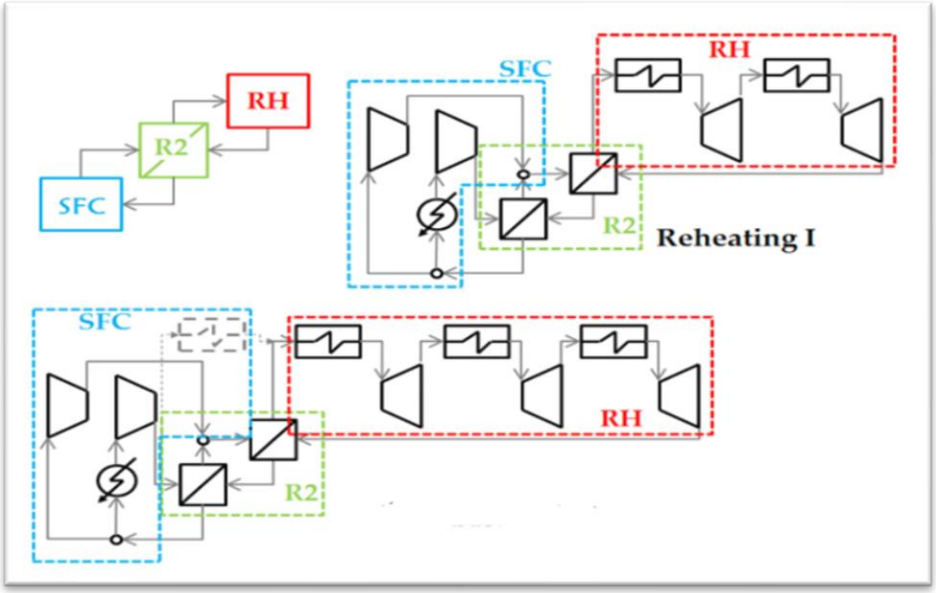

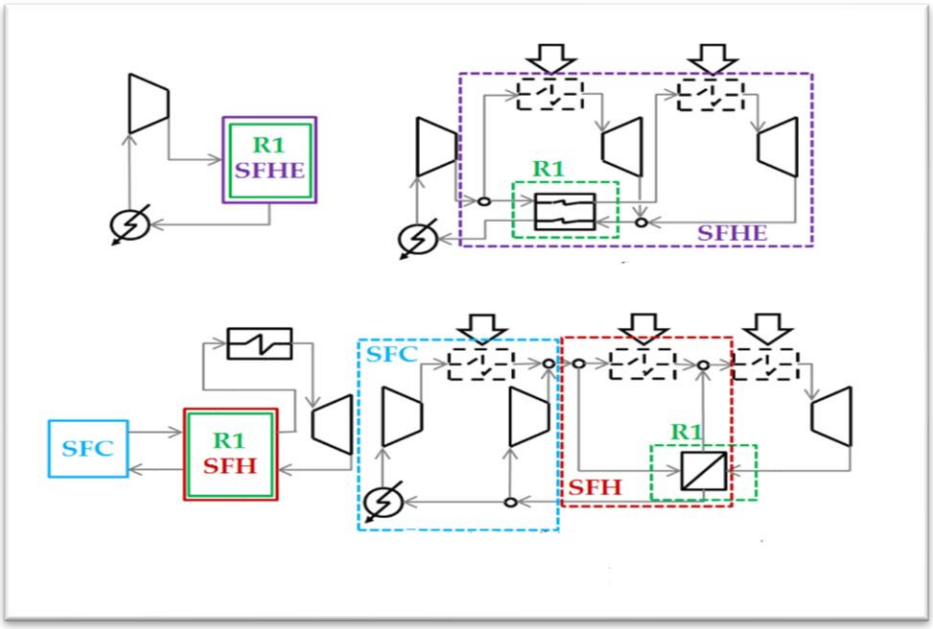

Figure 12. Various reheating cycles confirgurations [20]

The application of such cycle configurations usually in hybrid systems where one heat is not consistent as in renewable energy integration [34] [24] [19] [35], waste heat utilization [36] [37](although not consistent sometimes) and nuclear applications [38] [39] [22] [18].

2.1.4 Partial Intercooling Cycle (PIC)

This cycle layout came as a continuation of Feher's research [23] whereas the lower pressure s$\mathbf{CO_2}$ goes into split flow at the compression phase of the cycle. The concept behind this layout is to split the flow before the compression process. Commonly this type of power cycles are equipped with dual recuperators (Low and high temperature recuperators) in which the one compressor outlet flow directly to the High Temperature s$\mathbf{CO_2}$ line and the other compressor outlet flows toward the Low Temperature Recuperator (LHR) as illustrated in the Figure 13. Usually this type of power cycles depends on parallel dual compressors, one of the compressors is generally associated with a dedicated cooler to enhance the compression efficiency [34].

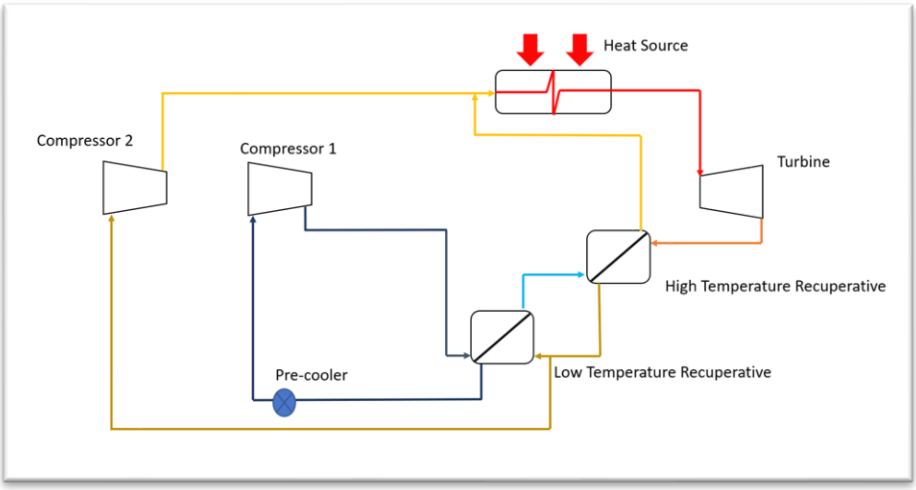

Figure 13. Partial cooling cycle configuration

The advantages of this type of power cycles is that is reduces the pinch point occurring at the Low Temperature Recuperator because of the reduction of the heat capacity resulted from the split flow toward the LTR. The thermal load is reduced due to reduced capacity resulted from the split flow where not all the flow goes through the cooler (prior compression stage), this drastically reduce the complexity of the compressor parts and its cost accordingly. Another advantage was noted by [40] that partial cooling cycle has the highest temperature difference in between the Low Temperature Recuperator and the turbine inlet temperature without compromising the compression efficiency. It was concluded by Thanganadar research [41] that the Partial Cooling cycle delivered the best performance in integrating the system with Concentrated Solar Power.

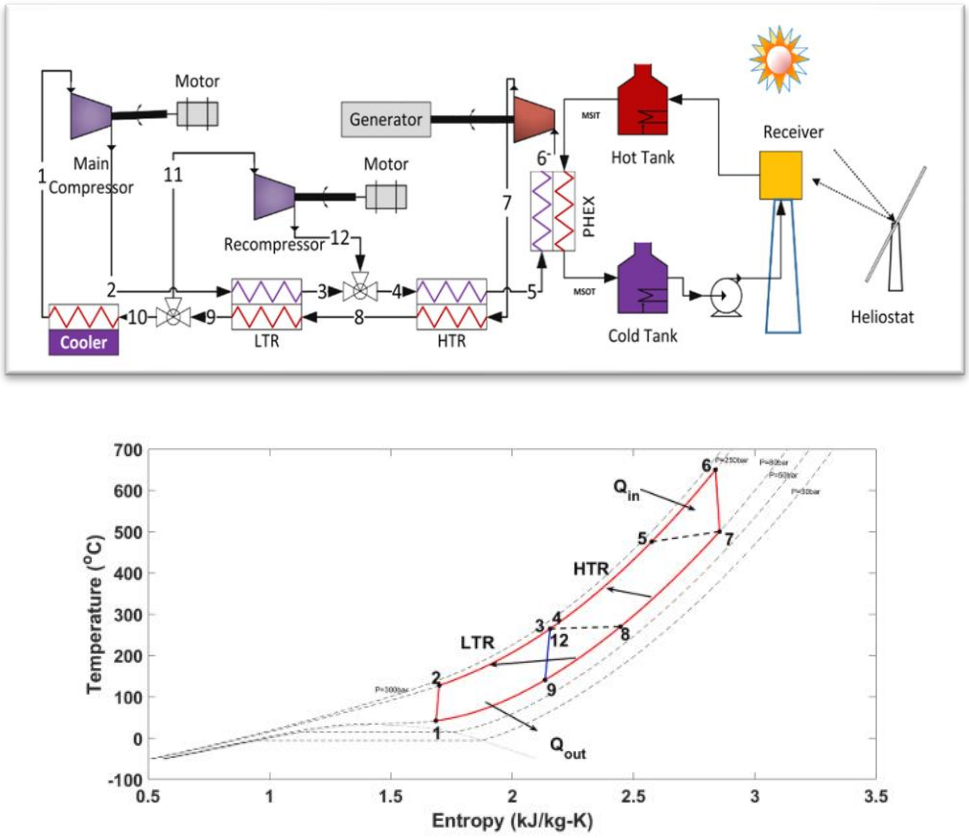

Figure 14. Thanganadar proposed partial cooling cycle [41]

2.1.5 Precompression Cycle (PCC)

Precompression cycle basic concept is the $\mathbf{sCO_2}$ goes through a multi-compression phases which is usually needed to meet a desire working pressure. Sometimes one compressor will not be enough or the size the compressor required to meet the desired pressure will be extremely large in size and very difficult to transport, install and maintain, accordingly the precompression cycle layout is introduced to overcome this challenge. The main difference between this cycle layout and the Intercooling Cycle (Recompression Cycle) is that in the Intercooling Cycle (Recompression Cycle) the second (Auxiliary) compressor is integrated within the cycle after the main compressor linked with an intercooler in between, however, in the Precompression Cycle, the pre-compressor in integrated within the cycle in between

the recuperators and classically associated with a dedicated intercooler [35] as illustrated in Figure 15.

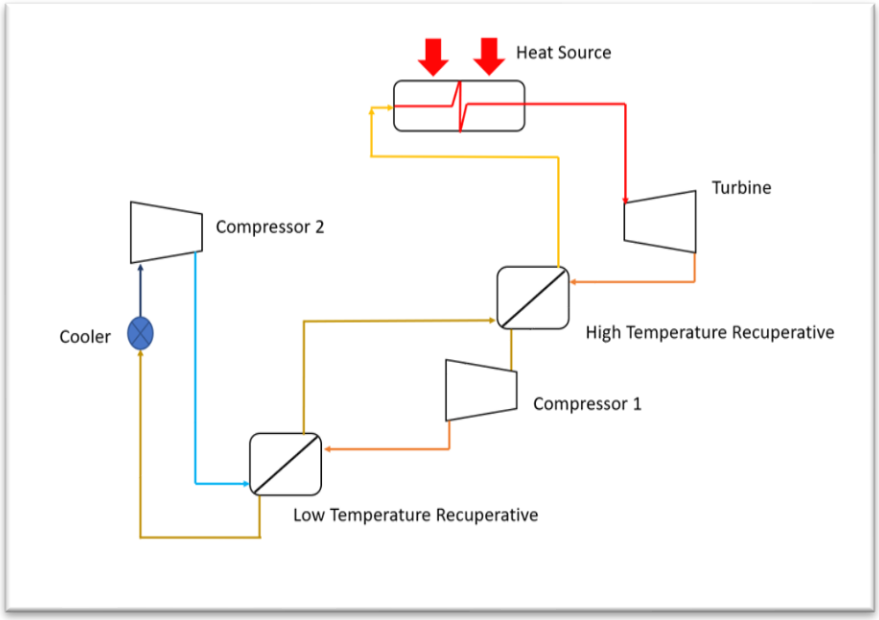

Figure 15. Precompression cycle configuration

In Wang's systematic comparison [35] between various $\mathbf{sCO_2}$ cycles configuration, it was confirmed that precompression cycle yields larger specific work in comparison to the recompression cycle. Another advantage of the precompression cycle layout is it reduces pinch-point taking place at the recuperative [42]. On key feature of the Precompression Cycle is relatively high main compressor inlet pressure coming via the Low Temperature Recuperator (LTR) with the help of the Pre-compressor component. One of the noted disadvantage of this cycle is the required equipment large size because there is no split flow and all the equipment handles all the mass flow rate available in the cycle [20]. The most common application of this cycle layout within the literature is in nuclear application [43] [38] and waste heat application [44].

2.1.6 Split Expansion Cycle (SEC)

This type of power cycle layout focuses on the splitting the flow after the addition of heat (via combustor, heater, waste heat, etc.) in two parallel streams toward a main and auxiliary turbine. The main steam passes the main turbine will complete a standard Brayton cycle where the stream will pass via an auxiliary turbine toward an ejector which will regulate the stream back toward the heater and back the turbines. The introduction of the ejector has been discussed thoroughly in Vasquez paper [45] where he proved its addition will significantly increases the thermal efficiency of the cycle. It worth noting that this type of cycle layouts was found in the literature integrated with single or multiple recuperators and combined with split-flow compression cycle (inter cooled and regular compression). The advantage behind the split-flow before compression (specially the intercooled) is to reduce the compression workload and eventually contribute to increased efficiency of the cycle.

2.1.7 Preheating Cycle (PHC)

This cycle emphasizes on preheating the $\mathbf{sCO_2}$ as a preparation for further heating process (via combustion or renewable source) for the purpose of minimizing the thermal load (and its associated cost) on the main heater by utilizing an alternative heating source which is usually cheaper but maybe instable, inconsistence, not reliable like renewable energies (without thermal storage) [19][46][47], waste heat [20][48][44], Geothermal [49][47][50], etc. A lot of researches are being conducted in this cycle configuration because of its cost competitiveness, reliability, and wider range of applications. Figure 16 illustrates a general preheating cycle configuration.

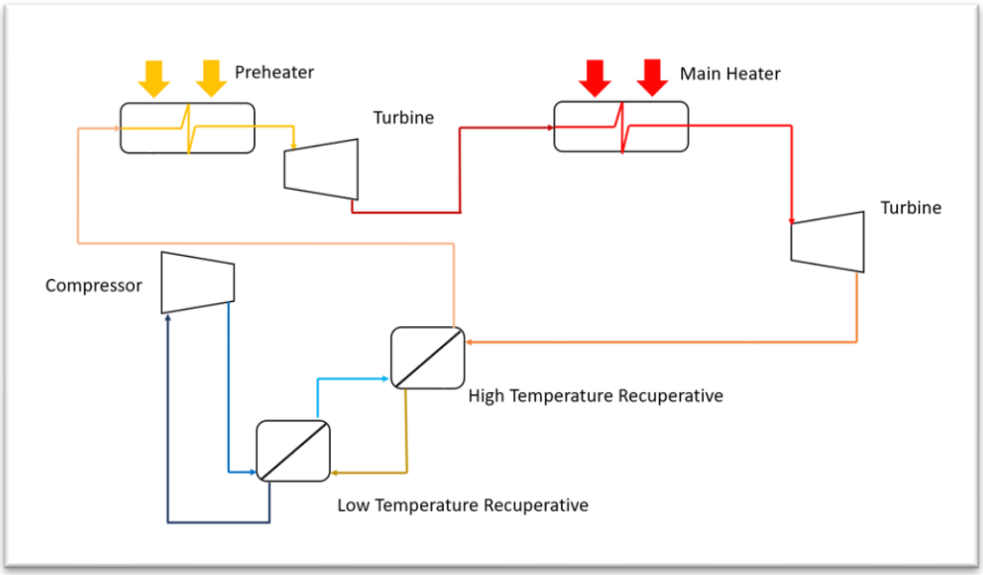

Figure 16. Preheating cycle configuration

After passes via the preheaters, the heated $\mathbf{sCO_2}$ proceed further with the expansion in the turbine and follow the ordinary $\mathbf{sCO_2}$ cycle process. This cycle configuration will be elaborated more in the coming sections as the investigated cycle configuration uses the CSP as pre-heater where the oxy combustor acts as the main heater. The main advantage of this cycle configuration is depends on dual heat sources in which if both sources are operational, the thermal load on main the heater is minimized to reduce its operating expenditures (like fuel consumption) and increase the efficiency of the cycle, on the other hand, during any interruption of the preheating source, the main heater will instantly kicks in to substitute the heat requirement.

2.2 Integration of sCO_2 power cycle with various Energy Sources

As the world is exploring alternative energy sources other than energy based on fossil fuels like renewable energy (solar and wind energies has achieved significant improvements in the past decades), the technology is still not mature enough due to the inconsistency of power supply where the development of energy storage technologies is not coping up with the development. Accordingly there is an acknowledgement from

the industrial community that a hybrid multi energy profile is best solution for now to overcome concerns over various energy sources limitation [51]. In this chapter, a review on the $\mathbf{sCO_2}$ power cycle with various renewable energy sources which includes Nuclear Energy, Solar Energy, Geothermal Energy, Waste Heat, Fuel Cell, Direct/Indirect Coal Combustion and Direct Oxy Fuel Combustion. Figure 17 is a graphical representation about the $\mathbf{sCO_2}$ power cycle energy sources, its temperature range and potential power generation.

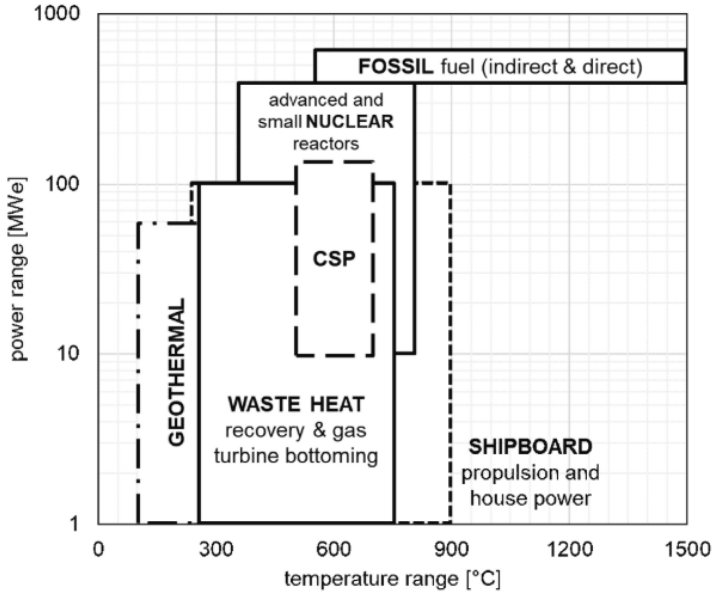

Figure 17. Power range versus temperature range for selected technologies [52]

2.2.1 sCO_2 power Cycle integration with Nuclear Energy

Initially the $\mathbf{sCO_2}$ was developed for nuclear applications [53] where the $\mathbf{sCO_2}$ is the working fluid and nuclear reactor is the heat source due it positive potential of thermal efficiency, low volume to power ratio, erosion free turbines and cavity free pumps [23]. Dostal [21] has carried a detailed study in utilizing the $\mathbf{sCO_2}$ in the nuclear application for the power industry and he concluded that the use of the $\mathbf{sCO_2}$ will

enhance the cycle thermal efficiency which reaches the range of 45.3% - 50% depending on the reactor operating temperature that ranges between 550°C and 650°C which was a very promising results at the time which was considered as the revival of the nuclear $\mathbf{sCO_2}$ research industry. Hoffman [54] was one the pioneers to develop a 150 KW $\mathbf{sCO_2}$ power cycle plant model in combination with helium cooled nuclear energy as an energy source. The authors justify the preference of $\mathbf{sCO_2}$ as a working fluid because of its good physical properties at the critical point, thermal stability, low corrosion levels, safe and its available abundance worldwide. The design plant operating temperature is 732°C and the pump inlet temperature is 66°C. The alternator shaft speed was configured at 40,000 rpm. The designed turbine inlet pressure is 11.4 Mpa and the turbine pressure ratio was set to 2.

Although the proposed cycle seemed operative and dependable, it needed continuous supply of very cold water (10°C - 15°C) to help condensing the $\mathbf{sCO_2}$ which was a major challenge to this proposed cycle. The authors believed although there were sufficient researches done in the $\mathbf{sCO_2}$ power cycles, it needed to be further expanded to reach to a level of maturity for further commercialization and some design improvement in the turbine sealants and bearings to avoid leakages during the expansion process. Ming [18] studied the use of $\mathbf{sCO_2}$ in nuclear applications, analyzed the applications of various $\mathbf{sCO_2}$ power cycle configuration and its advantages. It was noted that one of the $\mathbf{sCO_2}$ feature in such applications is the highly energy conversion and optimizable compressor work (using quasi-critical temperature). Driscoll [21] has concluded that the $\mathbf{sCO_2}$ power cycle becomes more efficient in comparison to the Ranking Cycle when the turbine inlet temperature exceeds the 550°C.

Ahn [55] has investigated various $\mathbf{sCO_2}$ cycles and it was concluded that the intercooling (recompression) cycle configuration achieve the highest efficiency for the

nuclear application. This conclusion was re-confirmed in another research [37], furthermore, it was highlighted that the relatively compact size the $\mathbf{sCO_2}$ power cycle is one of the major advantages of this cycle in comparison to the standard Ranking Cycle.

White [51] has reviewed the $\mathbf{sCO_2}$ power cycle various cycle configurations, components and applications. Regarding the Nuclear power, it was concluded that although the current $\mathbf{sCO_2}$ power cycle is proven to be a reliable and efficient power cycle specifically with the newly designed nuclear reactors that includes the integration of the $\mathbf{sCO_2}$, further development in this research area is progressing in considerably slow pace trying to overcome the challenges of high cost and safety concerns regarding the plants operation and the nuclear waste.

2.2.2 sCO_2 power cycle integration with solar energy

Significant researches were carried out in the field of $\mathbf{sCO_2}$ power cycle integrated with Solar powers for the use of power generation. This combination sometimes is presented integrated with a more consistent heat source which work in sequence (or in parallel) to the solar energy to overcome the solar power inconsistency. Such primary heat sources with integration potential with Solar Energy usually are heaters, combustors, coals furnace, nuclear power etc. The integration with the Combustor (specifically oxy combustor) is being discussed in-depth below in a separate chapter as this is directly related to the proposed cycles. On the other hand, Solar Power in general are sub-categorized into Photovoltaic (PV) and Concentrated Solar Power (CSP) [56]. Usually Concentrated Solar Power (CSP) are related to bigger system capacity requirement, higher investment cost, higher efficiency and based of the Direct Normal Irradiance (DNI) [57][58]. There are various CSP techniques to capture the Solar heat which are as Parabolic Dish, Parabolic Trough, Linear Fresnel and Solar

Power Tower [1]. The Solar Power has gained a lot of interest to its high potential in combination with $\mathbf{sCO_2}$ and its high efficiency specially in Arid climate [11]. As the thesis proposed cycle is power tower cycle, a dedicated chapter is allocated for the $\mathbf{sCO_2}$ integrated with Solar Power Tower. An overview of all the scientific published works about the $\mathbf{sCO_2}$ power cycle integrated with CSP cycle (Excluding Power Tower as it will be discussed separately) will be presented in this section.

Bennett [59] investigated the application of $\mathbf{sCO_2}$ power cycle integrated with Photovoltaic panels for the purpose of balancing power load. Figure 18 represents is a schematic of the model discussed above.

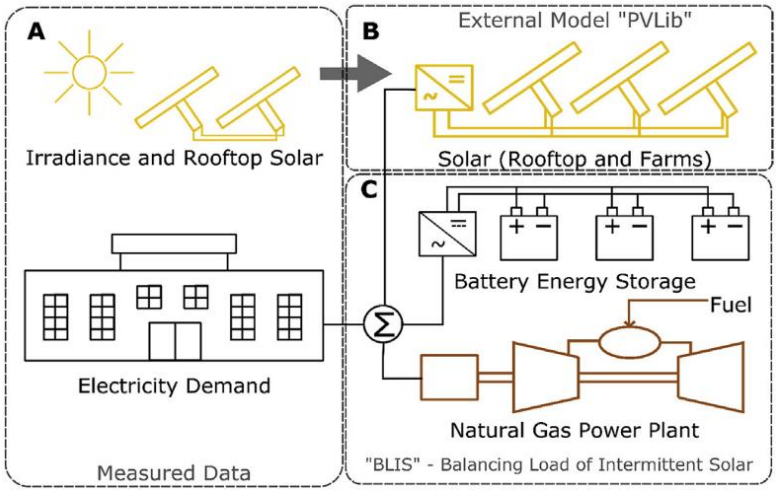

Figure 18. $\mathbf{sCO_2}$ power cycle combined with PV system [59]

A mathematical model was developed manage the demand load the power from the 3 sources of electricity (PV panels directly, Batteries and Natural Gas power plants) according to previously set algorithm. Levelized Cost of Electricity (LCOE) was calculated and found that it is at least 0.005$/kWh less expensive compared to the open cycle turbine. The proposed system was proven to be functional, cost efficient and solving the intermittency of the power generated from the Photovoltaics.

Khan [60] has researched the performance of the $\mathbf{sCO_2}$ integrated with Solar Dish for the power generation purposes using the nanofluid as heating medium. The $\mathbf{sCO_2}$ power cycle investigated is the re-compression combined with reheating cycle. The effect the ambient temperature, wind velocity, mass flow rate, receiver temperature, pressure ratios, nano-partials and other factors were considered as a part of this research. It was concluded that $\boldsymbol{Al_2O_3}$ (thermaloil nano-fluid) is the most suitable medium for this application where is reach a first law efficiency of 33.73%. Figure 19 represents the cycle diagram.

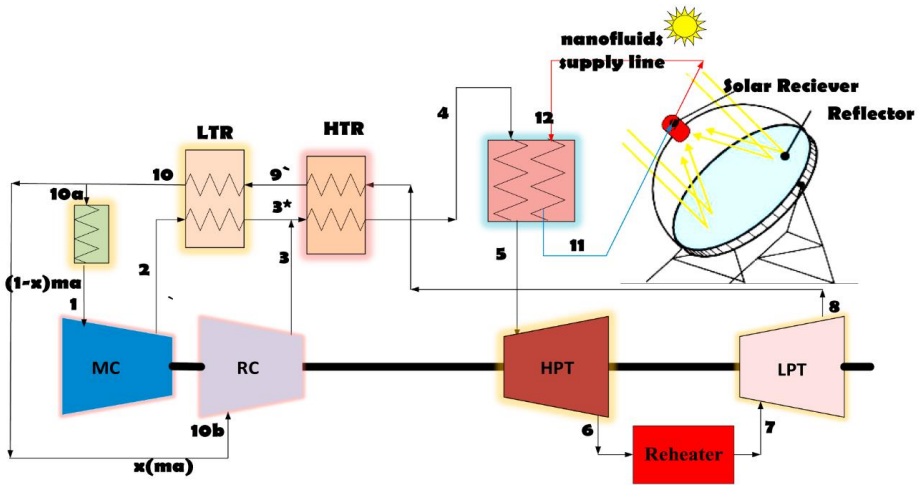

Figure 19. The power cycle investigated by [60]

Another CSP technology that is a very promising is the Linear Fresnel technology, there are power plants that is currently in operation [61][62] and some are under construction [63] and others are under design and study [64] [65] [66] which confirms the great potential of this technology specially in the region of Middle East, North Africa and Southern Europe.

Muñoz-Antón [67] published a paper elaborating more about the integration of the $\mathbf{CO_2}$ with Linear Fresnel CSP technology with the potential of using a gas cooled

linear receiver in reference to the Plataforma Solar de Almeria (PSA) plant. The paper presented a very interesting results in terms of thermal efficiency of the system, however, further study needs to be elaborated in terms of modification associated cost.

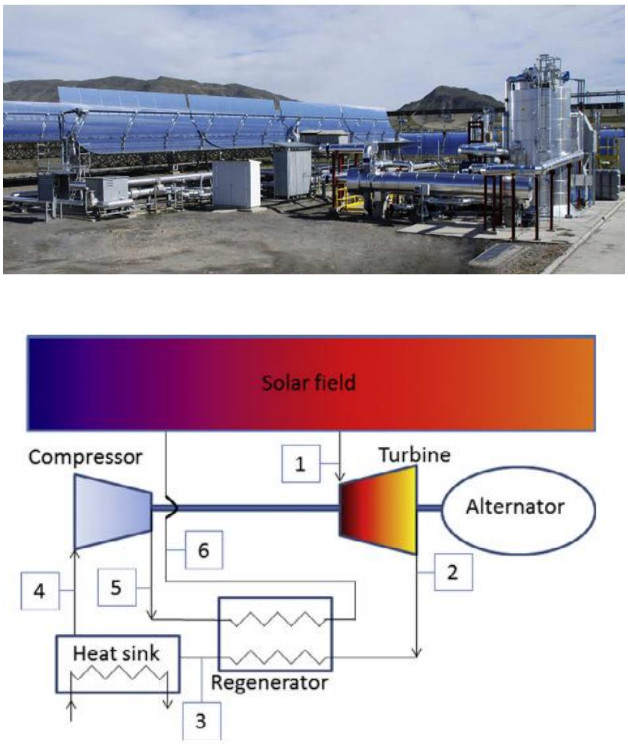

Figure 20. PSA plant overview and Brayton cyle in operation [67]

It is worth noting that a recent research [68] investigated the performance of using a pure $\mathbf{sCO_2}$ in comparison to the $\mathbf{sCO_2}$ combined with He, Kr, $\mathbf{H_2S}$, $\mathbf{CH_4}$, $\mathbf{C_2H_6}$, $\mathbf{C_3H_8}$, $\mathbf{C_4H_8}$, $\mathbf{C_4H_{10}}$, $\mathbf{C_5H_{10}}$, $\mathbf{C_5H_{12}}$, $\mathbf{C_6H_6}$ in a plant operation of 50 MW. The binary mixtures were classified into two groups based on: mixture ability to reduce the critical temperature (Group A: $\mathbf{sCO_2}$/He, $\mathbf{sCO_2}$/Kr, $\mathbf{sCO_2/CH_4}$, and $\mathbf{sCO_2/C_2H_6}$) and its ability to increase the critical temperature (Group B: $\mathbf{sCO_2/H_2S}$, $\mathbf{sCO_2/C_3H_8}$, $\mathbf{sCO_2/C_4H_{10}}$, $\mathbf{sCO_2/C_5H_{10}}$, $\mathbf{sCO_2/C_5H_{12}}$, $\mathbf{sCO_2/C_4H_8}$ and $\mathbf{sCO_2/C_6H_6}$). It was resulted that mixture group A contributes to the enhancement of the plant efficiency with around 3-4% in

comparison to the pure $\mathbf{sCO_2}$ power cycle. The best mixtures found were $\mathbf{sCO_2}$/He (90%/10%), $\boldsymbol{sCO_2}$/Kr (68% / 32%). This research extends another research which might contribute the further development of $\mathbf{sCO_2}$ power cycle integrated with solar energy.

2.2.3 sCO_2 power Cycle integration with Geothermal Energy

Wang [69] carried out an extensive investigation about the use of $\mathbf{sCO_2}$ power cycles integrated with geothermal energy. He investigated various $\mathbf{sCO_2}$ power cycle's configuration utilizing the geothermal energy via a thermodynamic model referring baseline parameters available in the literature like the geothermal heat, pressure drops due to separator. Figure 21 illustrates the use of the geothermal energy and the mechanism of heat transfer.

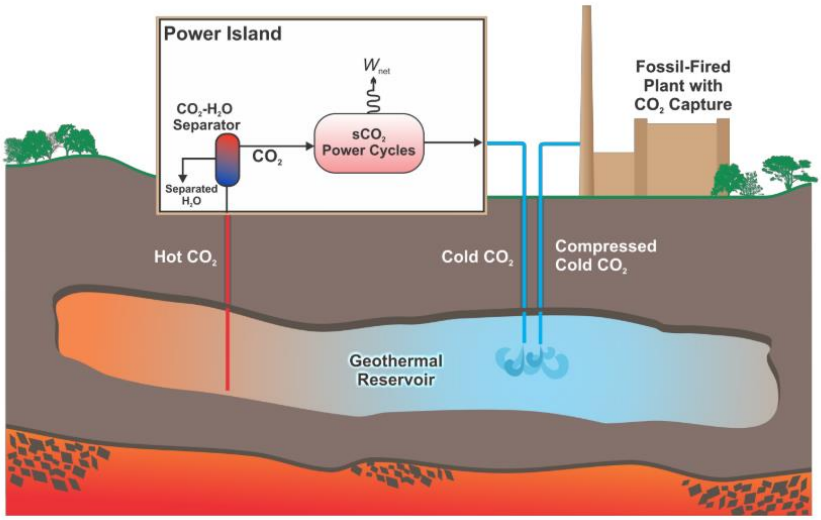

Figure 21. $\mathbf{sCO_2}$ power cycle integrated with Geothermal [69]

The assessment was carried out in various $\mathbf{sCO_2}$ configuration cycle and promising results were found as presented in the Table 1 below which concludes that the pre-compression, inter-cooling and reheat are obviously the most suitable option

for such application and further processing.

Table 1. $\mathbf{sCO_2}$ power cycle integrated with Geothermal Energy [69]

$\mathbf{sCO_2}$ Cycle Configuration	Net Power [MWe]	m'_{CO2} [kg/s]	Thermal Efficiency [%]	Exergy Efficiency [%]	Specific Power [kWe/kg.s]
Simply $\mathbf{sCO_2}$	2.785	87.58	13.92 – 9.52	40.71 – 53.47	31.49
Recuperative	2.584	90.26	8.92 – 14.64	38.14 – 53.75	28.63
Pre-compression and Inter-Cooling	3.194	90.44	11.02 – 13.28	47.15 – 56.32	35.32
Reheating	5.970	90.00	10.30 – 19.28	N.A.	66.34
Pre-compression, Inter-cooling and Reheat	6.904	90.00	11.91 – 18.76	N.A.	76.71

Figure 22 represents the system schematic about the selected Pre-Compression, Inter-cooling and Reheat cycle. The $\mathbf{sCO_2}$ Pre-Compression, Inter-cooling and Reheat cycle was further investigated as presented in the Table 2.

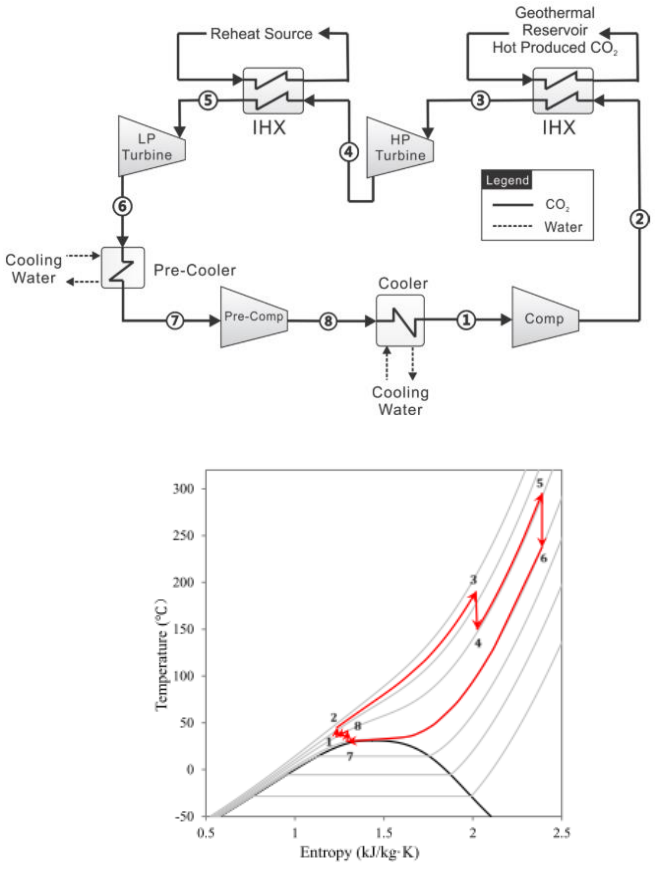

Figure 22. $\mathbf{sCO_2}$ pre-compression, inter-cooling and reheat cycle [69]

Table 2. Selected $\mathbf{sCO_2}$ power cycle detailed analysis

Case with Optimization	Net Power [MWe]	$\boldsymbol{m'_{CO2}}$ [kg/s]	Thermal Efficiency [%]	Exergy Efficiency [%]	Specific Power [kWe/kg.s]
Direct Expansion	4.226	90	14.58	62.37	46.95
Pre-Compression and Inter-cooling	3.194	90.44	11.02	47.15	35.32
Transcritical $\mathbf{sCO_2}$ Cycle	3.922	88.34	13.53	57.89	44.38

In [70], the use of geothermal reservoirs was investigated for the power generation using $\mathbf{CO_2}$. The concept behind this technology is to utilize the geothermal properties were the recycled (and captured) $\mathbf{CO_2}$ gets compressed to the underground reservoir in which it gets heated and utilized (with the help of water separator) to heat a an organic fluids to turn the turbine and generator power. The potential of using geothermal power to heat the $\mathbf{CO_2}$ has been investigated with the help of a dynamic thermodynamic model. It was noted that the extracted $\mathbf{sCO_2}$ temperature was 195°C. Although this is not direct application of the $\mathbf{sCO_2}$, it is related to the application and further studies can be developed depending on those findings to directly utilize the $\mathbf{sCO_2}$ for the power generation will be major breakthrough [70].

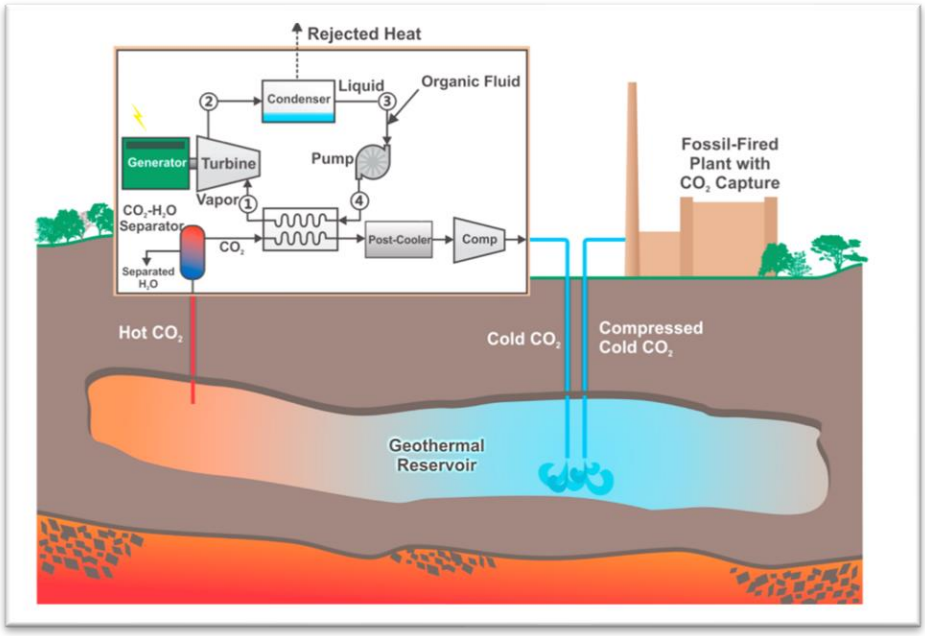

Figure 23. $\mathbf{sCO_2}$ geothermal reservoir [70]

Qiao [47] studied a novel hydrocyclone separator as a continuation to the work done by Wang [70]. A double-inlet conical hydro-cyclone was numerically investigated using Reynolds Stress Model (RSM) and Discrete Particle Model (DPM) to analysis the flow behavior (inlet, velocity, droplet size and water mass fraction and split ratio). The research concluded that the proposed separator is functional and contribute to enhancement of the cycle efficiency.

2.2.4 sCO_2 power cycle integration with waste heat energy

Utilizing nearby waste heat is the optimum scenario where the targeted heat is considered waste and thus free to be used. However, in real life applications, sometimes the physical location of high power demand doesn't have nearby waste heat resource, characteristic of waste heat source and managing power demands in line with the available waste [71]. Under this section, a review of the $\mathbf{sCO_2}$ combined with Waste Heat Recovery applications. Manente [72] has investigated the $\mathbf{sCO_2}$ application integrated with waste heat recovery application aiming maximizing the total heat

recovery efficiency in addition to the thermal efficiency and power outlet. A comparison study was carried between the traditional $\mathbf{sCO_2}$ power cycle layouts (Single Recuperative Cycle) and compared to the novel $\mathbf{sCO_2}$ power cycles (Single flow with split dual expansion and double flow split with dual expansion) was proposed as a part of this work as shown in Figure 24. The main difference between those further studied $\mathbf{sCO_2}$ cycles for the heat recovery applications and ordinary $\mathbf{sCO_2}$ power cycle is that the compressed $\mathbf{sCO_2}$ gets compressed directly to the turbine (or heater/recuperator) which make a better use if the heat used contributing to a better cycle thermal efficiency.

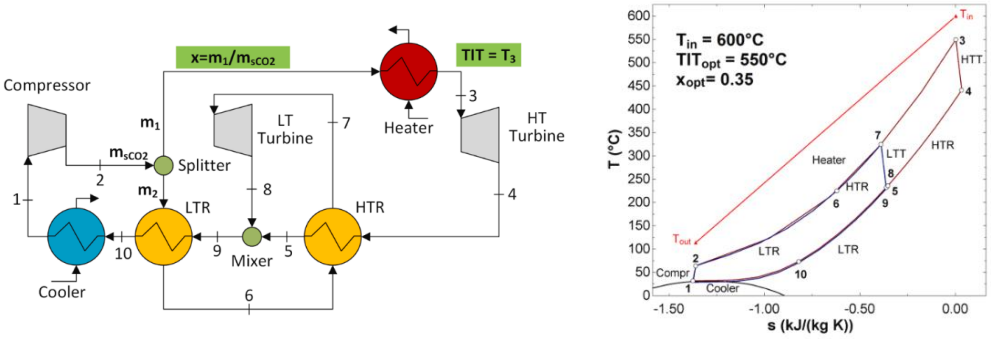

(a) Single flow with split dual expansion $\mathbf{sCO_2}$ power cycle.

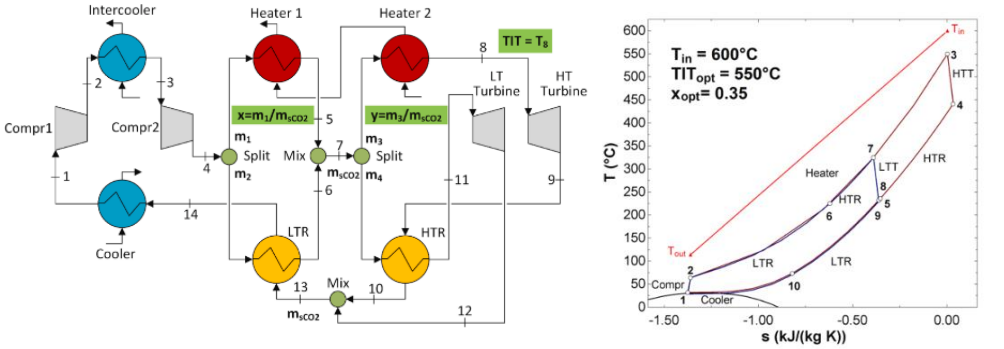

(b) Double flow split with dual expansion $\mathbf{sCO_2}$ power cycle.

Figure 24. Investigated $\mathbf{sCO_2}$ power cycle [72]

The $\mathbf{sCO_2}$ power cycle investigation was carried out on the four cycles considering a waste heat temperature ranges between 400°C to 800°C where it was proven that the double flow split with dual expansion achieve the higher efficiency

and is the most suitable $\mathbf{sCO_2}$ waste heat recovery application. The Exergy model done of the three models confirmed the same results where the least exergy losses was noted in the dual flow split with dual expansion cycle layout with its recuperators accounts of the most recorded exergy loss of 2227.6 kW as shown in Figure 25. Figure 26 presents the illustrates the exergy loss (in kW) at main cycle component across all three investigated cycle configurations.

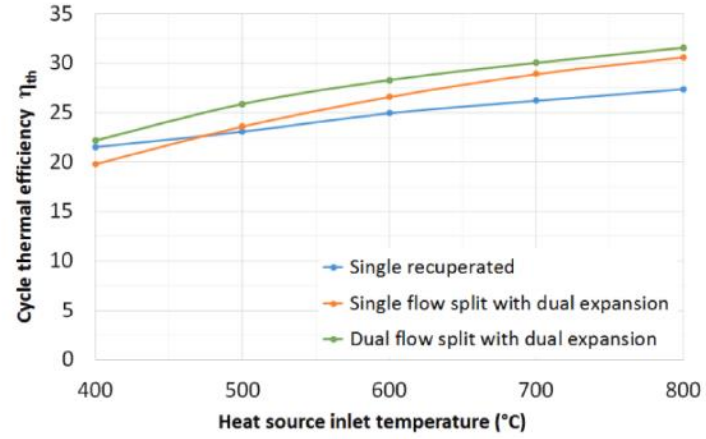

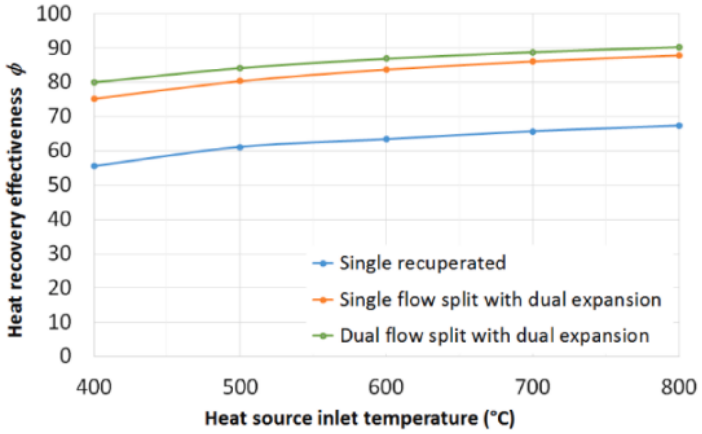

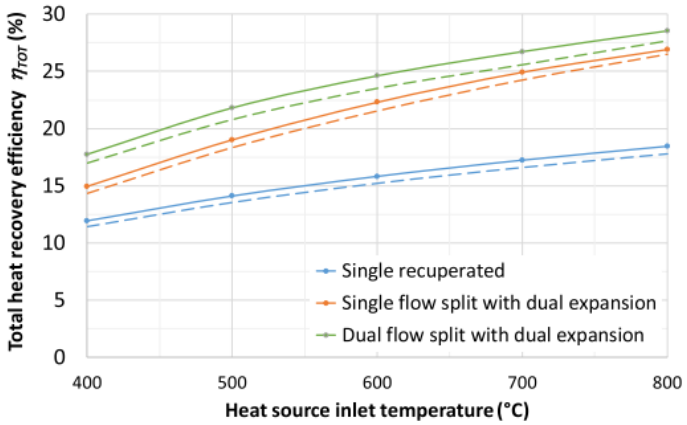

Figure 25. Comparitive results of the 3 investigated $\mathbf{sCO_2}$ power cycles [72]

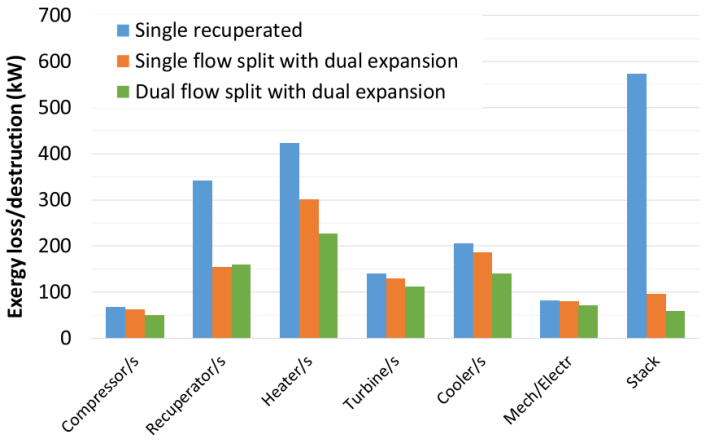

Figure 26. $\mathbf{sCO_2}$. power cycle configurations exergy loss per cycle component [72]

It is worth noting that another analysis [73] as a continuation to [72] research was done comparing the single flow split with dual expansion cycle configuration in comparison to the partial heating and dual recuperated cycle configurations and it was confirmed that the single flow split with dual expansion found to be more efficient in comparison to the other standard $\mathbf{sCO_2}$ power cycle. Elson [50] has published another interesting research in the area of $\mathbf{sCO_2}$ for a waste heat power cycle application where the $\mathbf{sCO_2}$ power cycle advantages were highlighted against the standard

Ranking Cycle with being low cost, non-toxic, non-flammable working fluid ($\mathbf{sCO_2}$), smaller size component foot prints and size (due its high fluid density) and the ability to place the exhaust heat exchanger directly with the waste heat source due to technical challenges like inflammability, thermal stability and the physical properties of the $\mathbf{sCO_2}$.

2.2.5 sCO_2 power Cycle integration with fuel cell

Very interesting paper [74] elaborated more into integrating a $\mathbf{sCO_2}$power cycle with a SOFC. This hybrid system works by using fuel (Methane) to heat the SOFC to generate electrical power and abundance of heat that gets transferred to the $\mathbf{sCO_2}$ Brayton cycle in order to turn the turbine and generate more of electrical power. The excessive heat of this process gets recirculated back to the reformer to contribute to lesser fuel consumption by a reheating process.

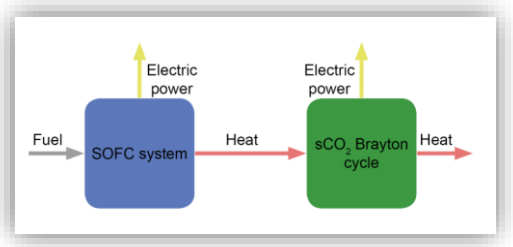

Figure 27. Integrating $\mathbf{sCO_2}$ with SOFC [74]

Various cycle combinations (15 cycles combinations) were studied (Recompression, Cathode recirculation, heat recovery steam, etc) and it was resulted that the Recompression cycle + Cathode Recirculation is most efficient cycle with the thermodynamic analysis (energy/exergy analysis) of this hybrid system has shown an LVH efficiency of 66.58%. Figure 28 represents the proposed system schematic.

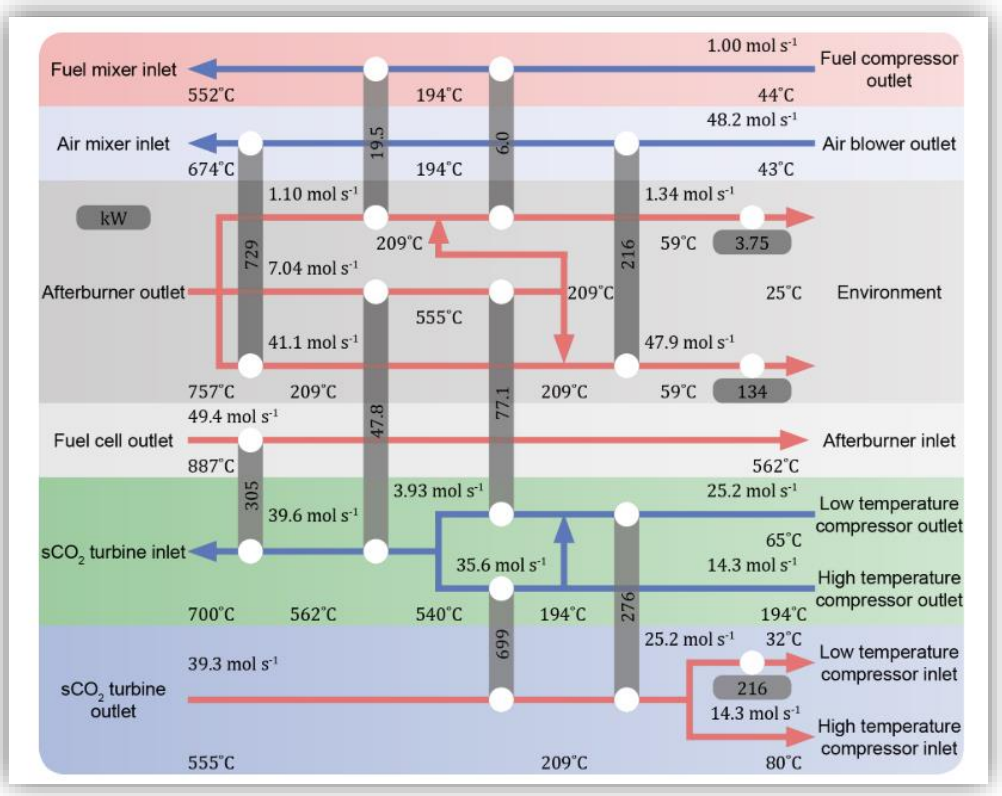

Figure 28. Recompression cycle + cathode recirculation cycle [74]

Another paper [75] investigated the integration of the $\mathbf{sCO_2}$ with SOFC in which an external heat source is used to heat the SOFC in which it produces electricity and the excessive heat is used via a recuperator to heat the $\mathbf{sCO_2}$ power cycle. It concluded that the combination between both systems resulted in a higher cycle's efficiency. It was also concluded that maximum power output also largely depends on the heat transfer coefficient between SOFC and Brayton cycle heat engine.

2.2.6 sCO_2 power Cycle integration with Direct/Indirect Coal Combustion

Although using coal for the energy production is not a sustainable option for power generation, however, it is the most cheaper technology for electricity generation and accordingly the majority of the electricity is being produced using coal despite international efforts to limit the carbon dioxide emission to the atmosphere.

Accordingly, this section elaborates more in utilizing $\mathbf{sCO_2}$ power cycle for the electricity production using coal fired heat. Liu [76] has presented the effectiveness of such combinations in various power plants capacities (ranges from 50 – 1000 MW). It was concluded that such model would be applicable for plant size of 1000 MW to allow enough $\mathbf{sCO_2}$ to heat which achieve a thermal efficiency of 50.46%.

2.3 sCO_2 power cycle integrated with CSP (Solar Power Tower)

As the renewables (in general) experienced major development in the recent years with the help of the technological advancement, which led to growing interest and further researches were done related to power generation industries. White [51] highlighted that the CSP installation around the world has increased 5 times the capacity back in 2010 and LCOE has decreased from 0.346 $/kWh to 0.182 $/kWh [77]. Although the CSP LCOE has noticeably decreased with around 50% of its price 10 years ago, it is still not financially attractive in comparison to other renewable technologies like Photovoltaic panel for example in which its LCOE is only 0.068 $/kWh. Researcher are working to reduce the CSP LCOE for further commercialization by targeting the major cost element of this system (Solar Collectors) which accounts for almost 40% of the system [78]. In addition, the use of $\mathbf{sCO_2}$ as a working fluid contribute the system cost reduction since equipment size gets reduced, smaller plants foot prints and lower operation and maintenance costs which contributes to lower LCOE [79].

Neises [80] has published a paper exploring the $\mathbf{sCO_2}$ power cycle options to reduce the LCOE when integrated with solar power tower operating at 650°C using molten salt thermal storage. It was noted that the partial intercooling cycle configuration has the lowest LCOE driven by relatively cheaper thermal storage due to the larger temperature difference, lower thermal loss and lesser HTF pump electricity

consumption due smaller HTF mass flow rate.

Allison [81] investigated the $\mathbf{sCO_2}$ power cycle integrated with CSP in a commercial scale via Sunshot program and it achieved an high potential results with a LCOE of 0.06 $/kWh, thermal efficiency of 50%, plant capacity 1 MW powered by a turbine inlet temperature is 750°C and pressure is 250 bar [82].

An investigation research was carried out by Wang [35] on the effect of various Brayton Cycle's layout (simple recuperation cycle, recompression cycle, pre-compression cycle, inter-cooling cycle and partial-cooling cycle) in combination with Concentrated Solar Power. The team proposed using a combination between Molten Salt (60 wt% of $\boldsymbol{N_aNO_3}$ and 40wt% of $\boldsymbol{KNO_3}$) loop and Carbon Dioxide as a medium of transferring the heat as shown in Figure 29.

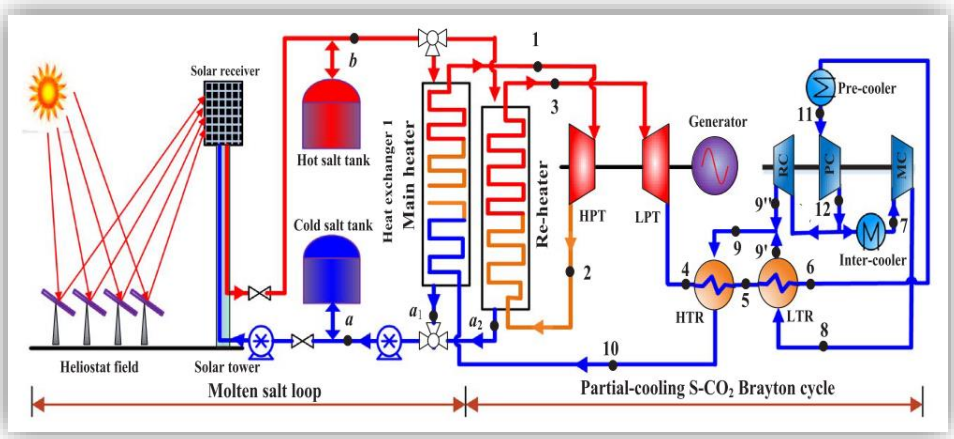

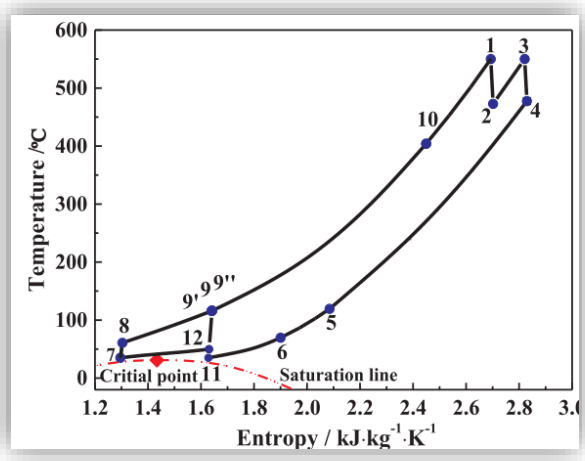

Figure 29. Partial-cooling with re-heating cycle layout and its TS diagram [35]

All 5 different layouts were analyzed thermodynamically, and it was concluded that the inter-cooling and partial cooling with re-heating cycle are the most efficient layout across other cycle's studied. It was noted that the partial cooling cycle achieves the highest efficiency in the range of specific works between 160 kw/kg to 190 kw/kg in which the efficiencies ranges between 27% to 32%.In addition, it was also noted that the inter-cooling cycle yields the maximum efficiency with the specific work ranges between 140 kw/kg to 170 kw/kg in which the efficiency ranges between 29% to 31%. [35].

Another research was carried out [33] to investigate the application of Supercritical Carbon Dioxide integrated with CSP with two different scenarios which are as follow:

- Standard Power Tower CSP plant with simple regenerative $\mathbf{sCO_2}$ cycle.

  This is one of the simplest applications of CSP and $\mathbf{sCO_2}$ cycle, it basically relays on the absorbed heat via the Heliostats at the Solar Tower and transmitted to the working gas ($\mathbf{sCO_2}$) via the PHE to increase its temperature as a preparation for the expansion process at the turbine.

- Multi-heating

  This proposed layout is slightly different from the simple layout above with the addition of an auxiliary absorber and heat exchanger to contribute in the pre-heating process and ultimately enhance the efficiency of the system. Figure 30 illustrates the graphical representation about the cycle.

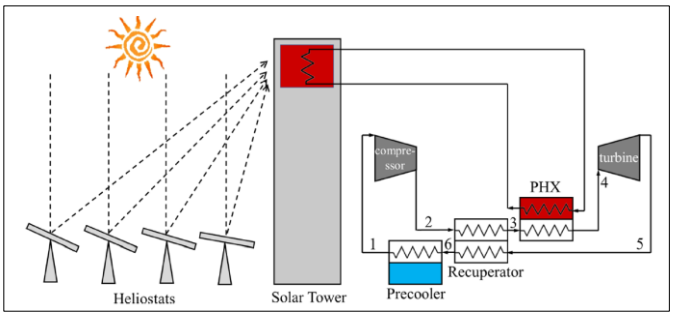

(a) Simple regenerative $\mathbf{sCO_2}$ cycle

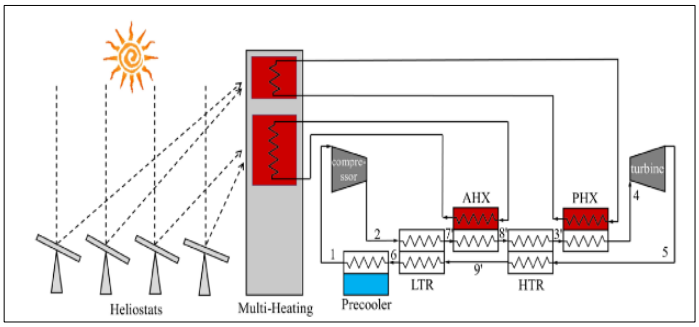

(b) Multi-heating $\mathbf{sCO_2}$ cycle

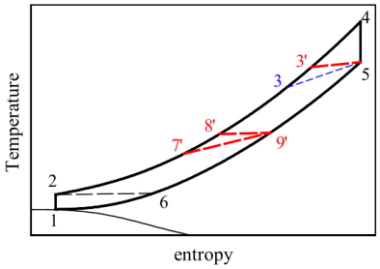

(c) TS diagram where the simple regenerative s$\mathbf{CO_2}$ cycle presented in black and blue, the multi-heating s$\mathbf{CO_2}$ cycle is presented in black and red.

Figure 30. Simple regenerative Vs. multi-heating $\mathbf{sCO_2}$ cycle [33]

In this paper a molten salt has been used for the power tower cycle and the $\mathbf{sCO_2}$ was used for the compressions/expansion cycle. Coating used for the power tower was Pyromark for the primary heat exchanger part and Cermet for the auxiliary part. As a part of this research paper, the relationship between the Tmax, Heat flux and the receiver efficiencies were studied. It was noted that the higher the temperature, the receiver efficiency decreases, the author claims that this information has been verified using SAM and EES and accordingly the auxiliary heat exchanger part was dedicated to the low temperature. [33]

It was concluded that the multi-heating cycle is more efficient in comparison to the standard CSP tower specially when it comes to the Turbine Inlet Temperature and the Compressor Inlet Temperature as shown in the graph represented in Figure 31.

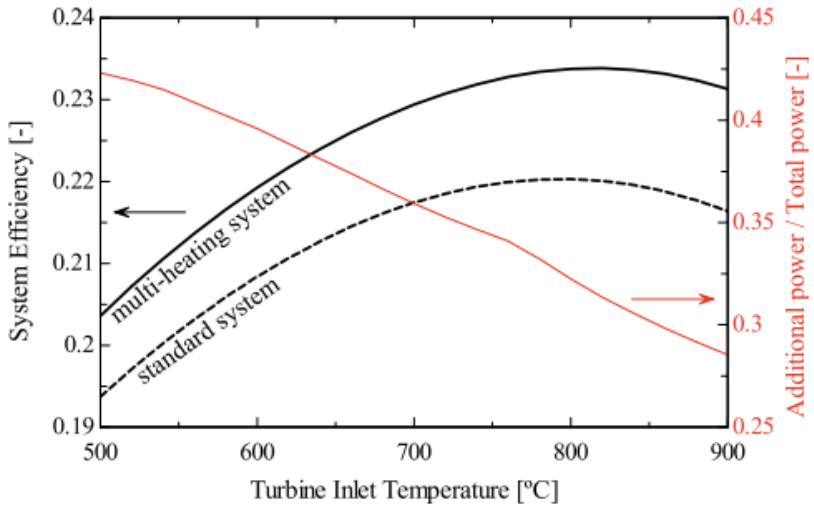

Figure 31. Turbine inlet temperature vs systems efficiency [33]

Binotti [83] has published a research on the assessment of $\mathbf{sCO_2}$ cycle integrated with Concentrated Solar Power [83]. Based on his assessment, it was confirmed that the Power Tower is most promising Concentrated Solar Power technology in terms of

efficiency and potential to reduce the Levelized Cost Of Electricity (LCOE) due the high potential concentration ratio (between 500 to 2000). It was noted that around 430 MW of electricity is currently being generated in the US and Spain using CSP - Power Tower Technology while another 430 MW capacity of power plants are currently under construction in China, US, Chile and South Africa and other 1500 MW capacity of power plants are under planning phase. [83].

In this research paper, it was noted that the two main challenges with integrating $\mathbf{sCO_2}$ cycle with CSP (PT) are the heat exchanger design and material selections and the high pressure at the receive. To overcome the challenges above, the heat exchanger design was considering the implementation of protective barrier with stable oxides (like chrome, nickel, alumina) specially at the $\mathbf{sCO_2}$ cycle to enhance the resistance to the high temperature corrosion. The high-pressure cycle challenge was attended by using indirect configuration using a suitable fluid (HTF) which gives a better control of the fluid dynamics at the severe transient conditions.

Binotti [83] has studied three alternative $\mathbf{sCO_2}$ integrated with CSP (PT) plants layout and analyzed each layouts advantages, dis-advantages and efficiencies of each scenario. These alternative system's layouts were analyzed by Marco and his team and they are a Recompression Cycle (RR), Partial Cooling Cycle (PI) and Recompression Main Compressor Intercooling (RMCI) layouts. The below thermodynamic model was used for the purpose of this study in which it was referenced to Gem solar plant (Operating Temp. 290°C – 565°C) available details which seems in acceptable range and matching the available information within literature. Equation (1) represents the thermodynamic model followed by Binotti and his team [83].

$$\boldsymbol{m_{HTF}}, \boldsymbol{c_{P,HTF}}, \boldsymbol{T_{HTF\,(in)}} + \boldsymbol{Q_{abs,t}} = \boldsymbol{m_{HTF}}, \boldsymbol{c_{P,HTF}}, \boldsymbol{T_{HTF\,(out)}} + \boldsymbol{Q_{cl,t}}(\boldsymbol{Tw}) + \boldsymbol{Q_{rad,t}}(\boldsymbol{Tw}) \quad (1)$$

It was calculated in [83] that the maximum net electrical power is being generated via the RMCI model with a TIT of 750°C is found to be equal to 24.7 MW. Table 3 represents the operational data of all 3 investigated models (PC, RR and RMCI) at their maximum efficiency as presented in paper [83].

Table 3. Tabulated Results for All Three Models.

Parameter Investigated	PC	RR	RMCI
Optimum TIT (°C)	780	740	750
Minimum cycle pressure (bar) at optimum TIT	5.23	9.37	7.06
RPR at Optimum TIT	0.356	-	0.548
Available Solar Power (MW)	282.8	282.8	282.8
Thermal Power at the Receiver (MW)	193.1	193.1	193.1
Thermal Power to the HTF (MW)	146.2	147.6	147.7
Receiver Thermal Losses (MW)	46.9	45.5	45.4
Thermal Power to Power Block, SM=1 (MW)	52.2	52.7	52.8
Power Block Gross Power Output, SM=1 (MW)	25.42	24.73	25.62
Auxiliaries Consumptions, SM=1 (MW)	0.74	0.92	0.83
Net Power Output, SM= 1 (MW)	24.68	23.81	24.78

Sensitivity analysis was performed to identify the critical assumptions made within this model and its impact to the results and it was resulted that the High Temperature Regenerator (HTR) effectiveness and the effect of an increase of the receiver efficiency. It was noted that a noticeable impact is reflected when HTR effectiveness is changed to ε_{HTR} equals 98% and ε_{HTR} 90% at the other scenario (originally it was assumed to be at 95%). The reflect of the effectiveness to the overall systems generated power and efficiencies is represented in Figure 32.

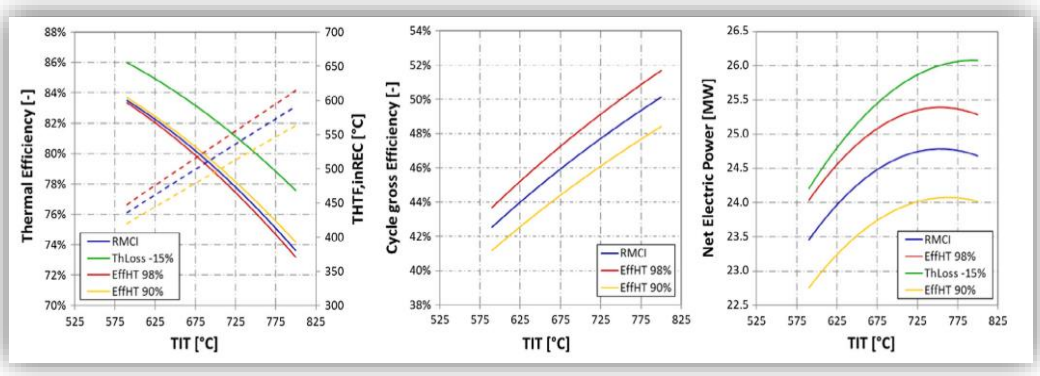

Figure 32. Reciever efficiency (Left), cycle Gross efficiency (Center) and net power for all the three HTR effectivness [83]

In a research paper published by Ma [84], the superstructure design of the $\mathbf{sCO_2}$ cycles was carried out. Various system combinations were found in the literature at both the hot and cold sides of the cycle (Hot Side: from the CSP/Thermal Energy Storage side toward the turbine. Cold Side: from the Recuperator and back to it via the compressor). Those combinations were presented and the systems efficiencies and the temperature difference against the pressure ratios calculations were demonstrated. The conducted study resulted that the presented four cycle combinations below are the most optimized and efficient power cycle [84] as follow:

1- MCIC-S: Main Compressor Inter-Cooler – Simple.

2- PC-S: Pre-Cooling – Simple.

3- MCIC-IS: Main Compressor Inter-Cooler – In Series.

4- PC- IS: Pre-Cooling – In Series.

Sensitivity analysis was carried out as a part of this research investigation the effect of Maximum Pressure and the calculated Levelized Cost Of Electricity per kWh combined with four different operating temperatures as follow:

Case 1: $\boldsymbol{T_{max}}$ = 550°C $\boldsymbol{T_{min}}$ = 35°C

Case 2: $\mathbf{T_{max}}$ = 550°C $\mathbf{T_{min}}$ = 55°C

Case 3: $\mathbf{T_{max}}$ = 700°C $\mathbf{T_{min}}$ = 35°C

Case 4: $\mathbf{T_{max}}$ = 700°C $\mathbf{T_{min}}$ = 55°C

As a conclusion to this research, it was founded that the most optimal system's design for an operating condition of a Maximum Temperature not exceeding 600°C is the PC-S system as shown in Figure 33.

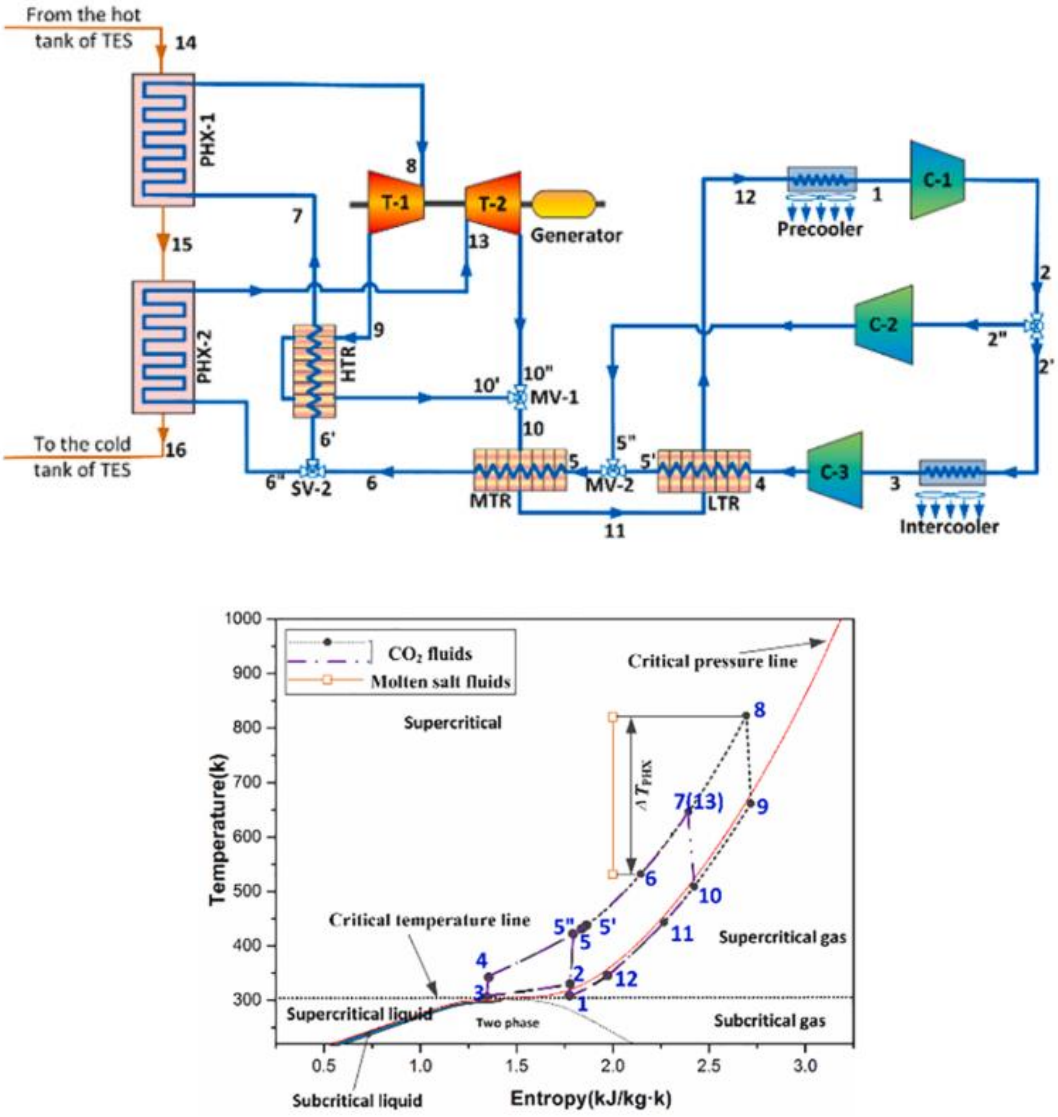

Figure 33. Most optimum design (PC-S) for T_{max} less than 600 °C [84]

On the other hand, it was found that for high operating Temperature ($\mathbf{T_{max}}$ = 700 °C) PC-S and MCIC-S system's combinations are the most optimum system's combinations depending on the actual minimum temperature. Niese and Turchi [40] have conducted a comparison study to evaluate various Carbon Dioxide power cycle configurations with an emphasis on CSP cycle that generate a total power output of 35 MW. They have emphasized on the advantages in using the s$\mathbf{CO_2}$ cycle by utilizing the high density near the critical point to minimize the compressor works and yield a potentially higher cycle efficiency compared to steam cycles. Also, other advantages were referred to in terms of the size and volume, thermal mass, and less complexity in comparison to the Rankine Cycle. The three studied cycle configurations are Simple Cycle, Recompression Cycle and Partial Cooling Cycle.

As a part of thermodynamic modeling of the different cycles, the recuperators effectiveness was used to calculate the thermal efficiencies of each cycle and optimize it against the total recuperators conductance as shown in Figure 34.

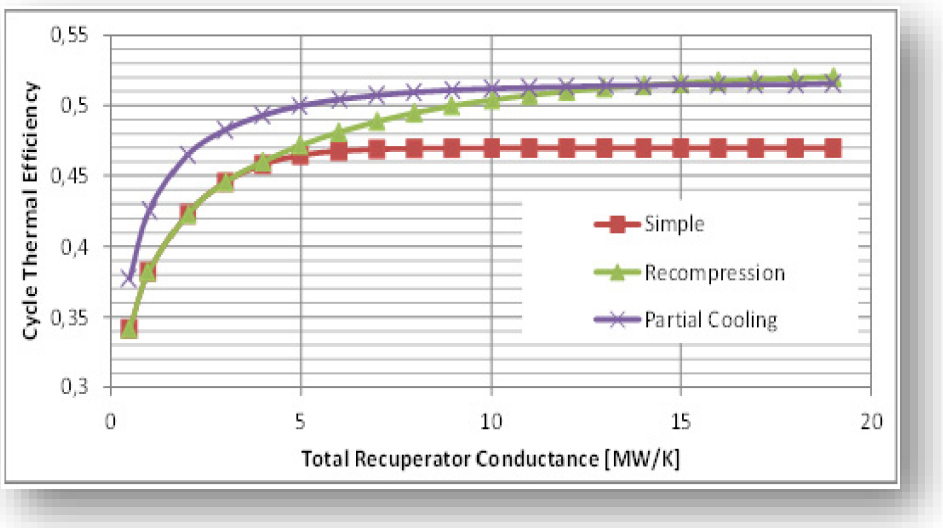

Figure 34. Cycle thermal efficiency vs. total recuperator conductance [13]

From the Figure 34 above it can be observed that the simple cycle efficiency is not increasing by increase of the recuperator's conductance. On the other hand, the higher the recuperators conductance the higher the efficiency gets specially when it exceeds 15 MW/K. Above results was confirmed and further design parameter was further elaborated in the paper published by Louis [85]. Figure 35 illustrates the T-S diagram of the recompression and partial cooling cycles which explains the thermodynamic behavior in each cycle.

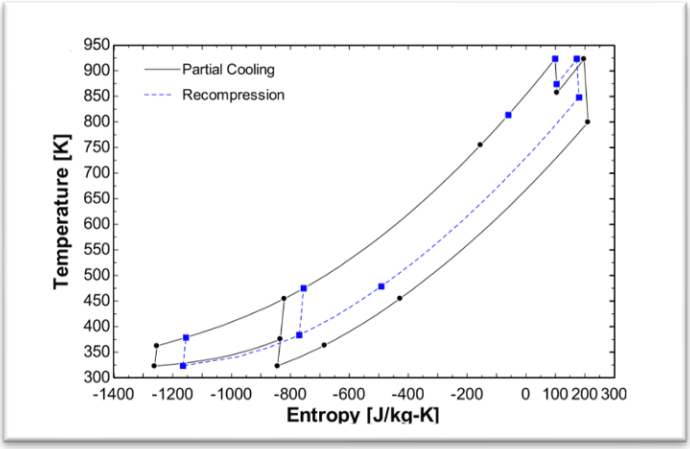

Figure 35. TS diagram of the partial cooling and recompression cycles [40]

As a conclusion, although the Partial Cooling and Recompression cycle configurations have performed equally under CSP relevant conditions when an effectiveness model was specified. However, when specifying a conductance model, it was resulted that the Partial Cooling cycle configuration slightly outperformed the recompression cycle configuration. It was noted that it is better to use the conductance model rather than effectiveness model considering the physical heat exchanger size. A key benefit of the Partial Cooling cycle configuration is the high temperature difference within the primary heat exchanger which allow for more efficient implementation of

thermal storage in CSP applications.

2.4 sCO_2 power cycle integrated with CSP and oxy combustor

A paper was published by Son [46] investigated various options to extract $\mathbf{CO_2}$ in 3 different scenarios from Pre-combustion, Post-combustion and oxy combustion scenarios as shown in Figure 36.

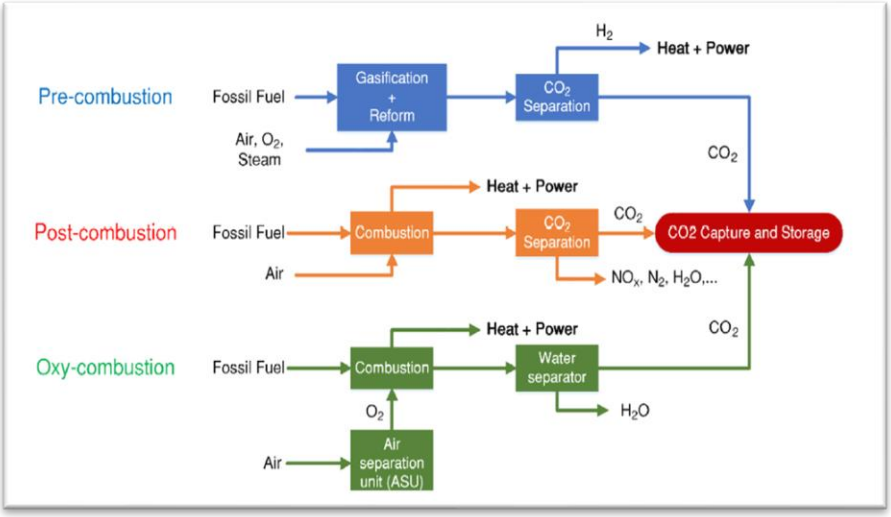

Figure 36. Different $\mathbf{CO_2}$ extration (Capturing) scenarios [46]

Table 4 presents a comparison between various paper's investigated scenarios with its key advantages and disadvantages.

Table 4. Comparison between various $\mathbf{sCO_2}$ capturing techniques

CO2 Extraction	Advantages	Disadvantages
Post-Combustion	• Proven CCS technologies for small scale plants • Mostly preferred for existing plants.	• Large Parasitic Load. • Electricity production cost would increase by 32% [86]
Pre-Combustion	• Relatively less load and cheaper compared to Post-Combustion.	• Lower Efficiency [86]
Oxy Combustion	• Potential to capture CO2 at high concentrations.	• The use Oxygen at the ASU comes at energy cost of over 7%.

The author had also emphasized on the combination of $\mathbf{sCO_2}$, CSP and Oxy combustion. The simple recuperated cycle was used where the carbon capturing process takes place after the compression process . The paper has noted two major advantages in integrating CSP with $\mathbf{sCO_2}$ and Oxy combustion [46] are as follow:

1- Overall gained efficiency
    a. 25% - 30% of the total heat is supplied via the CSP
    b. Achievable 55% - 60% performance efficiency [46].
2- Solving the solar intermittency challenge without contributing to production of $\mathbf{CO_2}$ to the atmosphere and thus eliminates the need of thermal storage.

As it was noted that a common problem with CSP systems is the heat loss due radiation. The heat loss increases by the increase of the receiver temperature. In other words, the more efforts we try to increase the receiver temperature, the heat loss due to radiation increases too and this led the researches to the conclusion that CSP is incapable to significantly increase the turbine inlet temperature beyond a certain temperature and accordingly the overall system efficiency. A chart explaining the relationship between the TIT and the efficiency of the system (Ideal Solar-to-work energy conversion efficiency) was also presented which illustrates the CSP limitation to drastically increase the TIT. There are few assumptions were made concerning the investigated model, the top assumptions made are summarized below as follow:

1. Turbine Inlet Temperature and Cooler Outlet Temperature are assumed to be given values and defined as a boundary condition.
2. Solar receiver temperature is assumed to be equal to the solar heat exchanger outlet temperature and the pinch temperature.

The integrated system of CSP and oxy combustor represented in this thesis has couple of major advantages in comparison to the systems presented in [46]. Firstly, the

efficiency of the recuperators efficiency increases with the proposed integration in comparison to the independent systems (CSP and oxy combustion systems) with the addition of the oxy combustor between the CSP and the turbine. In the other hand, the addition of the CSP reduces the fuel consumption required by the oxy combustion process due the heat provided by the CSP. The second systems advantage is proposed integrated system solves the intermittency problem of the CSP without the need of energy storage system and the carbon emission free electricity production.

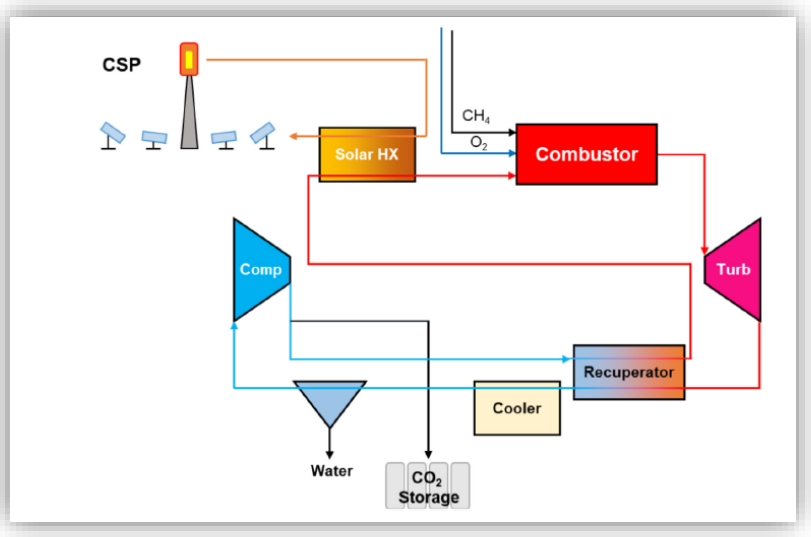

(a)

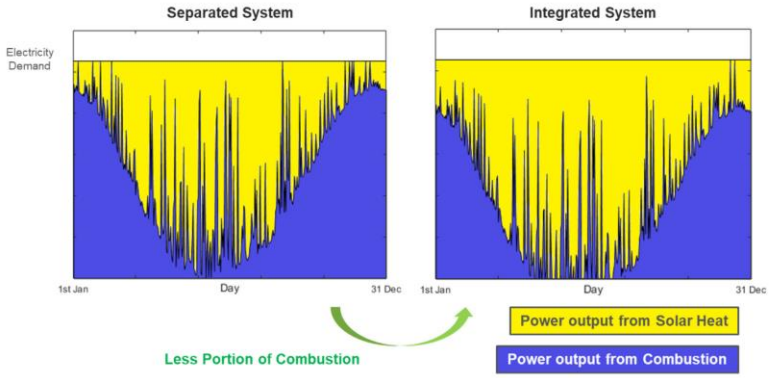

(b)

Figure 37. Simple s$\mathbf{CO_2}$ oxy combustion cycle integrated with CSP [46]

The authors investigated a model that studied Shouhang Dunhuang Plant in China comparing the power production using combustion alone vs the integrated system with CSP. Figure 37 (a) illustrates the cycle's layout. Figure 37 (b) presents the advantage of integrating the CSP with the oxy combustor and it reductions of fuel dependency needed for the combustion process as presented in blue and yellow color. Considering the most conservative calculations, the integrated power system will save around 16% of the independent combustion system. However, it ranges between 16% and up to 38% of the fuel consumption. This was found to be one the most relevant paper to my intended research, however, no energy/exergy analysis has been provided as a part of this research as it focused mainly on the CSP potential and its efficiency without carrying out energy/exergy analysis of the integrated system, however, in this thesis a complete energy exergy model is presented of the integrated system.

Another interesting paper published by Abengoa Solar and German Aerospace Center (DLR) institute of Solar Research [24] in which the operation of the Solugas plant is presented. It was noted that the pressurized air (medium) was heated via the receiver and 69 heliostats up to 800°C. The plant layout is presented in Figure 38.

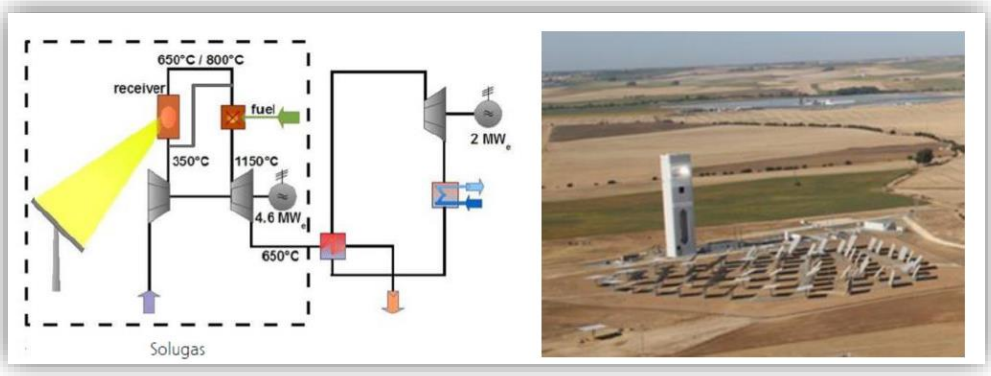

Figure 38. Solugas Plant's Layout [24]

This power plants generates about 50 MW with the help of modified gas turbine manufactured by Solar Turbines Incorporated. The paper highlighted that the plants operates consistently despite transitory clouds when operating at 600°C. it was noted that the receiver outlet temperature ranges in between 400°C - 800°C, mass flow rate ranges in between 3.5 – 5.75 kg/s, system pressure ranges in between 3.6 to 8.8 barg and turbine load is 4.5 MWe. It was mentioned that the plant was already prepared for integrating volumetric receiver to further help rising the operating temperature to 1000°C. This plant used a fuel combustor for the purposes of gaining thermal heat and not an oxy combustor as presented in this research, so the contribution of this paper is the integration of an oxy combustor in a place of this ordinary gas combustor of this cycle. Nkhonjera [87] has published a paper about the integration of oxy combustor, s$\mathbf{CO_2}$ Biomass and CSP for power conversion applications. This proposed system uses the generated syngas from the biomass for the combustion process in which the author believe is cleaner than the Natural Gas (due to lower carbon content and its emission). The working fluid used for the power cycle is s$\mathbf{CO_2}$and for the syngas generation cycle is $\mathbf{CO_2}$. This proposed cycle produces by products of pure water at both cycles (Power and syngas cycle) as a result of the oxy combustion and Gasification processes, In addition, $\mathbf{CO_2}$ will be also produced as a result of the oxy combustion process. Figure 39 illustrates the proposed cycle by the author.

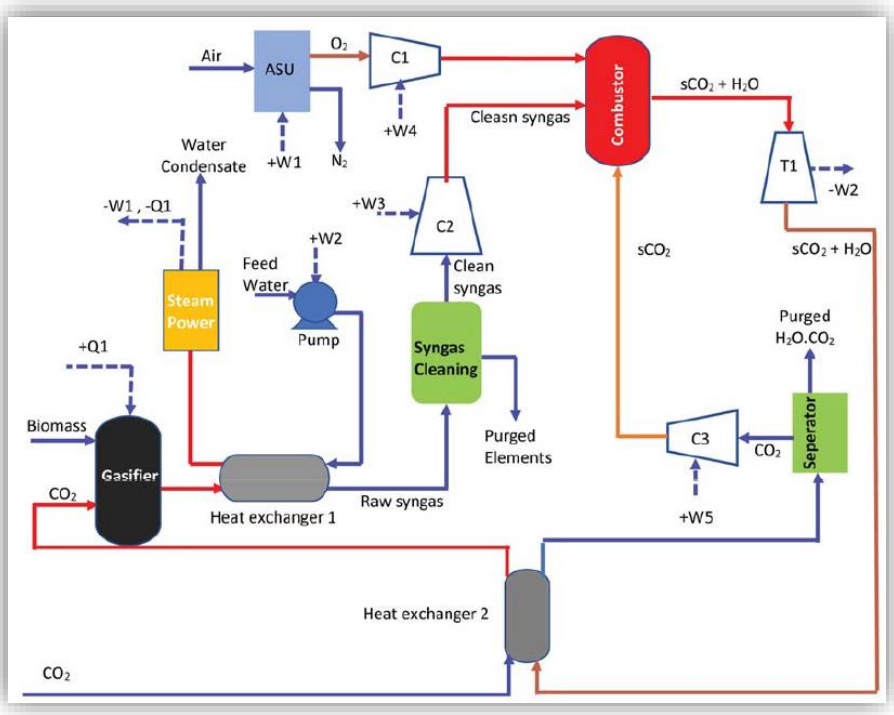

Figure 39. Proposed cycle by Nkhonjera [87]

The authors proposed the integration of CSP within their proposed cycle as a source of heat to be supplied to the Gasifier which results in the generation of the Syngas will have a positive impact on the cycle efficiency.

Another paper published by McClung [36] where two $\mathbf{sCO_2}$ integrated with oxy combustor power cycle concepts were investigated (CPOC & $\mathbf{sCO_2}$ recompression cycle). Both models were investigated via Aspen Plus were both cycle configurations were compared in terms of their thermal and the overall cycle efficiency. It was concluded that the recompression cycle achieved higher thermal efficiency 47% (at 650°C operating temperature and 290 atm) whereas the CPOC cycle achieved only 38% in the similar operating condition.

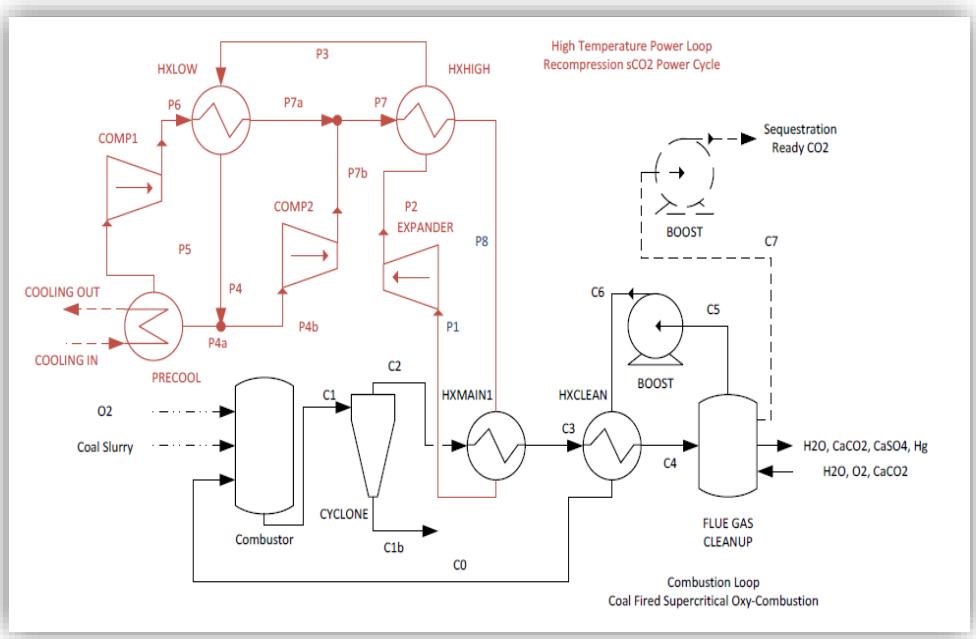

Figure 40. Investigated $\mathbf{sCO_2}$ recompression cycle [36]

Furthermore, the authors investigated the operation of integrating this cycle with the coal fired combustor integrated with high and low $\mathbf{sCO_2}$ power cycles which resulted in 1% reduced efficiency and slightly higher cost in comparison to the independent cycle due to equipment losses. This paper concluded that the introduction of recuperators has a very positive impact to the cycle efficiency (specially for the CPOC cycle) where the revised a line diagram was prepared highlighting the impact of the recuperator as a part of the layout in the thermal efficiency of the cycle as shown in Figure 41 below.

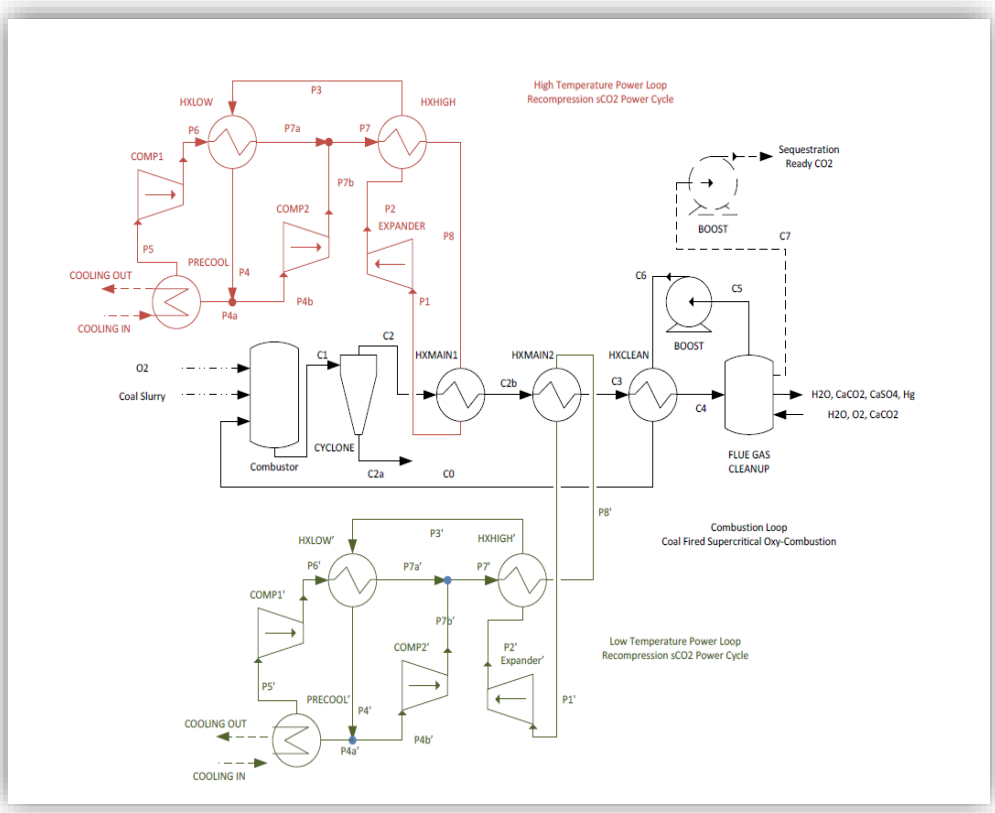

Figure 41. High/Low Temperature $\mathbf{sCO_2}$ cycles integrated with coal fired cycle [36]

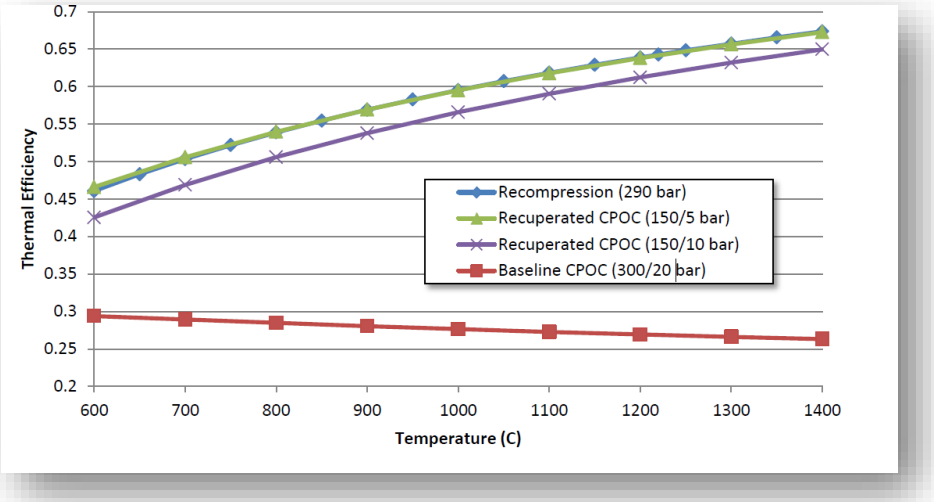

Figure 42. Comparision of the CPOC efficiency considering introduction of various recuperators and its effect in the thermal efficiency [36].

CHAPTER 3: DESCRIPTION OF PROPOSED SCO_2 CYCLE CONFIGURATION LAYOUTS

In this chapter, a proposed **sCO_2** cycle layout integrated with CSP and oxy combustor is studied and compared to other two cycles. All the cycle's configurations investigated and analyzed further are as follow:

1. Configuration 1 (CONF1): This cycle depends solely on the oxy combustor to run the turbine.
2. Configuration 2 (CONF2): This cycle depends solely on the CSP to run the turbine.
3. Configuration 3 (CONF3): This cycle depends on the integration of oxy combustor and CSP used to turn the turbine.

All the three different cycle will be discussed independently in the below sections describing how each cycle works and its components.

3.1 Investigated sCO_2 power cycle (CONF1)

This investigated cycle depends solely on the oxy combustor to generate the needed thermal power with the help of fuel (Methane) and pure Oxygen to power the turbine. Figure 43 illustrates the investigated **sCO_2** power cycle configuration (CONF1).

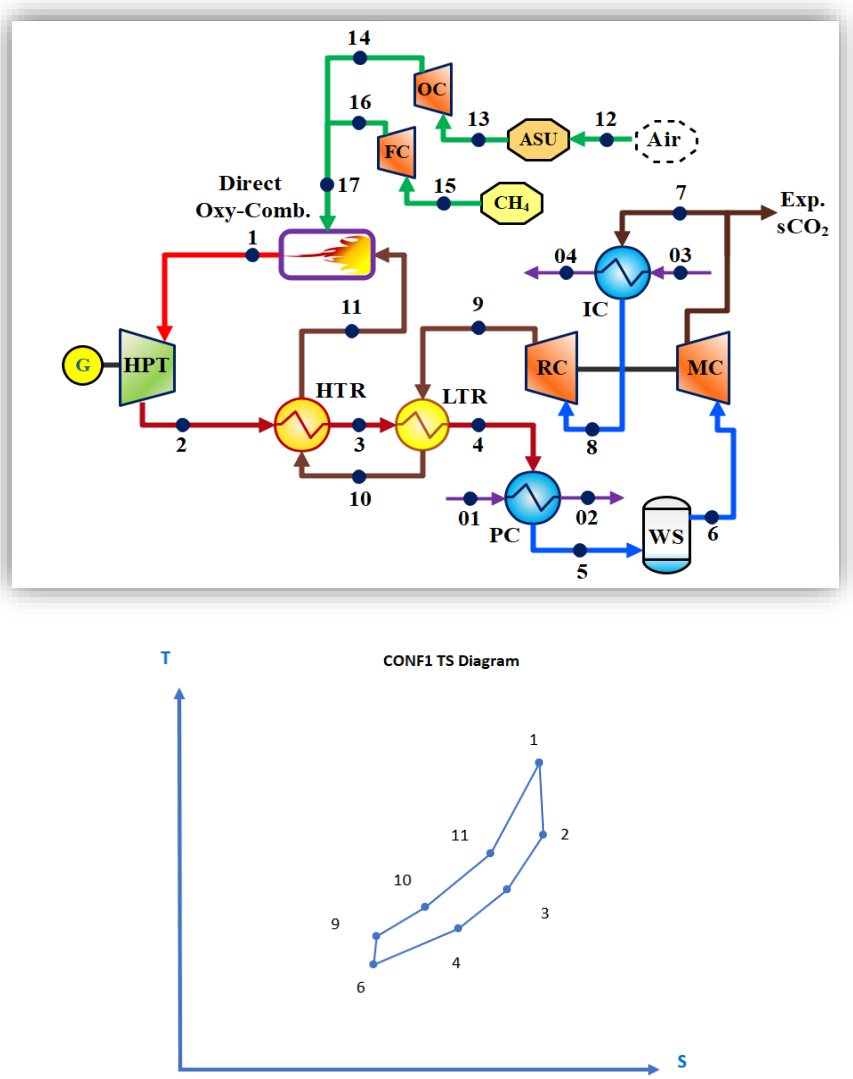

Figure 43. CONF1 power cycle configuration

The above cycle schematic describes the cycle's process flow and the cycle configuration. Each cycle's component will be discussed in the following headings as follow:

3.1.1 The oxy combustor (States 17, 11 to 1)

In this state, the oxy combustor is responsible for combusting the mixed oxygen and fuel coming from state 17 and the high temperature recycled Carbon Dioxide coming from the HTR (state 11). This combustion is fueled by the Methane (supplied via the fuel loop state 16) and ignited with the help of the pure Oxygen (supplied via

the oxygen loop state 14), the combustion of the fuel and oxygen mixture contribute results in increasing Carbon Dioxide temperature as a preparation for the upcoming expansion process.

As both the recycled and the generated $\mathbf{sCO_2}$ depends on the oxy combustion processed, the combustion rate governs the quantities of the $\mathbf{sCO_2}$ within the cycle.

This cycle configuration (CONF1) solely depends on the combustion process to generate enough thermal power to rotate the turbine blades and generate electricity and unlike the other investigated cycle configurations (CONF2 and CONF3) and accordingly it will consume more fuel and oxygen which makes the operation of this cycle a slightly more expensive to operate which leads to a higher LCOE. This is presented in detail in the following chapter (Chapter 4: Energy and Exergy Analysis).

As a result of the chemical reaction took place in the oxy combustion, newly generated $\mathbf{CO_2}$ process which will be resulted from the Oxy/fuel burning in addition to Water Vapor in which those will be extracted later on the cycle for commercial purposes. This chemical reaction is presented in chemical formula as in the balanced Equation (2). As the oxy combustor receive high temperature recycled $\mathbf{CO_2}$ presented as $\mathbf{CO_2}$ in Equation (2) and produces additional $\mathbf{CO_2}$ resulted from the combustion process (presented as $\mathbf{2CO_2}$) both gets combustion in the oxy combustor with the help of the fuel and the oxygen and enters the turbine after the combustion process with the highest temperature and pressure to turn the turbine blades for the purpose of power generation.

3.1.2 Turbine (States 1 to 2)

In between state 1 and 2, the combusted $\mathbf{sCO_{2\,(Overall)}}$ and water vapor mixture enters the turbine at a high temperature 619°C for the purpose of rotating the turbine blades and generate electricity via the generator attached to it. After the expansion

process, the hot air exists the turbine at roughly 470°C toward the High-Temperature Recuperators (HTR) and Low Temperature Recuperators (LTR) respectively.

3.1.3 High and Low Temperature Recuperators (HTR & LTR) between states 2-4 and 9-11

In between states 2 to 4 in the forward flow and states 9 to 11 in the reverse flow. The purpose of those recuperators is utilize the high-temperature exhaust $\mathbf{sCO_2}$ out of the turbine (which is 470°C) to pre-heat the recycled $\mathbf{sCO_{2\,(Recycled)}}$ after the water vapor is removed at stage 5-6(at a temperature 32°C) and $\mathbf{sCO_{2\,(Generated)}}$ is exported at stage 7 (at temperature of 80°C). The $\mathbf{sCO_{2\,(Recycled)}}$ enters state 9 (LTR) at 80°C and leaves the HTR in state 11 at a temperature of 420°C. So, the thermal gain at those recuperators is 340°C which contribute the preparation of the $\mathbf{sCO_2}$ for the combustion process at the oxy combustor.

The removal of the water vapor and the exportation of $\mathbf{sCO_2}$ reduces the thermal load on the oxy combustor which subsequently reduces the fuel and oxygen dependency, on the other hand, it contribute to cooling the exhausted $\mathbf{sCO_{2\,(Overall)}}$ and prepare it for the compression stage ana accordingly this reduce the work delivered by the compressor. formulas 9-20 are used to calculate thermal heat gain/loss of the recuperators in addition to recuperator's effectiveness.

3.1.4 Pre-Cooler (States 4 to 5), Inter-Cooler (States 7 to 8), Cooling Agents (States 1 to 4) and Water Separator (State 5-6)

At this part of the cycle, the $\mathbf{sCO_2}$ and Water Vapor mixture get cooled to facilitate the water extraction process as a part of the preparation for the $\mathbf{sCO_2}$ extraction and further compression process. The pre-cooler cools the $\mathbf{sCO_{2\,(Overall)}}$ (including water vapor) to a relatively cool temperature to allows liquification of the water and so the water separation process (state 5-6). The cooling takes place with the

help of an external cooling agent presented in purple line (state 1-2) as shown in Figure 44.

When this mixture enters the water separation column with a temperature near the room temperature (32°C), the mixture condensate at the column and water vapor condensate at the bottom of the separation column (with the help of baffle plates) which form a clean potable water. Although this extracted potable water is a by-product of this combustion process, this produced potable water is a big advantage to this cycle configuration which contribute to the efforts of the providing clean potable water to the surrounding communities. The extracted water can be estimated (using Equations (21) and (22)) with reference to the fuel mass flow rate. In other words, for every 1 kgs of Methane burned at oxy combustor, around 4 kgs of Oxygen is required to facilitate the burning which will results in 2.75 kgs of $\mathbf{CO_2}$ and around 2.25 kgs of water vapor ($\boldsymbol{H_2O}$).

Figure 44. Pre-cooler cooling agent (presented with the purple line between state 1-2)

At state 6, all the water content within the mixture is extracted and only the $\mathbf{sCO_2}$ is remaining within the mixture proceeding the main compressor. It is worth mentioning that the water vapor content within the mixture after this step is minimal (estimated to be around 1%) and that's why it is neglected and considered to be 100% $\mathbf{sCO_2}$ for the sake of thermodynamic calculations [19]. At state 7 (After the $\mathbf{sCO_2}$ was

compressed and $\mathbf{sCO_{2\ (Generated)}}$ was exported) get cooled again in the intercooler after it was compressed via the main compressor (state 6-7) which contribute the reduction of the compression load (and its electrical consumption) at the recompression cycle state 8 to 9.

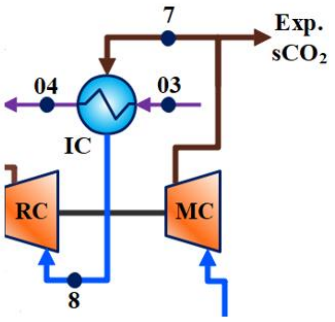

Figure 45. Inter-Cooler in between compression stages

3.1.5 Main Compression (state 6 to 7) and Re-Compression (states 8 to 9)

The compression process takes place in those states with the two compression phases (Main Compressor and the Re-Compressor). At the main compression phase, the $\mathbf{sCO_{2\ (Overall)}}$ gets compressed to 135 bar. This pressure facilitates the export of the $\mathbf{sCO_{2\ (Overall)}}$ that takes place directly after the compression process. A market survey was carried out and it confirmed that pressure in between 75-150 bar is within acceptable pressure range for storing and exporting the Carbon Dioxide for further commercial applications. At the recompression phase (state 8 to 9), the $\mathbf{sCO_{2\ (Recycled)}}$ gets recompressed to around 250 bar (after the generated part of $\mathbf{sCO_2}$ is exported and the remaining $\mathbf{sCO_2}$ gets cooled in the intercooler) as a preparation for combustion process.

3.1.6 Oxygen Loop (States 12 to 14 and 17)

At this part of the cycle, the atmospheric air gets into the Air Separation Unit

(ASU) where the pure Oxygen get separated and produced (in between state 12 to 13). The generated Oxygen from the ASU gets compressed and injected into the combustor using the oxygen compressor in between state 13 to 14. By applying the energy/exergy model (Chapter 4), it was noted that this cycle configuration will need an Oxygen flowrate of 13.64 Kg/s. Accordingly, the compressor size was defined, and its electrical power was determined and added to the cycle's electrical consumption. As this cycle solely depends in the oxy combustor to generated the needed heat to turn the turbine blades, accordingly a constant flow of the oxygen will be required and this is not variable load that might change during the day as in CONF3 cycle configuration.

3.1.7 Fuel Loop (States 15 to 17)

At state 15 the Natural Gas (Methane) gets injected into the power cycle and compressed by the Fuel Compressor (state 15-16) to the desired mass flowrate. Accordingly, the compressor size and its fuel consumption are highlighted and added to the cycle's electrical consumption. The compression process is an essential step to prepare the fuel for the combustion process. At state 17, the compressed fuel and Oxygen gets mixed gets injected to the oxy combustor for further combustion process. The quantity of the fuel consumed differs based on the combustor's outlet temperature and recuperators efficiencies, however in general, the fuel consumption of this cycle is expected to be equals to rate 3.411 kg/s since this cycle solely depends on the oxy combustor to generate the needed thermal power and there is no alternative thermal power or thermal storage like CONF3 cycle configuration. It worth noting that the amount of generated $\mathbf{CO_2}$ depends on the amount of fuel burned in the combustor which is governed by Equation (21) as presented in Chapter 4.

3.2 Investigated sCO_2 power cycle (CONF2).

The second scenario represented is a $\mathbf{sCO_2}$ cycle that depends solely on CSP

to generate the required heat via its heliostat and its receiver to power the turbine. As the CSP is not an objective of thesis, a literature review was conducted on the average receiver temperatures in the available CPS installation worldwide ranges between 800°C - 1000°C. Accordingly an average receiver temperature was considered to be 901°C. the receiver temperature contributes the heating of the $\mathbf{sCO_2}$ to prepare it for further expansion in turbine. As this cycle doesn't have the oxy combustor as a component, it doesn't have an Oxygen and Fuel loops and the cycle doesn't generate $\mathbf{CO_2}$ and potable water (as in the CONF1 power cycle), accordingly this power cycle is cheaper to operate and have the cheapest LCOE, however, it has major challenge with the generated power consistency as it depends on the solar radiations which might not consistent during the day (because of rain, clouds as an example) and no power generation will take place during the night. This fluctuation and inconsistency of the generated power is a major disadvantage with this cycle (and other similar renewables applications). Figure 46 represents the CONF2 cycle configuration layout.

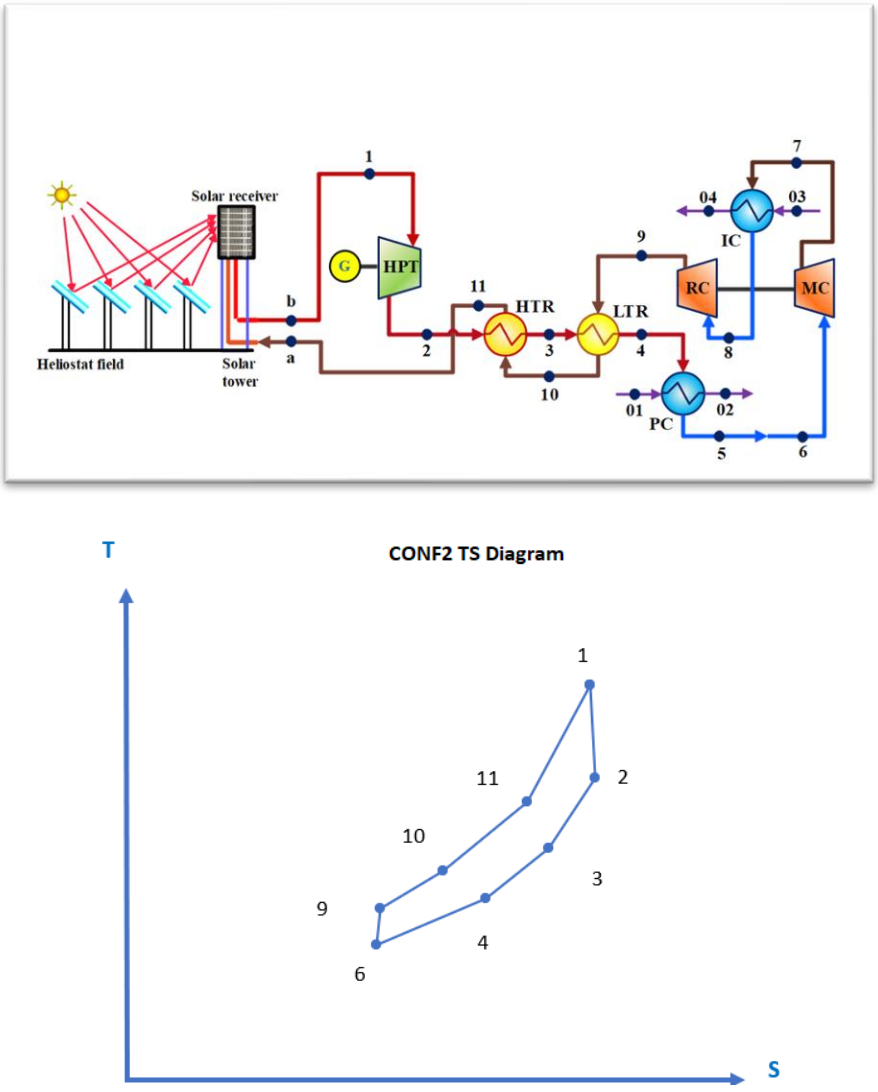

Figure 46. CONF2 power cycle configuration

3.2.1 The CSP (state a to b)

The CSP is the main driver of this power cycle. The Heliostat reflects the solar radiations toward the power tower, in which it focuses the radiation to the solar receive which heats the $\mathbf{sCO_2}$ coming from state a toward state b. The receiver temperature is considered to be 901°C (Receiver Temperature) and accordingly the T1 is considered to be 705°C where it rotates turbine for power generation purposes (state 1 to 2). As this $\mathbf{sCO_2}$ power cycle configuration depends solely on the CSP as the heat source and there is no thermal storage covering, this cycle operating hours will be limited to during

the daytime. It is worth mentioning that this cycle configuration doesn't have oxy combustion integrated with this cycle configuration scenario (like CONF1 and CONF3), there is no $\mathbf{sCO_2}$ is being exported and no water is being extracted from the cycle due the absent of combusting of fuel and oxygen.

3.2.2 Turbine (States 1 to 2)

In between state 1 and 2, the heated $\mathbf{CO_{2\,(Overall)}}$ enters the turbine at a high temperature and pressure (at temperature of 658 °C and pressure of 250 bar) to rotate turbine blades which generates power via rotating the generator. After the expansion process, the expanded air exists the turbine toward the High-Temperature Recuperators (HTR) and Low Temperature Recuperators (LTR) respectively for the purpose of recovering this heat to warm the compressed air before entering the power tower receiver. Equations used to calculate the work of the turbine are same used in Equations (5), (6), (7) and (8).

3.2.3 High and Low Temperature Recuperators (HTR & LTR) between states 2-4 and 9-11

In between states 2 to 4 in the forward flow and states 9 to 11 in the reverse flow. The purpose of those recuperators is utilize the high-temperature exhaust $\mathbf{sCO_2}$ out of the turbine to pre-heat the recycled $\mathbf{sCO_2}$ before it enters the Solar Power Tower Receiver which makes it easier for the receiver to heat the $\mathbf{sCO_2}$ to the desired Turbine Inlet Temperature of 705 °C. Equations used to calculate the thermal gain/loss at each recuperator is similar to Equations (9), (10), (11) and (12) with the condition that $\boldsymbol{m_{co2\,(Overall)}} = \boldsymbol{m_{Co2\,(Recycled)}}$ because there is no $\mathbf{sCO_2}$ is being generated in this cycle and no $\mathbf{sCO_2}$ is being exported as well. It is a closed loop $\mathbf{sCO_2}$. The effectiveness of those recuperators ($\mathcal{E}_{htr}$ & $\mathcal{E}_{ltr}$) is very essential to the overall efficiency of the power cycle which can be calculated using the Equations (13), (14), (15), (16), (17), (18), (19)

and (20) with the condition that $\boldsymbol{m_{co2\,(Overall)}} = \boldsymbol{m_{Co2\,(Recycled)}}$ for the same reason mentioned above.

3.2.4 Pre-Cooler (States 4 to 5), Inter-Cooler (States 7 to 8), Cooling Agents (States 1 to 4)

At this part of the cycle, the $\mathbf{sCO_2}$ gets cooled to facilitate for the compressions processes at the main compressor (state 6 to 7) more efficiently. The pre-cooler cools the $\mathbf{sCO_2}$ (including water vapor) to a relatively cool temperature with the help of an external cooling agent presented in purple line (state 1-2). At state 7, $\mathbf{sCO_2}$ gets cooled again in the intercooler after it was compressed via the main compressor (state 6-7). This process of intercooling contributes to the reduction of the recompression load (and its electrical consumption) at the re-compressor state 8 to 9. Kindly refer to Figure 44 for reference from the power cycle.

3.2.5 Main Compression (state 6 to 7) and Re-Compression (states 8 to 9)

The compression process takes place at those states with the two compressors (Main Compressor and the Re-Compressor). At the main compression phase, the $\mathbf{sCO_2}$ gets compressed to 135 bar. At the recompression phase (state 8 to 9), the $\mathbf{sCO_2}$ gets recompressed to around 250 bar as a preparation for recuperative process and further heating in the solar receiver. The work of the Main Compressor and Re-compressor is calculated using Equations (24) and (25).

3.3 Investigated sCO_2 power cycle (CONF3)

This cycle configuration (CONF3) depends on the integrated system between the oxy combustor and the CSP. The CSP receiver works as preheater to in which reach to a temperature of 1073°C ($\mathbf{T_b}$= 950°C) while leaving the receiver and entering the combustor, so the thermal load decreases on the oxy combustor as it will heat the $\mathbf{sCO_2}$ that is already at already high temperature. This cycle has the most reliable

configuration among the previously investigated configurations (CONF1 and CONF2) because of the combination between the oxy combustor and the CSP where the system doesn't consume relatively high fuel (as it will be presented in the following chapter) like the cycle configuration in CONF1 and the power inconsistency that comes with CONF2 cycle configuration because of cycle depends solely in CSP. The CSP will act as a pre-heater to the oxy combustion process for the purpose of reducing the thermal load on the oxy combustor and its fuel consumption. Below Figure illustrates the CONF3 cycle configuration.

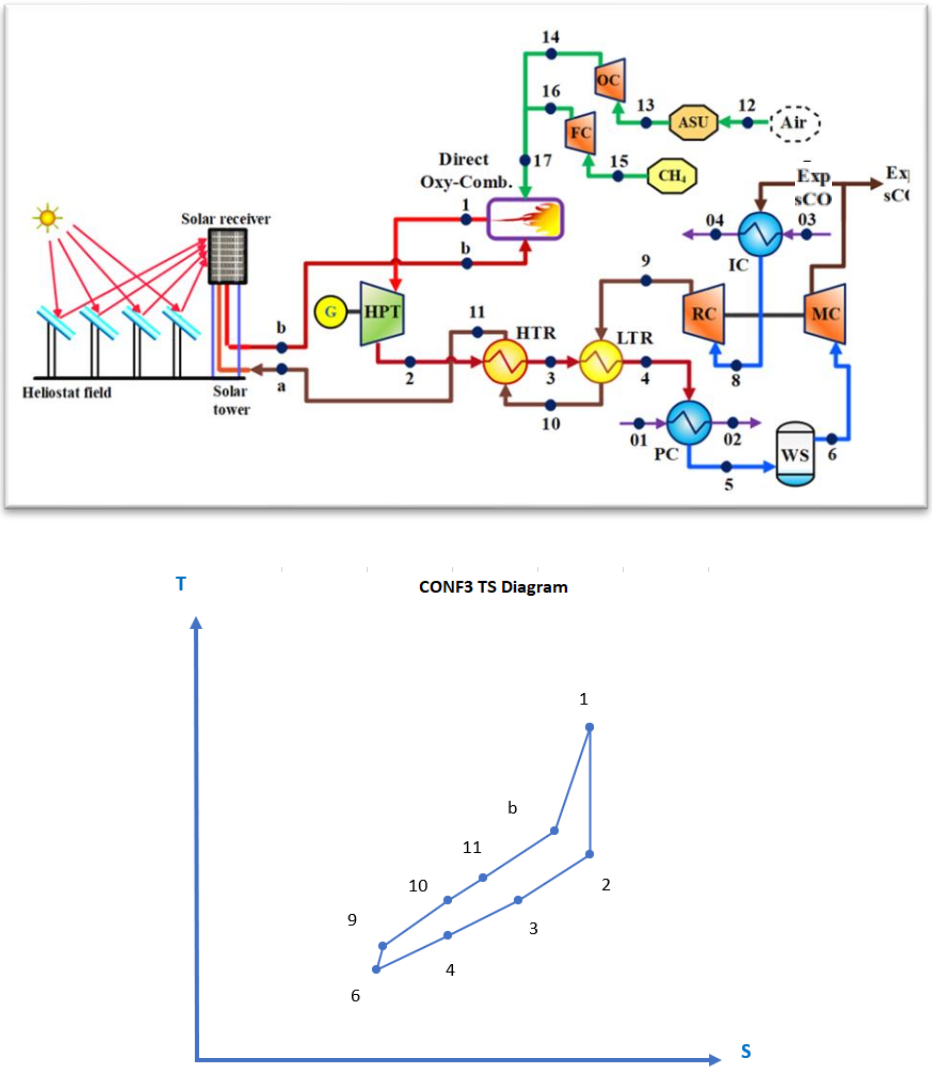

Figure 47. CONF3 power cycle configuration

3.3.1 The oxy combustor (Between States 3+17-1)

In this state, the oxy combustor is responsible for combusting the mixed Oxygen and fuel with the recycled $\mathbf{sCO_2}$ coming heated by the CSP receiver coming from the state 3. The oxy combusting process generated $\mathbf{sCO_2}$ that gets added and extracted (after the expansion process) for further commercial applications. Furthermore, this oxy combusting process also generate clean potable water that is condensed via the water separator and extracted also for further commercial applications. Equations (2), (3) and (4) are governing the relationship between the combustion process and its generation

of the by-products. Equation (1) is used to calculate the thermal gain at the combustor.

3.3.2 Turbine (Between States 1-2)

In between state 1 and 2, the high temperature $\mathbf{sCO_2}$ and water vapor mixture enters the turbine at a very high temperature (TIT= 1125 °C) for the purpose of rotating the turbine blades and generate electricity. After the expansion process, the hot air exists the turbine toward the High-Temperature Recuperators (HTR) and Low Temperature Recuperators (LTR) respectively. The rotation of the turbine blades generates electricity via the attached generator. The work of the turbine is calculated via Equations (5), (6) and (7) and efficiency of the turbine is calculated via Equation (8) above.

3.3.3 High and Low Temperature Recuperators (HTR & LTR) between states 2-4 and 9-11

In between states 2 to 4 in the forward flow and states 9 to 11 in the reverse flow. The purpose of those recuperators is utilize the high-temperature exhaust out of the turbine ($\mathbf{T_2}$= 890°C) to pre-heat the recycled $\mathbf{sCO_2}$ before it enters the Solar Receiver (from $\mathbf{T_9}$ at 80°C to $\mathbf{T_{11}}$ at 840°C), on the other hand, it contribute to cooling the exhaust $\mathbf{sCO_2}$ and prepare it for the cooling stage, water extraction process and the compression stage. Equations (9), (10), (11) and (12) are used to determine the heat gain/loss among those recuperators. The effectiveness of those recuperators was calculated via Equations (13), (14), (15), (16), (17), (18), (19) and (20) as presented in the chapter 4.

3.3.4 Pre-Cooling (state 4-5), Inter-Cooler (state 7-8) and Water Separation Process (state 5-6)

At this part of the cycle, the $\mathbf{sCO_2}$ and water vapor mixture gets cooled to facilitate the water extraction process and further compression process. The pre-cooler

cools the mixture temperature to around 32°C and accordingly ease the water extraction process in state 5-6. The cooling takes place with the help of an external cooling agent presented in purple line (state 1-2) as shown in Figure 44. The equations to quantify the produced water from this cycle and the fuel/oxygen consumed for the cycle were calculated via Equations (21), (22) and (23). At state 6, all the water content within the mixture is already extracted and only the $\mathbf{sCO_2}$ is remaining within the mixture proceeding the main compressor. $\mathbf{sCO_2}$ at state 7 (After exportation at a pressure of 135 bar) gets re-cooled after the main compressor (state 6-7) in the Inter-Cooler which increases the cycle efficiency by reducing the operating temperature of the $\mathbf{sCO_2}$ to 32°C before the recompression cycle via an external cooling agent presented in purple line (state 3-4) as shown above in Figure 45.

3.3.5 Main Compression (states 6-7) and Re-Compression (state 8-9)

At the main compressor (state 6-7), the cooled $\mathbf{sCO_2}$ gets compressed to 135 bar which facilitate the exportation of the $\mathbf{sCO_2}$ for further commercial applications. On the contrary, the re-compressor compresses the $\mathbf{sCO_2}$ to high pressure 250 bar to prepare the $\mathbf{sCO_2}$ for further heating, combusting, and expanding process. It was proven that this "inter-cooling" cycle layout allow the flexibility to partially pressure the $\mathbf{sCO_2}$ and exported in a relatively low pressure and then continue pressurizing the $\mathbf{sCO_2}$ to maintain the required pressure by the cycle, furthermore, it was noted from the literature review in similar cycles that the intercooling cycle achieves higher cycle efficiency in comparison to other cycle's layout. Equations (6), (24) and (25) above were used to calculate the compressors works.

3.3.6 Concentrated Solar Power Receiver Tower (State a-b)

As this cycle works in integrated mode between CSP and oxy combustor, the $\mathbf{sCO_2}$ gets to the CSP-PT after the LTR and HTR in which the CSP-PT works as a pre-

heater to the oxy combustor. Although no CSP thermodynamic model is not considered as a part of this thesis deliverables, a reference is made already published papers of existing power plants like Solugas power plant allocated near Seville as an example. This power plants uses 69 heliostat units with a reflective area of 121 $\boldsymbol{m^2}$ with a receiver height of 65m, the cycle is equipped with a gas turbine that operates via natural gas in which the receiver tower acts as a pre-heater to reduce the fuel dependency [24]. It was noted that the receiver heats the working gas to in between 650°C - 800°C and after the combustion the operating temperature reaches to 1150°C in an average working day [24]. Another example is in Elbeih dissertation [11] were various tower designs were reviewed and it was confirmed that receivers can absorb temperatures up to 1500°C with the help of Siliconized Silicon Carbide (SiSiC). In light of the above and for the purpose of this thesis energy and exergy analysis (chapter 4), the receiver outlet temperature ($\mathbf{T_b}$) is considered to be equals to 950°C entering the oxy combustor for further combusting process.

3.3.7 Oxygen Loop (state 12 to 14, 17)

At this part of the cycle, the atmospheric air gets into the Air Separation Unit (ASU) where the pure Oxygen get separated and produced (in between state 12 to 13). The generated Oxygen from the ASU gets compressed and injected into the combustor using the oxygen compressor in between state 13 to 14. As this cycle configuration depends on the combination of the oxy combustor and CSP where the CSP acts a pre-heater, the combustion rate (and accordingly the oxygen consumption) varies according to the gained thermal power in the receiver. By applying the energy and exergy analysis (chapter 4), it was noted that this cycle oxygen consumption is 6.579 Kg/s (considering receiver outlet temperature of 950°C) and 13.64 kg/s during the night operation (where there is no thermal power gained by the receiver which makes it same as CONF1 during

the night operation). After the generated pure Oxygen gets compressed by the Oxygen Compressor to 250 bar, it gets mixed with the compressed Methane (at state 17) as a preparation for the combustion process at the oxy combustor. The Air Separation process is a very energy intensive process which accounts for around 44% of the overall power plants energy consumption [86]. The Air Separation Process is hot research topic and any progress in this field will have a positive impact to such power plant efficiency.

3.3.8 Fuel Loop (state 15 – 17)

At state 15 the Natural Gas (Methane) gets injected into the power cycle and compressed by the Fuel Compressor (state 15-16) to the desired mass flowrate 1.645 kg/s to the combustor at the optimum operating condition whereas the $\mathbf{sCO_2}$ enters combustor at 950°C heated by the CSP receiver. However, as this cycle layout depends in the integration of the oxy combustor and CSP, in the absent of CSP receiver thermal heat (during the night for example) the fuel consumption is calculated to be equals to 3.411 kg/s (similar to CONF1 cycle configuration) as the system will solely depends on the oxy combustor to generate the required thermal load to run the turbine. At state 17, the compressed fuel and Oxygen gets mixed gets injected to the oxy combustor for further combustion process. It worth noting that the amount of generated $\mathbf{CO_2}$ depends on the amount of fuel burned in the combustor which is governed by Equation (21) below.

CHAPTER 4: ENERGY AND EXERGY MODEL

In this chapter, the energy and exergy model will be presented of all the three cycles highlighting the assumption and the input parameters used for this study. The model has been developed with the help of Engineering Equations Solver (EES) in which each model has been solved separately and results were studied and presented in a comparison table as presented in Table 7. There are general assumptions for all the three assumptions as the system capacity is 50 MW. CIT was considered 32°C and the Oxygen and Fuel inlet temperature is 250°C. The generator efficiency is set at 97%, turbine efficiency is at 93% and compressors (main and re-compressor) are set at 93%. The cycle highest pressure is considered is considered at 250 bar and its lower pressure is considered at 73.5 bar.

hereby are the formulas used to calculate produced heat from the combustion process ($\boldsymbol{Q_{OC}}$) as presented below in Equations (2) and (3).

$$\boldsymbol{Q_{OC}} = [\boldsymbol{m_{CO2\,(Recycked)}}\,(\boldsymbol{h1} - \boldsymbol{h3})] + [\boldsymbol{m_f\,LHV_f}] \quad (2)$$

$$\boldsymbol{CH_4} + \boldsymbol{CO_{2\,(Recycled)}} + \boldsymbol{2O_2} \longrightarrow \boldsymbol{2CO_2} + \boldsymbol{2H_2O} \quad (3)$$

Equation (3) represents the relationship between the recycled and generated $\boldsymbol{CO_2}$ in which both (along with water vapors) are expanded in the turbine as explained in the following sub-section. Equation (4) highlights that the generated $\boldsymbol{CO_2}$ gets exported at state 7 (after the main compression) for further commercial applications.

$$\boldsymbol{CO_{2\,(Recycled)}} + \boldsymbol{CO_{2\,(Generated)}} = \boldsymbol{2CO_{2\,(Overall)}} \quad (4.1)$$

$$\boldsymbol{CO_{2\,(Generated)}} = \boldsymbol{CO_{2\,(Exported)}} \quad (4.2)$$

The work of the turbine is calculated using Equations (5) and (7) as shown below:

$$\boldsymbol{W_t} = \frac{\boldsymbol{W_e}}{\boldsymbol{n_g}} + \boldsymbol{W_C} \quad (5)$$

$$W_C = W_{Main\ Compressor} + W_{Recompressor} \quad (6)$$

$$W_t = n_t[m_{CO2}(h_1 - h_2)] \quad (7)$$

Where W_e represents the total targeted electrical power, which is 50 MW in this thesis, W_c presents the work consumed by the compressors and n_t is the isentropic efficiency of the turbine. The isentropic efficiency of the turbine (n_t) is calculated using the below equation.

$$n_t = \frac{(h_1 - h_{2a})}{(h_1 - h_{2s})} \quad (8)$$

The characteristic equations used to determine the heat gain/loss (Q_{htr} & Q_{ltr}) for the High Temperature Recuperator (HTR) and Low Temperature Recuperator (LTR) respectively are as follow:

$$Q_{htr} = m_{co2\ (Overall)}\ x\ CP_{htr,h}\ (T_2 - T_3) \quad (9)$$

$$Q_{htr} = m_{Co2\ (Recycled)}\ x\ CP_{htr,c}\ (T_{11} - T_{10}) \quad (10)$$

$$Q_{ltr} = m_{co2\ (Overall)}\ x\ CP_{htr,h}\ (T_3 - T_4) \quad (11)$$

$$Q_{ltr} = m_{Co2\ (Recycled)}\ x\ CP_{htr,c}\ (T_{10} - T_{11}) \quad (12)$$

The specific heat (CP) is a constant value depending on the recuperator's design and materials which might varies from the hot and the cold side. Those recuperators plays an important role to recovering the expanded high-temperature Carbon Dioxide heat as a pre-heat to the recycled Carbon Dioxide and raise its temperature as a preparation to the combustion phase. The recuperators (HTR & LTR) thermal effectiveness (Σ_{htr} & Σ_{ltr}) are calculated using the below equations with reference to the minimum value of Heat Capacity Rate (C_{min}) as follow:

$$\Sigma_{htr} = \frac{Q_{htr}}{C_{min,htr}\ (T_2 - T_{10})} \quad (13)$$

$$C_{min,htr} = Min\ (C_{htr,h}\ , C_{htr,c}) \quad (14)$$

$$C_{htr,h} = m_{CO2\ *\ (Overall)}\ x\ CP_{htr,h} \quad (15)$$

$$C_{htr,c} = m_{CO2*(Recycled)}\, x\, CP_{htr,c} \quad (16)$$

$$\Sigma_{ltr} = \frac{Q_{ltr}}{C_{min,ltr}\,(T_3 - T_7)} \quad (17)$$

$$C_{min,ltr} = Min\,(C_{ltr,h}\,, C_{ltr,c}) \quad (18)$$

$$C_{ltr,h} = m_{CO2\,(Overall)}\, x\, CP_{ltr,h} \quad (19)$$

$$C_{ltr,c} = m_{CO2\,(Recycled)}\, x\, CP_{ltr,c} \quad (20)$$

Since this produced potable water and newly produced $\mathbf{CO_2}$ is related amount of fuel being burned at the oxy combustor, the following formulas is used to calculate the mass flow as follow:

$$m_{CO2\,(Generated)} = 2.75\, m_{fuel} \quad (21)$$

$$m_{water\ vapor} = 2.25\, m_{fuel} \quad (22)$$

$$m_{Oxygen\,(O2)} = 4\, m_{fuel} \quad (23)$$

The work of the Main Compressor and Re-compressor is calculated using the below equation:

$$W_{Main\ Compressor} = \frac{m_6\,(h_7 - h_6)}{n_{\,main\ compressor}} \quad (24)$$

$$W_{Recompressor} = \frac{m_7\,(h_9 - h_8)}{n_{Recompressor}} \quad (25)$$

4.1 CONF1 sCO_2 Power Cycle Energy and Exergy Model

This cycle solely depends on the oxy combustor to meet its thermal requirements of heating the $\mathbf{sCO_2}$ to its critical region. Its energy and exergy model of this cycle (Figure 36) was developed and solved with the help of EES. There are some inputs fed to the model to facilitate the simulation as the Turbine Inlet Temperature was estimated to be 619°C and the Turbine Inlet Pressure at 250 bar. The work of the turbine was calculated using Equation (7) and (8) was used to calculate the turbine isentropic efficiency. The system's power capacity was calculated via Equation (5) to ensure the achievement of the power capacity of 50 MW.

CIT was considered to be equals to 32°C. the work of the compressors were calculated via Equations (6), (24) and (25). As this cycle solely depends on the oxy combustor, the recycled $\mathbf{sCO_2}$ flowrate is considered to be 550 kg/s and fuel (Methane) flow rate of 3.146 kg/s which are slightly higher than CONF2 and CONF3 models as it will be presented. Equations (2), (3) and (4) were used to govern the relationship between the recycled and generated $\mathbf{sCO_2}$. The mass flowrates of fuel, $\mathbf{sCO_2}_{\mathbf{(Generated)}}$, oxygen, and water vapors were calculated via Equations (21), (22) and (23). HTR and LTR recuperators heat capacity and thermal effectiveness were calculated via Equations (13), (14), (15), (16), (17), (18), (19) and (20). The heat transfer in between the recuperators were calculated using the set of Equations (9), (10), (11) and (12).

4.2 CONF2 sCO_2 Power Cycle Energy and Exergy Model

This cycle is operated via the thermal heat collected by CSP in order to heat the $\mathbf{CO_2}$ to beyond its supercritical state (Supercritical $\mathbf{sCO_2}$). As the CSP is not the main focus of this thesis, no detailed CSP design model will be presented in this chapter, however, the CSP will be considered as a source of heating that heats the $\mathbf{sCO_2}$ as a preparation to turbine the turbine. The work generated by the turbine is calculated using Equation (7) whereas the turbine isentropic efficiency is calculated using Equation (8). The system's power capacity is calculated using Equation (5) to ensure the generated net power is 50 MW.

CSP-PT general model input parameters are ambient temperature of 35°C, another assumption made is the Receiver Outlet Temperature equals the Turbine Inlet Temperature which is considered to be 705°C the heat $\mathbf{sCO_2}$ in order to run the turbine. Heliostat efficiency of 73%, heliostat area of 610 $\boldsymbol{km^2}$ and receiver effectives of 85% were recorded. SAM and Solar Polit were used for to validate the CSP parameters. Equations (6), (24) and (25) were used to calculate the compressors works

the relationship between the work of both compressors. Equations (13), (14), (15), (16), (17), (18), (19) and (20) are used to calculate the HTR and LTR thermal effectiveness heat capacity with the use the $\mathbf{sCO_2}$ mass flow rate. Equations (9), (10), (11) and (12) were used to calculate the thermal heat transfer within the recuperators.

4.3 CONF3 sCO_2 Power Cycle Energy and Exergy Model

This is the hybrid model where the $\mathbf{sCO_2}$ power cycle depends on the CSP and the oxy combustor where the CSP works as preheater to the combustor. The introduction of the CSP in this cycle contribute to drastically reduce the cycle consumption of Oxygen and Fuel in Comparison to CONF1 model as it will be shown. On the other hand, this integrated model (with the presence of the oxy combustor) will solve the CONF2 $\mathbf{sCO_2}$ power cycle inconsistency problem due to it dependency on solar power without thermal storage in addition to enhancing the cycle efficiency. CONF3 inputs parameters defied the receiver outlet temperature is 950°C in which it leaves the oxy combustor after heating at a temperature of 1100°C (TIT). Equation (1) was used to calculate the heat delivered by the oxy combustor.

Equations (2), (3) and (4) were used to govern the relationship between the recycled and generated $\mathbf{sCO_2}$, using this model, the recycled $\mathbf{sCO_2}$ flowrate was found to be equals to 437 kg/s.

Equation (7) were used to calculate the work generated by the turbine where the isentropic efficiency of the turbine was calculated using Equation (8). On the other hand, Equation (5) is used to calculate the net generated power of the system considering the generator efficiency which was used to verify the achievement of 50MW of power capacity. The heat transfer within the HTR and LTR was calculated using Equations (9), (10), (11) and (12) whereas their thermal effectiveness was calculated using Equations (13), (14), (15), (16), (17), (18), (19) and (20). The work of

both compressors was calculated using Equations (24) and (25) and Equation (6) is used to govern the relationship in between the work consumed by both compressors which is finally captured in Equation (5).

Equations (21), (22) and (23) are to calculate mass flowrate of $\mathbf{sCO_2}$ **(Generated)**, water vapor and oxygen (respectively) in terms of fuel flowrate which is found to be equal to

2.54 kg/s. This proves that this cycle consumes less fuels in comparison to the CONF1 cycle configuration as shown in the comparison presented in chapter 5 below.

CHAPTER 5: RESULTS AND DISCUSSION

In this chapter, the of the energy and exergy analysis is presented and compared between with other investigated cycle configuration in addition verification and verification of the result obtained as categorized in the below sections.

5.1 Validation and Verification

Model verification and validation are performed by comparing the results of models of CONF 1 and 2 with similar power cycles available in literature. Since the model of the first configuration (CONF1) is close to Allam cycle, the major operating conditions were adjusted to be the same as [88] with same electrical output power. The calculated results were compared to those reported in [88] as shown in Table 5. A maximum error was found of -3.8% in the turbine outlet temperature. This is attributed to the slight difference in the composition of the exhaust flow from the combustor between the present study and Scaccabarozzi et al. [88] . At the same time, the error in the electric efficiency is only about 1%. Table 5 below illustrates the difference between the results obtained from CONF1 and the results published by the author [88].

Table 5. CONF1 results compared to the published model by Scaccabarozzi [88]

Items	Ref. [88]	CONF1	Error (%)
Thermal energy of the fuel, LHV (MW_{th})	768.31	775.20	-0.89
Turbine output power, $\dot{W}$_HPT (MW)	622.42	637.20	-2.37
Recycle flow compression, (MW)	111.15	112.86	-1.54
NG compressor consumption, (MW)	4.18	4.32	-3.35
Turbine outlet temperature, T_2 (°C)	741.20	769.60	-3.8
Recycle flow final temperature, T_{11} (°C)	721.20	734.80	-1.89
Total recycle flow rate (with oxygen), $\dot{m}_1$ (kg/s)	1353.90	1353.50	0.03
Thermal efficiency of the cycle, (%)	54.58	54.09	0.90
ASU penalty, (MW)	85.54	83.86	1.90
Turbine inlet flow rate, $\dot{m}_{1,\ co2}$ (kg/s)	1271.00	1268.00	0.24

Model of CONF2 is compared to the investigated by Yang et al. [89] for the same operating conditions as shown in Table 6. The maximum error of 1.09% in the temperature at the turbine inlet is due to the differences in the thermodynamic properties of the heat transfer fluids. However, the temperatures at the receiver outlet of both fluids are close. This is explained by that they received power from the receiver surface ($\boldsymbol{Q_{rec,}}$ $\mathbf{sCO_2}$) is almost the same.

Table 6. CONF2 results compared to the results works published by Yang et al. [89]

Items	Ref. [89]	CONF2	Error (%)
Turbine inlet pressure, $\boldsymbol{P_1}$ (bar)	230	230	Input
Compressor inlet pressure, $\boldsymbol{P_6}$ (°C)	73.50	73.50	Input
Compressor inlet temperature, $\boldsymbol{T_6}$ (°C)	32.00	32.00	Input
Turbine isentropic efficiency, $\boldsymbol{\eta_t}$ (%)	93	93	Input
Compressor isentropic efficiency, $\boldsymbol{\eta_c}$ (%)	89	89	Input
Receiver thermal power, $\boldsymbol{Q_{rec,\,sCO_2}}$ (MW_{th})	330.00	327.17	0.85
Thermal efficiency of the cycle,	40.40	40.75	-0.86
Turbine inlet temperature, $\boldsymbol{T_1}$ (°C)	550.00	556.00	1.09

5.2 Discussion

The results presented below includes the results of the energy and exergy and discussion driven from the analysis results of all the 3 three models. Those results are plotted in graphically format for easier presentation and comparison across important variations as it presented in coming plots. Furthermore, the impact of the integrated CSP system has been assessed and its impact on the fuel and oxygen consumption powering the combustion process has been presented. In addition, all states main components and its power requirement (like pumps and compressors works as an example) are presented in this section.

It was resulted that higher the maximum pressure in the $\mathbf{sCO_2}$ power cycle (Turbine Inlet Pressure - TIP), the higher the thermal efficiency of the cycle with a maximum of 46% of thermal efficiency when the TIP is 300 bar considering CONF3

$\mathbf{sCO_2}$ power cycle. It was also noted that CONF2 and CONF3 power cycles have almost the same thermal efficiency (37%) with the Turbine Inlet Pressure is 200 bar and as the pressure increases the CONF3 power cycle thermal cycles increases as it reaches a maximum of 46% at 300 bar. Figure 49 below presents the relationship between the thermal efficiency and the maximum pressure across all the three investigated $\mathbf{sCO_2}$ cycle's configuration.

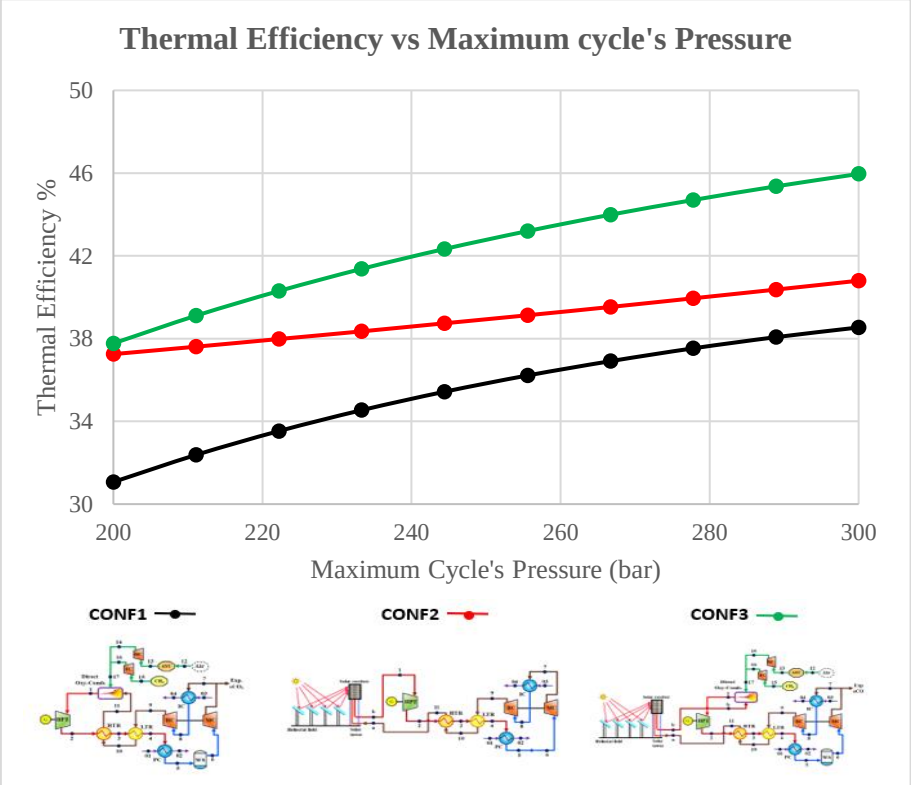

Figure 48. Thermal efficiency vs. maximum cycle's pressure.

The effect of the cycle's maximum pressure in the exergy efficiency of the cycle has been investigated. It was resulted that CONF3 cycle has the highest exergy efficiency in comparison to other investigated cycle configurations with an efficiency of 83.3% at a maximum pressure of 200 bar. It was noted that the exergy efficiency decreases by the increment of the cycle maximum pressure. This is due to the energy

losses that increases by the increment of high pressure. However, it is worth mentioning that the negative slope in the CONF1 and CONF3 cycle configurations is minimum, whereas in CONF2 cycle configuration exergy efficiency is badly affected by the increase of the maximum cycle's pressure. In other words, to maintain the exergy efficiency at its maximum, the cycle's highest pressure shall be reduced to the minimum although this will affect the thermal efficiency of the cycle, accordingly a compromising maximum cycle's pressure to be defined to consider the cycle's maximum thermal and exergy efficiencies. Figure 49 reflects the relationship between the cycle's maximum pressure (TIP) and its exergy efficiency.

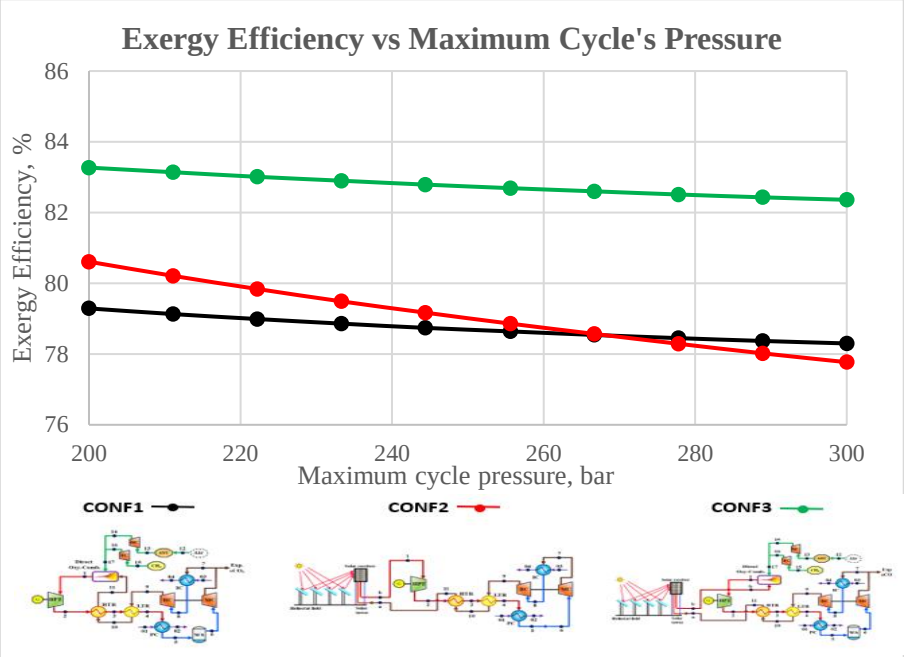

Figure 49. Exergy efficiency vs. maximum cycle's pressure

The effect of the minimum cycle's temperature on the thermal and exergy efficiencies has been investigated across all three investigated $\mathbf{sCO_2}$ power cycle configurations. It was found that the thermal efficiency decreases when the cycle's minimum temperature increases and this confirms the positive impact of the

intercooling cycle configurations as the $\mathbf{sCO_2}$ gets compressed with the lowest cycle's temperature which results in minimizing the load on the compressor. Furthermore, it was resulted that introduction of the oxy combustor (in CONF3 and CONF1) helped the power cycles to slightly reduce the effect of the minimum cycle's temperature on in the thermal as presented in Figure 50.

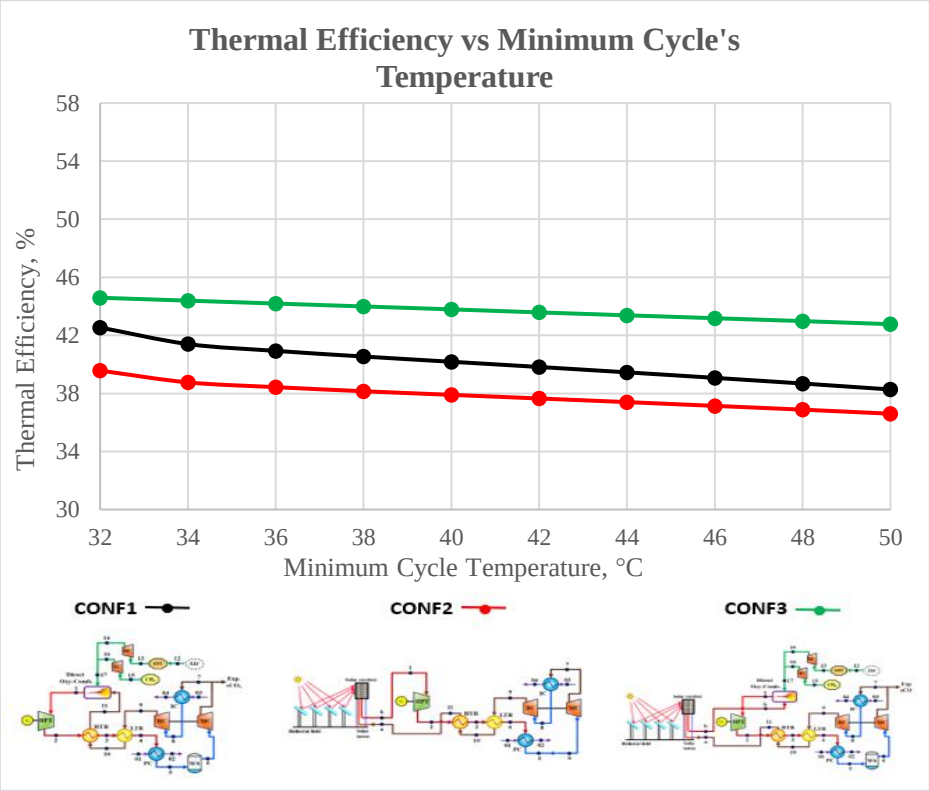

Figure 50. Thermal efficiency vs. minimum cycle's temperature (°C)

Figure 51 represents the relationship between the minimum cycle's temperature and the cycle's exergy efficiency. It was resulted that the cooler cycle's temperature achieves the highest cycle's efficiency. CONF3 cycle configuration was found to achieve the highest exergy efficiency in the same minimum cycle's temperature in comparison to CONF1 and CONF2 cycle configurations. CONF3 achieved exergy efficiency of 83.24% at temperature of 32°C (before the Main Compressor).

Figures 50 and 51 represents the relationship between the cycle's minimum temperature and its affect to the thermal and exergy efficiencies of the cycles and accordingly the systems shall be designed in an optimum minimum temperature considering the thermal and exergy efficiencies, cooling loads, compressors optimum compression temperature, waster separator design and exported $\mathbf{sCO_2}$.

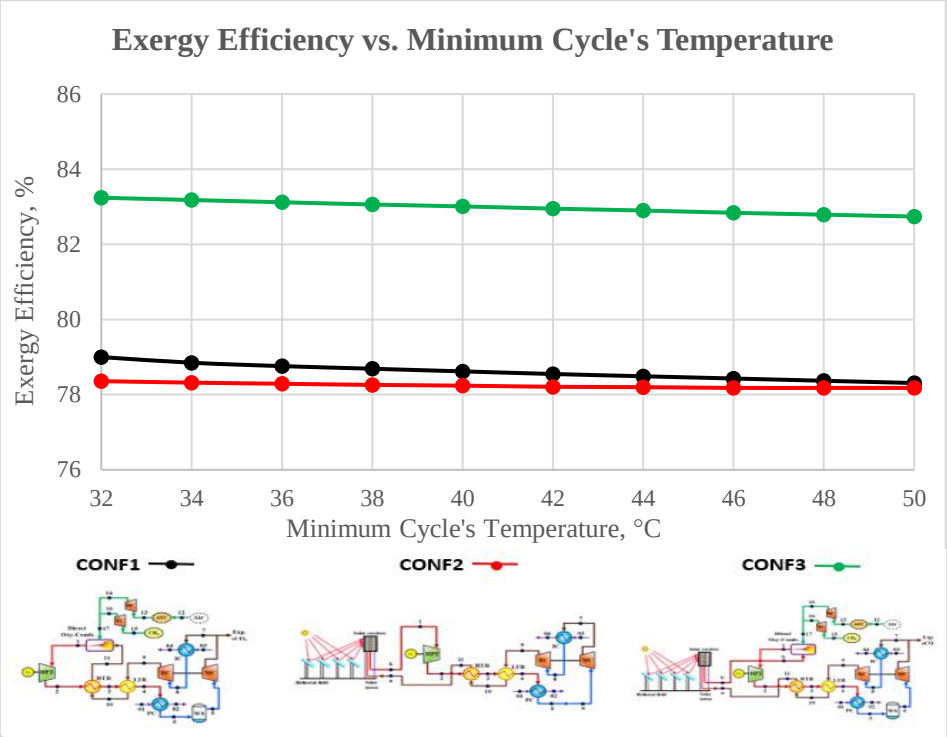

Figure 51. Exergy efficiency vs. minimum cycle's temperature (°C)

As it was found in the literature review that the recuperators play an important role to the efficiency of $\mathbf{sCO_2}$ power cycles, an investigation in the intermediate pressure (HTR and LTR) and its impact on the thermal and exergy efficiencies of the cycles, it was noted that the higher the intermediate pressure, the thermal efficiency of the cycle is positively impacted. The highest impact was observed at CONF1 and CONF2 cycle configuration in the which the increment of the intermediate pressure from 85 to 110 bar will results in increase of the thermal efficiency of CONF1 and

CONF2 from 34% to almost 39% (an increase of 5%). On the other hand, the higher the intermediate cycle pressure have a minimum impact to the cycle's thermal efficiency. To keep it in prospective, the increase of the intermediate pressure from 85 to 110 bar, the thermal efficiency of the cycle increases from 41.7% to 42.7% (enhancement of ~ 1%). Figure 53 presents the relationship between the intermediate cycle pressure and thermal efficiency across the range between 85 to 110 bar.

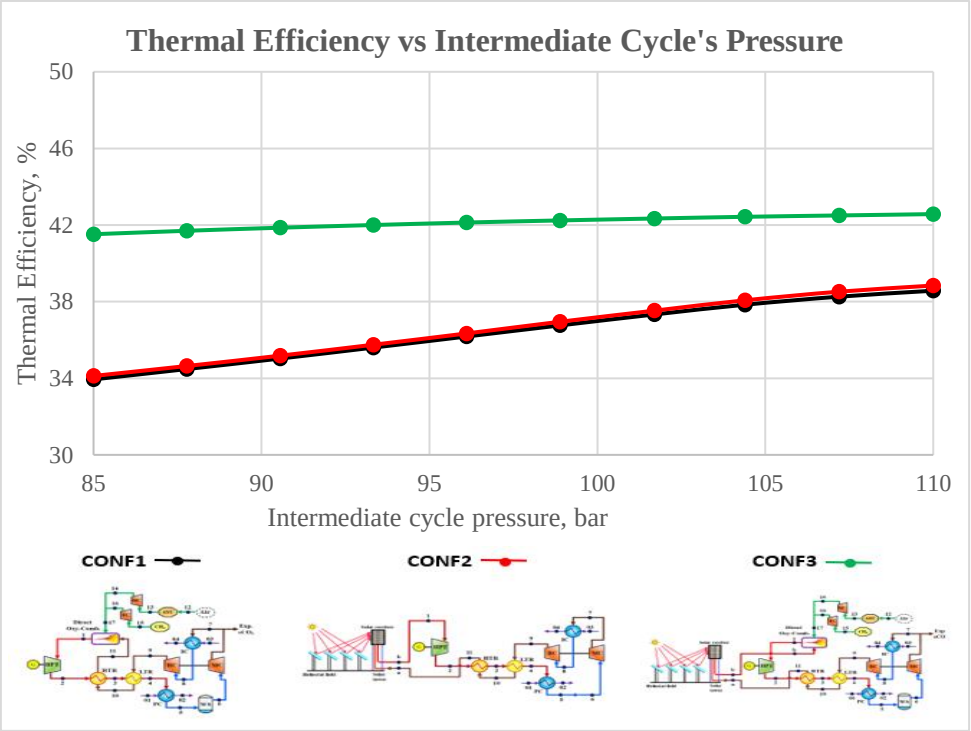

Figure 52. Thermal efficiency vs. intermediate cycle's pressure

On the other hand, an analysis was conducted on the effect of the intermediate cycle's pressure and its impact on the exergy efficiency of each cycle configuration. In general, it was noted in CONF1 and CONF3 $\mathbf{sCO_2}$ cycle configurations that the higher the intermediate cycle pressure, the higher is the exergy efficiency is achieved, however it is negative relationship when it comes to CONF2 $\mathbf{sCO_2}$ cycle configuration (Figure 53).

In CONF1 $\mathbf{sCO_2}$ cycle configuration, the pressurization of the intermediate cycle pressure from 85 to 96 bar didn't have any impact on the cycle efficiency (constant exergy efficiency at 77.1%), however, a drastic increase was noticed in the exergy efficiency when the intermediate cycle pressure increases beyond the 96 bar to 99 bar in which the exergy efficiency increases from 77.1% to 78.3% and then stays constant regardless of the increases of the intermediate cycle pressure up to 110 bar.

In CONF2 $\mathbf{sCO_2}$ cycle configuration, it was noted that the exergy efficiency continuously decreases when the intermediate cycle pressure increases (negative slope). It was recorded that when the cycle's intermediate pressure is at 85 bar, the recorded exergy efficiency is almost 78.8%. However, by the increases of the intermediate cycle pressure it was noted that the exergy efficiency decreases until it reaches 77.7% when the intermediate pressure is considered at 110 bar. This cycle has similar relationship to the one presented in Figure 49 which represents the relationship between the exergy efficiency and maximum cycle pressure.

In CONF3 $\mathbf{sCO_2}$ cycle configuration, a slight constant increase was noticed in the exergy efficiency of the cycle by the increment of the cycle's intermediate pressure. At an intermediate cycle's pressure, the exergy efficiency found equals to 81.8%. However, it was noticed that by the increase of the cycle's intermediate pressure, it the cycle's exergy efficiency increases too which reaches to an efficiency of 82.3% at 110 bar of cycle's intermediate pressure. Figure 53 illustrates the relationship between the intermediate pressure and the cycle's exergy efficiency.

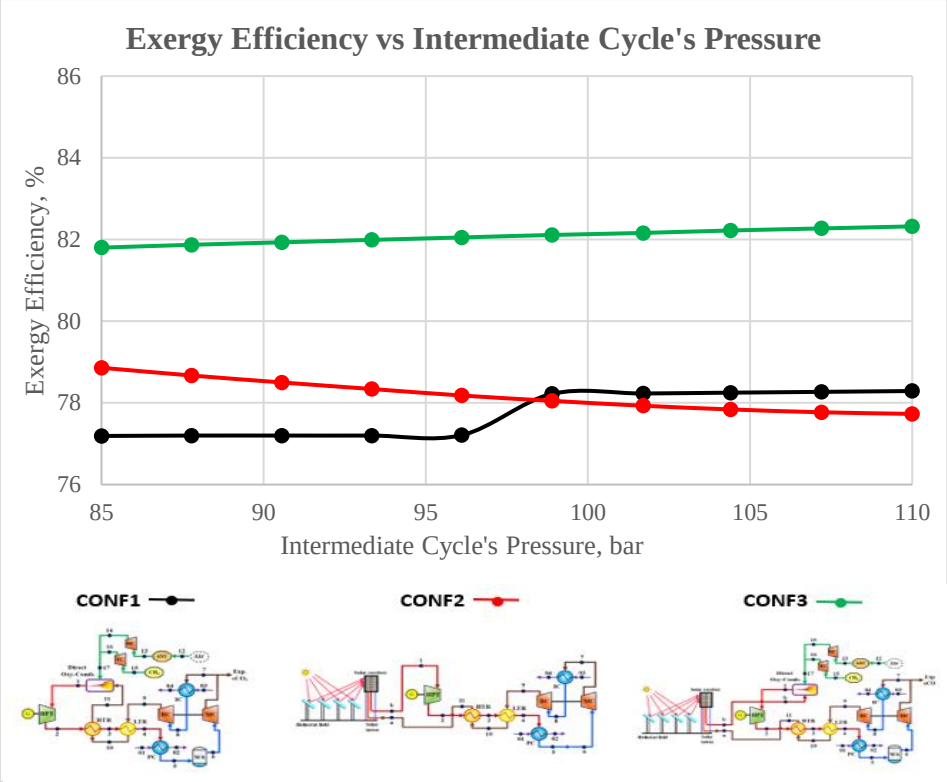

Figure 53. Exergy efficiency vs. intermediate cycle pressure

As a part of the analysis conducted on the investigated $\mathbf{sCO_2}$ cycle configurations, an investigation was conducted on the effect of the solar radiation and its impact on the thermal and exergy efficiency of the $\mathbf{sCO_2}$ power cycles.

It was observed that the increase of the solar radiation contributes to the increase thermal efficiency of the CONF2 and CONF3 $\mathbf{sCO_2}$ cycle configurations (Figure 55). In other words, it is a positive relationship between the solar radiation and thermal efficiency of the cycle. This is an expected behavior as the solar radiation adds thermal load to the investigated cycle which will contribute to the enhancement of the cycle's efficiency. As CONF3 is integrated with an oxy combustor, its thermal efficiency is slightly higher than CONF2 cycle which at 400 W/$\boldsymbol{m^2}$ of solar radiation, CONF2 achieved 18.7% of thermal efficiency whereas CONF3 achieved 36.2%. However, both thermal efficiencies increase by the increment of the solar radiation, CONF2 achieves

40.25% of thermal efficiency and CONF3 achieves 48.75% of thermal efficiency at a solar radiation of 800 W/$\boldsymbol{m^2}$. On the other hand, the relationship between the solar radiation and its effect on the exergy efficiency of $\boldsymbol{sCO_2}$ power cycle configurations. It noted that the exergy efficiency decreases by the increases of the solar radiation at the CSP system. it was noted that when the solar radiation is at 400 W/$\boldsymbol{m^2}$ (at the minimum), the exergy efficiency of CONF2 is at 83.31% and CONF3 is at 84.3%. However, when the solar radiation increases to 800 W/$\boldsymbol{m^2}$, the exergy efficiency was noticed to be negatively impacted where the exergy efficiency of CONF2 is 78.65% and CONF3 is 83.39%. Figure 55 illustrates the relationship between the cycle's exergy efficiency and solar radiation.

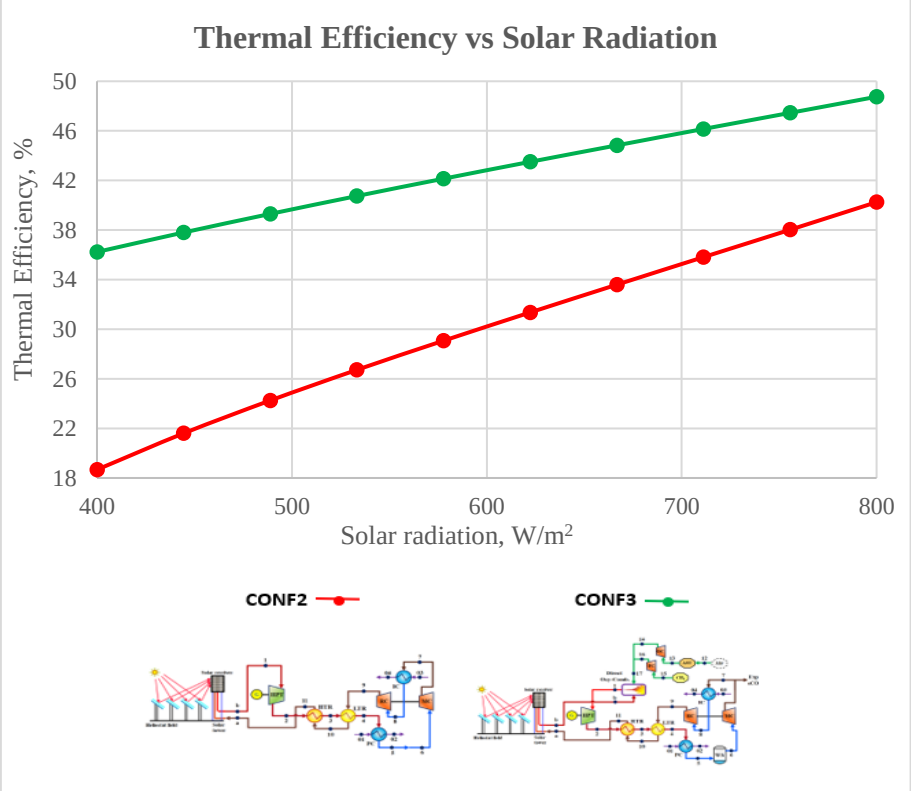

Figure 54. Thermal efficiency vs. solar radiation

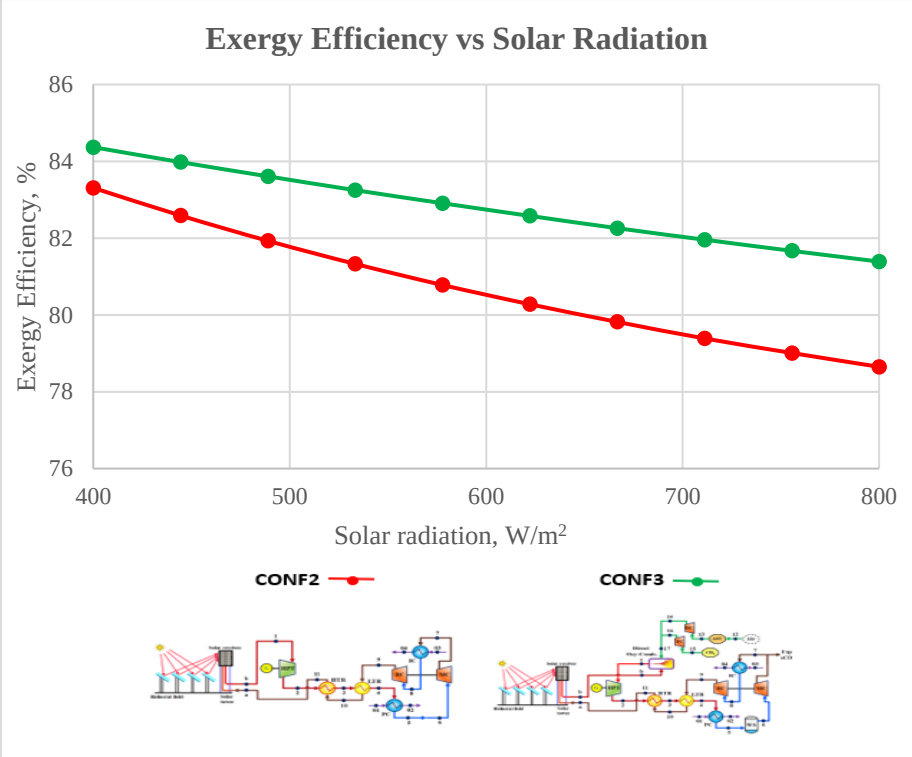

Figure 55. Exergy efficiency vs. solar radiation

Note: CONF1 is excluded from this comparison analysis (Figures 54 and 55) as it solely depends on the oxy combustor and doesn't dependent on CSP-PT Solar technology like CONF2 and CONF3.

From the above analysis, it is clear that the CONF3 model is most efficient cycle configuration among the investigated cycles. Furthermore, its flexibility in managing the thermal heat collected via the CSP without the need of thermal storage was found to be promising and with relatively simpler design. The CSP plays a crucial role in enhancing the thermal efficiency of the cycle. Figure 56 presents the relationship between the thermal/exergy efficiency and the CSP outlet temperature.

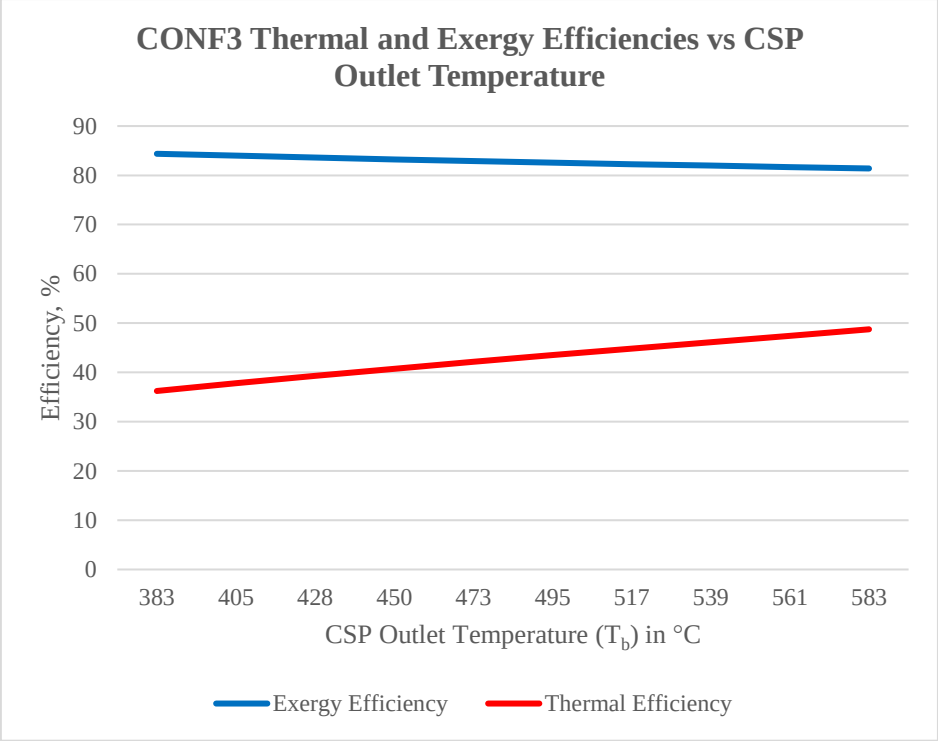

Figure 56. CONF3 thermal and exergy efficiency vs. CSP outlet temperature

Further to the above analysis of the thermal and exergy efficiencies, the effect of receiver temperature and how the intensity of the solar radiation will affect the receiver temperature at the CSP system are investigated. In CONF2 cycle configuration the heat gained at the CSP power tower heats the $\mathbf{sCO_2}$ within the cycle which is sent directly to the turbine for the expansion process. Accordingly defining the optimum receiver temperature in CONF2 cycle configuration directly depends on the optimum turbine inlet temperature. On the other hand, in CONF3 cycle configuration, the receiver temperature is used to heat the $\mathbf{sCO_2}$ (as a pre-heater) in which it will be sent to the oxy combustor for further heating as a preparation to the expansion process. The heat gained at the receiver will positively contribute to the cycle efficiency and reduce its fuels consumption as presented in Table 5 below (in comparison to CONF1 cycle).

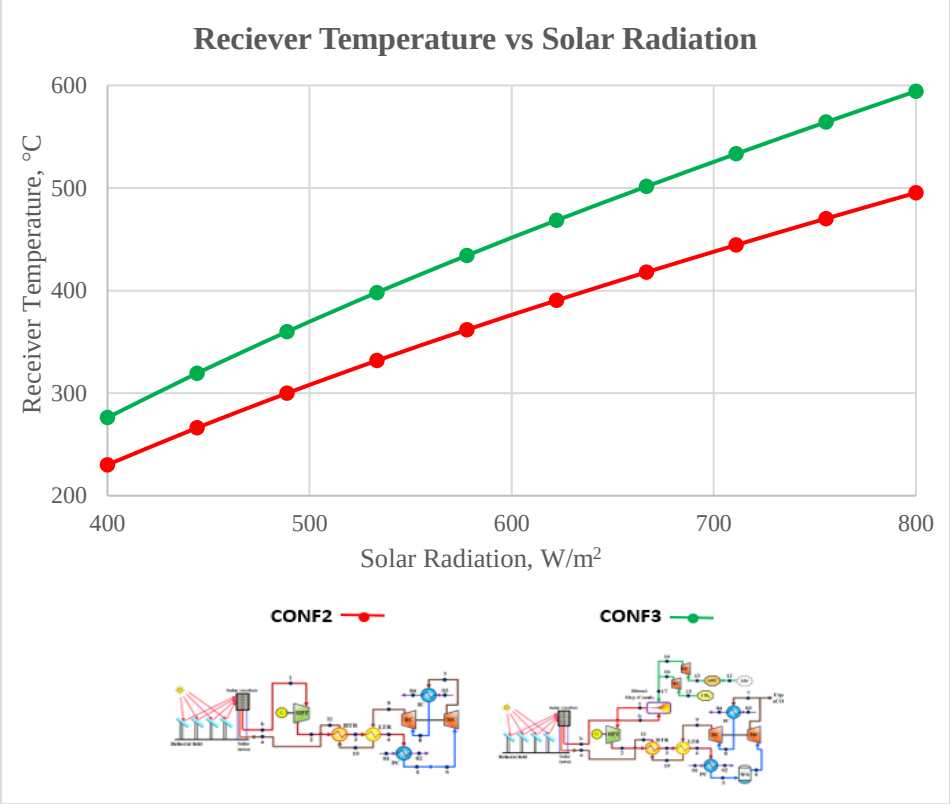

Figure 57. Reciever temperature vs. solar radiation

In CONF3 cycles configurations and in relation to the above Figures, it was concluded that the increase of the solar radiation and receiver temperature contributes positively to the thermal and exergy efficiency of the cycle in addition to increase the receiver temperature, this will contribution will reflect in the cycle's dependency on fuel and pure oxygen (heat load required by the oxy combustor). In other words, the higher the Solar Radiations (and subsequently the CSP outlet temperature $\boldsymbol{T_b}$), the lower cycle dependency on fuel and Oxygen to heat up the $\mathbf{sCO_2}$ at the desired TIT at the oxy combustor and accordingly the amount of newly generated $\mathbf{sCO_2}$ is shrinking too as a result of lesser burning of fuel and oxygen at the oxy combustor. Figure 58 below represents the variations of fuel and oxygen consumption in addition to the generated $\mathbf{CO_2}$.

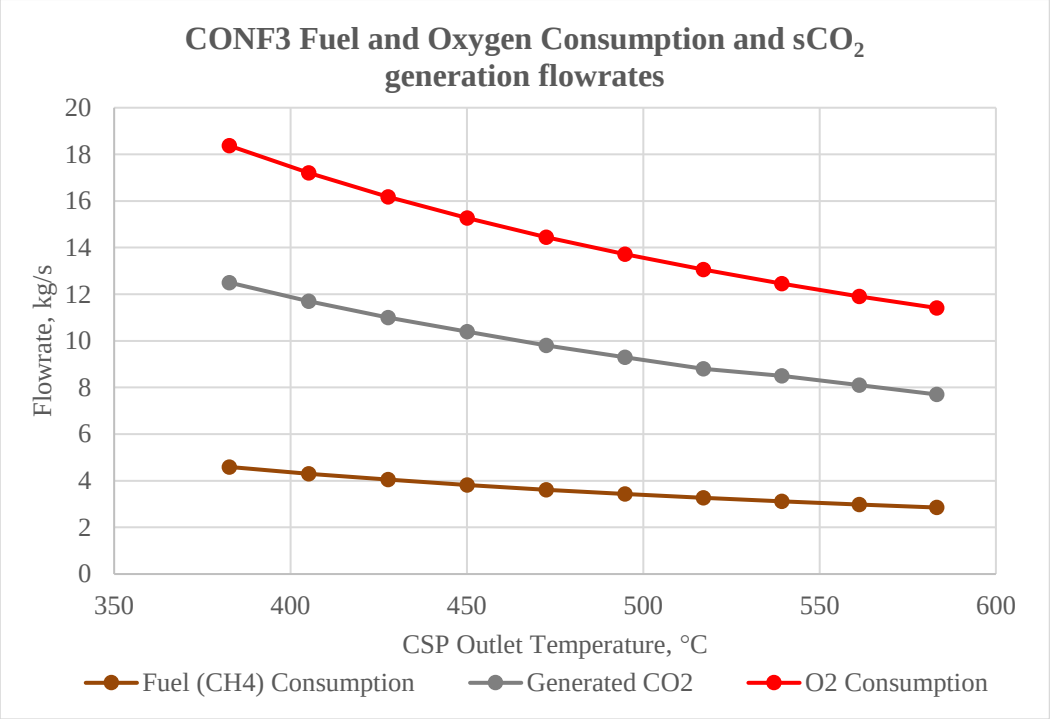

Figure 58. CONF3 fuel and oxygen consumption and $\mathbf{sCO_2}$ generation flowrate

Following the above analysis, it was noted that CONF3 is has a better potential, higher efficiencies, lower fuel/oxygen dependency in addition of the by-production potable water and CO_2 for further export (unlike CONF2 for example). As a part of the detailed comparison across the investigated configurations, Table 7 below presents cycle's configuration state physical condition for the sake of comparison, validation, and assessment.

Table 7. Comparison between $\mathbf{sCO_2}$ cycle configurations

Category	CONF1			CONF2			CONF3		
	T (°C)	P (bar)	**E** ($\mathbf{sCO_2}$)	T (°C)	P (bar)	**E** ($\mathbf{sCO_2}$)	T (°C)	P (bar)	**E** ($\mathbf{sCO_2}$)
1	619	250	360062	705	250	325154	1125	250	292400
2 ($\boldsymbol{T_{2a}}$)	470.3	73.5	252858	545.5	73.5	230256	890.4	73.5	215493
2 ($\boldsymbol{T_{2s}}$)	459.1	73.5	252858	533.5	73.5	230256	874.6	73.5	215493
4	267	73.5	182009	293.1	73.5	153108	435.5	73.5	111624
6	32	73.5	144178	32	73.5	116463	32	73.5	67359
7 ($\boldsymbol{T_{7a}}$)	80.76	135.6	167047	80.76	135.6	134936	80.76	135.6	78043
7 ($\boldsymbol{T_{7s}}$)	75.39	135.6	167047	75.39	135.6	134936	75.39	135.6	78043
8	32	135.6	161987	32	250	132976	32	135.6	75680

Category	CONF1			CONF2			CONF3		
	T (°C)	P (bar)	**E** ($\mathbf{sCO_2}$)	T (°C)	P (bar)	**E** ($\mathbf{sCO_2}$)	T (°C)	P (bar)	**E** ($\mathbf{sCO_2}$)
9 ($\boldsymbol{T_{9a}}$)	80.89	250	184429	80.89	80.89	151399	80.89	250	86164
9 ($\boldsymbol{T_{9s}}$)	75.51	250	184429	75.51	75.51	151399	75.51	250	86164
11	420.3	250	0	495.5	250	245848	840.4	250	218105
14	250	250	0	350	250	0	250	250	2530
16	250	250	0	350	250	0	250	250	1656
TIT	620.3 °C			658 °C			1125 °C		
$\boldsymbol{W_{fuel}}$	1978 KW			0 KW			953.7 KW		
$\boldsymbol{W_{o2}}$	2900 KW			0 KW			1398 KW		
$\boldsymbol{W_{MC}}$	25315 KW			20449 KW			11827 KW		
$\boldsymbol{W_{RC}}$	24866 KW			20413 KW			11617 KW		
$\boldsymbol{W_{turbine}}$	106605 KW			92408 KW			77343 KW		
Net Power	51546 KW			51546 KW			51547 KW		
$\boldsymbol{\dot{m}_{fuel}}$	3.411 kg/s			0 kg/s			1.645 kg/s		
$\boldsymbol{\dot{m}_{oxygen}}$	13.64 kg/s			0 kg/s			6.579 kg/s		
$\boldsymbol{\dot{m}_{WV}}$	7.752 kg/s			0 kg/s			3.621 kg/s		
$\boldsymbol{\dot{m}_{CO2\ Export}}$	9.6 kg/s			0 kg/s			4.5 kg/s		
$\boldsymbol{\dot{m}_{CO2\ Overall}}$	596.3 kg/s			481.7 kg/s			278.6 kg/s		
$\Sigma_{thermal}$	35.3 %			38.9 %			42.4 %		
$\Sigma_{Overall}$	78.7%			79.1 %			82.77 %		

CHAPTER 6: CONCLUSIONS, RECOMMENDATIONS AND FUTURE WORK

6.1 Conclusions and recommendations

Three different sCO_2 cycle configurations integrated with CSP and oxy combustor were investigated, and energy and exergy analyses were performed. The first investigated cycle (CONF1) was solely depending on the oxy combustor to heat the sCO_2 to its supercritical region and turn the turbine blades (Figure 43). The secondly investigated cycle (CONF2) solely depends on the CSP-PT to heat the sCO_2 to its supercritical region and run the turbine blades (Figure 46). The third cycle investigated in an integration of the mentioned above cycles where this cycle (CONF3) has the CSP-PT function as a pre-heater where the sCO_2 is heated further in the oxy combustor as a preparation for further expansion process in the turbine (Figure 47).

The utilization of sCO_2 as working fluid contribute to the world's effort (led by the UN Paris Agreement Framework) in reducing the carbon emissions by utilizing the sCO_2 as a working fluid to run the turbine. Furthermore, the newly generated sCO_2 from the combustion is being captured and exported for further industrial use such as working fluid for pumping and manufactured products.

CONF3 cycle configuration resulted in a very promising results whereas the combination of the CSP-PT and the oxy combustor improved the cycle's thermal and exergy efficiency as presented in the above results. The proposed cycle is a hybrid cycle, which overcomes the problem of the power intermediacy of the renewable energy without badly effecting the project's investment cost by integrating a storage facility (thermal or batteries storages), which will turn the project into a complex cycle. At TIP of 250 bar, the cycle achieved an exergy efficiency of 82.7% and thermal efficiency of 42.4%. As this cycle configuration depends on the solar power to preheat the sCO_2 before entering the oxy combustor. The impact of the solar power was measured in

terms of thermal and exergy efficiency of the proposed CONF3 cycle. At receiver temperature (T_b) of 700°C, the cycle achieved thermal efficiency of 43.38% and exergy efficiency of 82.36%. The receiver temperature of 700°C is achieved with a solar radiation of 651.8 W/m^2. This system was found to be reliable and efficient as the system will instantly function according to the available thermal solar power (via CSP-PT) and the oxygen/fuel consumption will vary accordingly. The main conclusions are:

1- CONF3 cycle configuration was found to be the most efficient cycle where it achieved thermal efficiency of 42.4% (whereas CONF1 achieved 35.4% and CONF2 achieved 38.97%) and exergy efficiency of 82.77% (whereas CONF1 achieved 78.73% and CONF2 achieved 79.08%).

2- This cycle configuration overcome the intermediacy and the inconsistency of the CSP (and renewables in general) without batteries or thermal storages.

3- By-product of this cycle is potable water which contributes to communities suffering from water scarcity or isolated/remote locations from potable water sources [8]. Furthermore, another by-product of the cycle is the sCO_2 which is exported from the cycle for further applications.

4- The combination of CSP and oxy combustor reduces the cycle dependency on fuel and oxygen and subsequently believed to reduces the LCOE too.

5- This proposed cycle configuration has a potential to be easily integrated with other energy sources like waste heat and geothermal when available.

Based on the obtained results, the novel CONF3 cycle configuration was found promising with high potential to contribute to the reduction of CO_2 emissions by utilizing renewable energy technologies without storage facility. It is believed that this proposed cycle configuration will bridge the current technological gap to the full transformation into renewables.

6.2 Future work

As this study is still on development stage, the following areas are highlighted for future work, researches, and potential improvements:

- Investigation to be conducted on the reason behind the sudden increase in the exergy efficiency of the CONF1 cycle in between 96 – 98 bars of intermediate pressure. If this increase in the exergy efficiency can be expedited, it will have a positive impact on the overall efficiency (Figure 53).
- LOCE can be calculated for all the 3 investigated configurations and compared to the existing conventional power generation technologies LOCE.
- A pilot project can be funded and built for the experimental analysis.
- Investigation of alternative cycle configurations that could contribute to the enhancement of the cycle thermal and exergy efficiency, while reducing the fuel and oxygen consumption.
- ASU can be investigated for further improvement as the current ASU technology is very energy intensive process which consumes around 5 – 10% of the cycle's consumed power.
- Further improvements on the CSP-PT technology to reach a receiver temperature of around 1000°C to achieve higher efficiencies.

REFERENCES

[1] P.D.I. Bari, Performance of a 50 Mw, (2011).

[2] IEA, World gross electricity production, by source, 2018, Int. Energy Agency. (2020). https://www.iea.org/data-and-statistics/charts/world-gross-electricity-production-by-source-2018.

[3] M. Shublaq, A.K. Sleiti, Experimental analysis of water evaporation losses in cooling towers using filters, Appl. Therm. Eng. 175 (2020) 115418. https://doi.org/10.1016/j.applthermaleng.2020.115418.

[4] A.K. Sleiti, W.A. Al-Ammari, M. Al-Khawaja, A novel solar integrated distillation and cooling system – Design and analysis, Sol. Energy. 206 (2020) 68–83. https://doi.org/10.1016/j.solener.2020.05.107.

[5] A.K. Sleiti, W.A. Al-Ammari, M. Al-Khawaja, Review of innovative approaches of thermo-mechanical refrigeration systems using low grade heat, Int. J. Energy Res. 44 (2020) 9808–9838. https://doi.org/10.1002/er.5556.

[6] A.K. Sleiti, M. Al-Khawaja, W.A. Al-Ammari, A combined thermo-mechanical refrigeration system with isobaric expander-compressor unit powered by low grade heat – Design and analysis, Int. J. Refrig. 120 (2020) 39–49. https://doi.org/10.1016/j.ijrefrig.2020.08.017.

[7] A.K. Sleiti, Isobaric Expansion Engines Powered by Low-Grade Heat—Working Fluid Performance and Selection Database for Power and Thermomechanical Refrigeration, Energy Technol. 8 (2020) 2000613. https://doi.org/10.1002/ente.202000613.

[8] A.K. Sleiti, H. Al-Khawaja, H. Al-Khawaja, M. Al-Ali, Harvesting water from air using adsorption material – Prototype and experimental results, Sep. Purif. Technol. 257 (2021). https://doi.org/10.1016/j.seppur.2020.117921.

[9] A.K. Sleiti, W.A. Al-Ammari, M. Al- Khawaja, Analysis of Novel Regenerative Thermo-Mechanical Refrigeration System Integrated With Isobaric Engine, J. Energy Resour. Technol. 143 (2021) 052103. https://doi.org/10.1115/1.4049368.

[10] G. Takalkar, A.K. Sleiti, Comprehensive performance analysis and optimization of 1,3-dimethylimidazolylium dimethylphosphate-water binary mixture for a single effect absorption refrigeration system, Front. Energy. (2021) 1–15. https://doi.org/10.1007/s11708-021-0720-9.

[11] M. Elbeih, A.K. Sleiti, Analysis and Optimization of Concentrated Solar Power Plant for Application in Arid Climate, Energy Sci. Eng. 2021 (2021) 1–14. https://doi.org/10.1002/ese3.742.

[12] K.A.R.S. Perera, K.H.W.L. De Silva, M.D. Amarasinghe, Potential impact of predicted sea level rise on carbon sink function of mangrove ecosystems with special reference to Negombo estuary, Sri Lanka, Glob. Planet. Change. 161 (2018) 162–171. https://doi.org/10.1016/j.gloplacha.2017.12.016.

[13] W. Qi, J. Liu, F. Leung, A framework to quantify impacts of elevated CO 2 concentration, global warming and leaf area changes on seasonal variations of water resources on a river basin scale, J. Hydrol. 570 (2019) 508–522. https://doi.org/10.1016/j.jhydrol.2019.01.015.

[14] L. Cozzi, T. Gould, S. Bouckart, D. Crow, T.-Y. Kim, C. McGlade, P. Olejarnik, B. Wanner, D. Wetzel, World Energy Outlook 2020, 2050 (2020) 1–461.

[15] U. Collier, Progress wiht solar heat in India, Int. Energy Agency. (2018). https://www.iea.org/commentaries/progress-with-solar-heat-in-india.

[16] IEA, Renewables 2018, Int. Energy Agency. (2018). https://www.iea.org/reports/renewables-2018.

[17] R.J. Allam, J.E. Fetvedt, B.A. Forrest, D.A. Freed, The OXY-fuel, supercritical CO2 allam cycle: New Cycle Developments to Produce Even Lower-Cost Electricity From Fossil Fuels Without Atmospheric Emissions, ASME Turbo Expo 2014 Turbine Tech. Conf. Expo. (2014) 9. https://doi.org/10.1115/GT2014-26952.

[18] M.J. Li, H.H. Zhu, J.Q. Guo, K. Wang, W.Q. Tao, The development technology and applications of supercritical CO2 power cycle in nuclear energy, solar energy and other energy industries, Appl. Therm. Eng. 126 (2017) 255–275. https://doi.org/10.1016/j.applthermaleng.2017.07.173.

[19] A.K. Sleiti, W.A. Al-ammari, Direct-fired oxy-fuel combustion supercritical CO 2 power cycle with novel preheating configurations, (2020) 1–24.

[20] F. Crespi, G. Gavagnin, D. Sánchez, G.S. Martínez, Supercritical carbon dioxide cycles for power generation: A review, Appl. Energy. 195 (2017) 152–183. https://doi.org/10.1016/j.apenergy.2017.02.048.

[21] V. Dostal, D. MJ, H. P.A, A supercritical carbon dioxide cycle for next generation nuclear reactors, MIT-ANP-TR-100, advanced nuclear power technology program report. Cambridge (MA): Massachusetts Institute of Technology, (2004).

[22] Y. Liu, Y. Wang, D. Huang, Supercritical CO2 Brayton cycle: A state-of-the-art review, Energy. 189 (2019) 115900. https://doi.org/10.1016/j.energy.2019.115900.

[23] E.G. Feher, The supercritical thermodynamic power cycle, Energy Convers. 8 (1968) 85–90. https://doi.org/10.1016/0013-7480(68)90105-8.

[24] M. Quero, R. Korzynietz, M. Ebert, A.A. Jiménez, A. Del Río, J.A. Brioso, Solugas - Operation experience of the first solar hybrid gas turbine system at

MW scale, Energy Procedia. 49 (2014) 1820–1830. https://doi.org/10.1016/j.egypro.2014.03.193.

[25] A.J. Sánchez, A.J. Gallego, J.M. Escaño, E.F. Camacho, Parabolic Trough Collector Defocusing Analysis: Two control stages vs four control stages, Sol. Energy. 209 (2020) 30–41. https://doi.org/10.1016/j.solener.2020.09.001.

[26] J. Guo, Design analysis of supercritical carbon dioxide recuperator, Appl. Energy. 164 (2016) 21–27. https://doi.org/10.1016/j.apenergy.2015.11.049.

[27] A.K. Sleiti, W.A. Al-Ammari, Energy and exergy analyses of novel supercritical CO2 Brayton cycles driven by direct oxy-fuel combustor, Fuel. (2021) 120557. https://doi.org/https://doi.org/10.1016/j.fuel.2021.120557.

[28] D. Vaclav, D. Jan, Supercritical CO2 Regeneration Bypass Cycle - Comparison to Traditional Layouts, Optimization. (2011) 2021.

[29] C.M. Invernizzi, Prospects of mixtures as working fluids in real-gas Brayton cycles, Energies. 10 (2017). https://doi.org/10.3390/en10101649.

[30] Y. Ma, M. Liu, J. Yan, J. Liu, Thermodynamic study of main compression intercooling effects on supercritical CO2 recompression Brayton cycle, Energy. 140 (2017) 746–756. https://doi.org/10.1016/j.energy.2017.08.027.

[31] J.D. Osorio, R. Hovsapian, J.C. Ordonez, Dynamic analysis of concentrated solar supercritical CO2-based power generation closed-loop cycle, Appl. Therm. Eng. 93 (2016) 920–934. https://doi.org/10.1016/j.applthermaleng.2015.10.039.

[32] J. Floyd, N. Alpy, A. Moisseytsev, D. Haubensack, G. Rodriguez, J. Sienicki, G. Avakian, A numerical investigation of the sCO2 recompression cycle off-design behaviour, coupled to a sodium cooled fast reactor, for seasonal variation in the heat sink temperature, Nucl. Eng. Des. 260 (2013) 78–92. https://doi.org/10.1016/j.nucengdes.2013.03.024.

[33] L.F. González-Portillo, J. Muñoz-Antón, J.M. Martínez-Val, Supercritical carbon dioxide cycles with multi-heating in Concentrating Solar Power plants, Sol. Energy. 207 (2020) 144–156. https://doi.org/10.1016/j.solener.2020.06.066.

[34] R.V. Padilla, Y.C. Soo Too, R. Benito, W. Stein, Exergetic analysis of supercritical CO2 Brayton cycles integrated with solar central receivers, Appl. Energy. 148 (2015) 348–365. https://doi.org/10.1016/j.apenergy.2015.03.090.

[35] K. Wang, M.J. Li, J.Q. Guo, P. Li, Z. Bin Liu, A systematic comparison of different S-CO2 Brayton cycle layouts based on multi-objective optimization for applications in solar power tower plants, Appl. Energy. 212 (2018) 109–121. https://doi.org/10.1016/j.apenergy.2017.12.031.

[36] A. McClung, K. Brun, L. Chordia, Technical and economic evaluation of supercritical oxy-combustion for power generation, Fourth Supercrit. CO 2 Power Cycles Symp. Pittsburgh, PA, Sept. (2014) 9–10. http://sco2symposium.com/www2/sco2/papers2014/systemConcepts/40-McClung.pdf.

[37] Y. Ahn, S.J. Bae, M. Kim, S.K. Cho, S. Baik, J.I. Lee, J.E. Cha, Review of supercritical CO2 power cycle technology and current status of research and development, Nucl. Eng. Technol. 47 (2015) 647–661. https://doi.org/10.1016/j.net.2015.06.009.

[38] D. Luo, D. Huang, Thermodynamic and exergoeconomic investigation of various SCO2 Brayton cycles for next generation nuclear reactors, Energy Convers. Manag. 209 (2020) 112649. https://doi.org/10.1016/j.enconman.2020.112649.

[39] V. Dostal, A Supercritical Carbon Dioxide Cycle, Massachusetts Inst. Technol. Cambridge. (2004) 1–16.

[40] T. Neises, C. Turchi, A comparison of supercritical carbon dioxide power cycle configurations with an emphasis on CSP applications, Energy Procedia. 49 (2014) 1187–1196. https://doi.org/10.1016/j.egypro.2014.03.128.

[41] D. Thanganadar, F. Fornarelli, S. Camporeale, F. Asfand, K. Patchigolla, Off-design and annual performance analysis of supercritical carbon dioxide cycle with thermal storage for CSP application, Appl. Energy. 282 (2021) 116200. https://doi.org/10.1016/j.apenergy.2020.116200.

[42] K. Wang, Y.L. He, H.H. Zhu, Integration between supercritical CO2 Brayton cycles and molten salt solar power towers: A review and a comprehensive comparison of different cycle layouts, Appl. Energy. 195 (2017) 819–836. https://doi.org/10.1016/j.apenergy.2017.03.099.

[43] A. Moisseytsev, J.J. Sienicki, Investigation of alternative layouts for the supercritical carbon dioxide Brayton cycle for a sodium-cooled fast reactor, Nucl. Eng. Des. 239 (2009) 1362–1371. https://doi.org/10.1016/j.nucengdes.2009.03.017.

[44] K. Mohammadi, J.G. McGowan, Thermoeconomic analysis of multi-stage recuperative Brayton cycles: Part II – Waste energy recovery using CO 2 and organic Rankine power cycles, Energy Convers. Manag. 185 (2019) 920–934. https://doi.org/10.1016/j.enconman.2019.01.091.

[45] B. Stankovic, Brayton or Brayton-Rankine combined cycle with hot-gas recirculation and inverse mixing ejector, Am. Soc. Mech. Eng. Int. Gas Turbine Institute, Turbo Expo IGTI. 2 A (2002) 571–580. https://doi.org/10.1115/GT2002-30140.

[46] S. Son, J.Y. Heo, N. Il Kim, A. Jamal, J.I. Lee, Reduction of CO2 emission for solar power backup by direct integration of oxy-combustion supercritical CO2

power cycle with concentrated solar power, Energy Convers. Manag. 201 (2019) 112161. https://doi.org/10.1016/j.enconman.2019.112161.

[47] Z. Qiao, Y. Cao, P. Li, X. Wang, C.E. Romero, L. Pan, Thermoeconomic analysis of a CO2 plume geothermal and supercritical CO2 Brayton combined cycle using solar energy as auxiliary heat source, J. Clean. Prod. 256 (2020) 120374. https://doi.org/10.1016/j.jclepro.2020.120374.

[48] S. Peng, H. Hong, H. Jin, Z. Wang, An integrated solar thermal power system using intercooled gas turbine and Kalina cycle, Energy. 44 (2012) 732–740. https://doi.org/10.1016/j.energy.2012.04.063.

[49] Z. Qiao, Y. Tang, L. Zhang, C. Pan, C.E. Romero, X. Wang, J. Charles, F. Si, C. Rubio Maya, Design and performance analysis of a supercritical CO2 (sCO2)-water separator for power generation systems using hot sCO2 from geothermal reservoirs, Geothermics. 81 (2019) 123–132. https://doi.org/10.1016/j.geothermics.2019.05.001.

[50] A. Elson, R. Tidball, A. Hampson, Waste Heat to Power Market Assessment (Report No.ORNL/TM-2014/620), 2015. http://info.ornl.gov/sites/publications/files/Pub52953.pdf.

[51] M.T. White, G. Bianchi, L. Chai, S.A. Tassou, A.I. Sayma, Review of supercritical CO 2 technologies and systems for power generation , Appl. Therm. Eng. 185 (2021) 116447. https://doi.org/10.1016/j.applthermaleng.2020.116447.

[52] C. Mendez, G. Rochau, sCO2 Brayton cycle: Roadmap to sCO_2 power cycles NE commercial applications, (2018) SAND2018-6187.

[53] G. Sulzer, Verfahren zur Erzeugung von Arbeit aus Warme, 1950.

[54] J.R. Hoffmann, E.G. Feher, 150 kwe Supercritical Closed Cycle System, J. Eng.

Power. 93 (1971) 70–80. https://doi.org/10.1115/1.3445409.

[55] Y. Ahn, S.J. Bae, M. Kim, S.K. Cho, S. Baik, J.I. Lee, J.E. Cha, Cycle layout studies of S-CO 2 cycle for the next generation nuclear system application, Trans. Korean Nucl. Soc. Autumn Meet. Pyeongchang. (2014) 2–5.

[56] M.T. Islam, N. Huda, A.B. Abdullah, R. Saidur, A comprehensive review of state-of-the-art concentrating solar power (CSP) technologies: Current status and research trends, Renew. Sustain. Energy Rev. 91 (2018) 987–1018. https://doi.org/10.1016/j.rser.2018.04.097.

[57] M.B. ELBEH, Concentrated Solar Power Plant For Key Locations In Doha, Qatar Univ. 549 (2017) 40–42.

[58] J. Hernández-Moro, J.M. Martínez-Duart, Analytical model for solar PV and CSP electricity costs: Present LCOE values and their future evolution, Renew. Sustain. Energy Rev. 20 (2013) 119–132. https://doi.org/10.1016/j.rser.2012.11.082.

[59] J.A. Bennett, J. Fuhrman, T. Brown, N. Andrews, R. Fittro, A.F. Clarens, Feasibility of Using sCO2 Turbines to Balance Load in Power Grids with a High Deployment of Solar Generation, Energy. 181 (2019) 548–560. https://doi.org/10.1016/j.energy.2019.05.143.

[60] M.S. Khan, M. Abid, H.M. Ali, K.P. Amber, M.A. Bashir, S. Javed, Comparative performance assessment of solar dish assisted s-CO2 Brayton cycle using nanofluids, Appl. Therm. Eng. 148 (2019) 295–306. https://doi.org/10.1016/j.applthermaleng.2018.11.021.

[61] M. Petrollese, G. Cau, D. Cocco, The Ottana solar facility: dispatchable power from small-scale CSP plants based on ORC systems, Renew. Energy. 147 (2020) 2932–2943. https://doi.org/10.1016/j.renene.2018.07.013.

[62] A. Boretti, S. Castelletto, S. Al-Zubaidy, Concentrating solar power tower technology: Present status and outlook, Nonlinear Eng. 8 (2019) 10–31. https://doi.org/10.1515/nleng-2017-0171.

[63] A. Alami Merrouni, R. Conceição, A. Mouaky, H.G. Silva, A. Ghennioui, CSP performance and yield analysis including soiling measurements for Morocco and Portugal, Renew. Energy. 162 (2020) 1777–1792. https://doi.org/10.1016/j.renene.2020.10.014.

[64] T. Solar, P. Plant, M.I. Soomro, A. Mengal, Q.N. Shafiq, S. Aziz, U. Rehman, Performance Improvement and Energy Cost Reduction under Di ff erent Scenarios for a Parabolic, Processes. 7 (2019) 1–23.

[65] W. Al-Kouz, J. Nayfeh, A. Boretti, Design of a parabolic trough concentrated solar power plant in Al-Khobar, Saudi Arabia, E3S Web Conf. 160 (2020) 1–5. https://doi.org/10.1051/e3sconf/202016002005.

[66] E.M.A. Mokheimer, Y.N. Dabwan, M.A. Habib, Optimal integration of solar energy with fossil fuel gas turbine cogeneration plants using three different CSP technologies in Saudi Arabia, Appl. Energy. 185 (2017) 1268–1280. https://doi.org/10.1016/j.apenergy.2015.12.029.

[67] J. Muñoz-Antón, C. Rubbia, A. Rovira, J.M. Martínez-Val, Performance study of solar power plants with CO2 as working fluid. A promising design window, Energy Convers. Manag. 92 (2015) 36–46. https://doi.org/10.1016/j.enconman.2014.12.030.

[68] R. Valencia-Chapi, L. Coco-Enríquez, J. Muñoz-Antón, Supercritical CO2 mixtures for advanced brayton power cycles in line-focusing solar power plants, Appl. Sci. 10 (2020). https://doi.org/10.3390/app10010055.

[69] X. Wang, E.K. Levy, Investigation of Geothermal Heat Extraction Using

Supercritical Carbon Dioxide (sCO2) and Its Utilization in sCO2-based Power Cycles and Organic Rankine Cycles - A The rmodynamic & Economic Perspective, Mech. Eng. Doctor of (2018) 240.

[70] X. Wang, E.K. Levy, C. Pan, C.E. Romero, A. Banerjee, C. Rubio-Maya, L. Pan, Working fluid selection for organic Rankine cycle power generation using hot produced supercritical CO2 from a geothermal reservoir, Appl. Therm. Eng. 149 (2019) 1287–1304. https://doi.org/10.1016/j.applthermaleng.2018.12.112.

[71] L. Liu, Q. Yang, G. Cui, Supercritical carbon dioxide(S-co2) power cycle for waste heat recovery: A review from thermodynamic perspective, Processes. 8 (2020) 1–18. https://doi.org/10.3390/pr8111461.

[72] G. Manente, F.M. Fortuna, Supercritical CO2 power cycles for waste heat recovery: A systematic comparison between traditional and novel layouts with dual expansion, Energy Convers. Manag. 197 (2019) 111777. https://doi.org/10.1016/j.enconman.2019.111777.

[73] G. Manente, M. Costa, On the conceptual design of novel supercritical CO2 power cycles for waste heat recovery, ECOS 2019 - Proc. 32nd Int. Conf. Effic. Cost, Optim. Simul. Environ. Impact Energy Syst. (2019) 2219–2231.

[74] S.I. Schöffer, A solid oxide fuel cell- sCO2 Brayton cycle hybrid system - System concepts and analysis, (2017) 29–65. https://repository.tudelft.nl/.

[75] Z. Yang, H. Zhang, M. Ni, B. Lin, A hybrid system using Brayton cycle to harvest the waste heat from a direct carbon solid oxide fuel cell, Appl. Therm. Eng. 160 (2019) 113992. https://doi.org/10.1016/j.applthermaleng.2019.113992.

[76] C. Liu, J. Xu, M. Li, Z. Wang, Z. Xu, J. Xie, Scale law of sCO2 coal fired power plants regarding system performance dependent on power capacities, Energy

Convers. Manag. 226 (2020) 113505. https://doi.org/10.1016/j.enconman.2020.113505.

[77] IRENA, Renewable power generation costs in 2019, Int. Renew. Energy Agency. (2020) 144.

[78] C.S. Turchi, J. Stekli, P.C. Bueno, Concentrating solar power, Elsevier Ltd, 2017. https://doi.org/10.1016/B978-0-08-100804-1.00011-6.

[79] M. Mehos, C. Turchi, J. Vidal, M. Wagner, Z. Ma, C. Ho, W. Kolb, C. Andraka, A. Kruizenga, Concentrating Solar Power Gen3 Demonstration Roadmap, Nrel/Tp-5500-67464. (2017) 1–140. https://doi.org/10.2172/1338899.

[80] T. Neises, C. Turchi, Supercritical carbon dioxide power cycle design and configuration optimization to minimize levelized cost of energy of molten salt power towers operating at 650 °C, Sol. Energy. 181 (2019) 27–36. https://doi.org/10.1016/j.solener.2019.01.078.

[81] T.C. Allison, J. Jeffrey Moore, D. Hofer, M.D. Towler, J. Thorp, Planning for successful transients and trips in a 1 MW e -Scale High-Temperature sCO 2 test loop, J. Eng. Gas Turbines Power. 141 (2019). https://doi.org/10.1115/1.4041921.

[82] J.J. Moore, S. Cich, M. Towler, T. Allison, J. Wade, D. Hofer, Commissioning of a 1 MWe Supercritical CO 2 Test Loop, 6th Int. Symp. - Supercrit. CO2 Power Cycles. (2018) 1–36.

[83] M. Binotti, M. Astolfi, S. Campanari, G. Manzolini, P. Silva, Preliminary assessment of sCO2 cycles for power generation in CSP solar tower plants, Appl. Energy. 204 (2017) 1007–1017. https://doi.org/10.1016/j.apenergy.2017.05.121.

[84] Y. Ma, T. Morosuk, J. Luo, M. Liu, J. Liu, Superstructure design and optimization on supercritical carbon dioxide cycle for application in

concentrated solar power plant, Energy Convers. Manag. 206 (2020) 112290. https://doi.org/10.1016/j.enconman.2019.112290.

[85] L.A. Tse, T. Neises, The 5 th International Symposium-Supercritical CO2 Power Cycles ANALYSIS AND OPTIMIZATION FOR OFF-DESIGN PERFORMANCE OF THE RECOMPRESSION sCO2 CYCLES FOR HIGH TEMPERATURE CSP APPLICATIONS, (2016) 1–13. http://sco2symposium.com/www2/sco2/papers2016/SystemModeling/100paper.pdf.

[86] M. Kanniche, R. Gros-Bonnivard, P. Jaud, J. Valle-Marcos, J.M. Amann, C. Bouallou, Pre-combustion, post-combustion and oxy-combustion in thermal power plant for CO2 capture, Appl. Therm. Eng. 30 (2010) 53–62. https://doi.org/10.1016/j.applthermaleng.2009.05.005.

[87] L. Nkhonjera, S. Ansari, X. Liu, Development of hybrid CSP biomass gasification process with supercritical carbon dioxide cycle for power generation Development of Hybrid CSP Biomass Gasification Process with Supercritical Carbon Dioxide Cycle for Power Generation, 080005 (2020).

[88] R. Scaccabarozzi, M. Gatti, E. Martelli, Thermodynamic analysis and numerical optimization of the NET Power oxy-combustion cycle, Appl. Energy. 178 (2016) 505–526. https://doi.org/10.1016/j.apenergy.2016.06.060.

[89] J. Yang, Z. Yang, Y. Duan, Off-design performance of a supercritical CO2 Brayton cycle integrated with a solar power tower system, Energy. 201 (2020) 117676. https://doi.org/10.1016/j.energy.2020.117676.

APPENDIX 1: NAMENCLATURES

Symbol	Description	Units
sCO_2	Supercritical Carbon Dioxide	-
CSP	Concentrated Solar Power	-
CSP-PT	Concentrated Solar Power – Power Tower	-
Oxy Combustion	Oxygen dependent Combustion	
HTR	High Temperature Recuperator	-
LTR	High Temperature Recuperator	-
EES	Engineering Equations Solver	-
SRC	Single Recuperative Cycle	-
DRC	Dual Recuperative Cycle	-
MC	Main Compressor	-
RC	Recompression	-
IC	Intercooler	-
PC	Pre-Cooler	-
LCOE	Levelized Cost Of Electricity	-
RSM	Reynolds Stress Model	
DPM	Discrete Particle Model	
PSA	Plataforma Solar de Almeria	-
SOFC	Solid Oxide Fuel Cell	-
PHE	Primary Heat Exchanger	-
CSP-PT	Concentrated Solar Power – Power Tower	-
ASU	Air Separation Unit	-
TIT	Turbine Inlet Temperature	-
TIP	Turbine Inlet Pressure	-
CIT	Compressor Inlet Temperature	-
CPOC	Cryogenic Pressurized Oxy Combustion Cycle	-
cp	Specific heat	$\frac{kJ}{kg}\,^{\circ}C$
C	Heat Capacity Rate	$\frac{kW}{^{\circ}C}$
h	Specific Enthalpy	$\frac{kJ}{kg}$
LHV	Lower Heating Value	$\frac{kJ}{kg}$
$\dot{m}$	Mass flow rate	$\frac{kg}{s}$
P	Pressure	kPa
Q	Heat Transfer Rate	kW
S	Specific Entropy	$\frac{kJ}{kg}\,^{\circ}C$

Appendix 1: Nomenclatures, Continued.

Symbol	Description	Units
S_r	Split Ratio	-
T	Temperature	$°C$
W	Work	kW
$n_{thermal}$	Thermal Efficiency	%
Σ_{htr}	Thermal effectiveness of the high temperature recuperator	%
Σ_{ltr}	Thermal effectiveness of the low temperature recuperator	%
W_{fuel}	Work consumed by the fuel pump	KW
W_{O2}	Work consumed by the oxygen pump	KW
W_{MC}	Work consumed by the Main Compressor	KW
W_{RC}	Work consumed by the Re-Compressor	KW
$m`_{fuel}$	Mass flowrate of the fuel consumed by the cycle	Kg/s
$m`_{Oxygen}$	Mass flowrate of oxygen consumed by the cycle	Kg/s
$m`_{WV}$	Mass flowrate of the Water Vapor within the cycle	Kg/s
$m`_{Exported\ CO2}$	Mass flowrate of the exported CO_2	Kg/s